Advanced labelling strategies for structural investigation of membrane protein dynamics by solid-state magic angle spinning NMR spectroscopy

Inaugural-Dissertation
to obtain the academic degree
Doctor rerum naturalium (Dr. rer. nat.)

submitted to the Department of Biology, Chemistry and Pharmacy
of Freie Universität Berlin

by

Gregorio Giuseppe de Palma

From Terlizzi (BA), Italy

December 2015

This Ph.D. thesis describes the work done between July 2009 and July 2012 at the Leibniz-Institut für Molekulare Pharmakologie (FMP), under the supervision of Prof. Dr. Hartmut Oschkinat. I hereby certify that all the work described in this thesis was done by me, unless specified otherwise in the text. The whole work was submitted to the Freie Universität Berlin (Department of Biology, Chemistry and Pharmacy).

Gregorio Giuseppe de Palma

Berlin, December 2015

Questa tesi di dottorato e´dedicata
a mia nonna recentemente scomparsa.

Reviewer: Prof. Dr. Hartmut Oschkinat

Reviewer: Prof. Dr. Udo Heinemann

Date of defense: 31.10.2016

Acknowledgements

I would like to say thanks to all the people who supported me during this work at the Leibniz-Institut für Molekulare Pharmakologie (FMP).

I would like to express my sincere and deep gratitude to my supervisor, **Prof. Dr. Hartmut Oschkinat**, for giving me both the opportunity to work on this project in a well-equipped laboratory with expert scientists and the financial support.

I would like to thank **Prof. Dr. Udo Heinemann** for being my second reviewer.

A particular thanksgiving is for **Dr. Matthias Hiller** for his patience to teach me the techniques for membrane protein expression, purification, refolding, reconstitution in 2D crystals and to record different spectra for solid-state MAS NMR studies.

Thank you very much also to **Dr. Anne Diehl** for the huge support in the laboratory (especially during the experiments) and for the helpful discussions about my project during seminars and in her office.

Thank you very much to **Lilo Handel** for the co-operation in the OmpG project.

Thank you very much to **Joren-Sebastian Retel** for the inspiring and useful discussion in NMR, an introduction to the use of the UNIX machine and for teaching me an important and useful programme like CCPN or Analysis.

Thank you very much to **Dr. Dorothea Lorenz** for recording images of the 2D crystals on the transmission electron microscopy.

Thank you very much to **Andrea Steuer** for helping with the bureaucracy.

Thank you very much to **Dr. Anne Honer** for the introduction to the Marie Curie network and its rules.

And of course I would also like to thank all colleagues I forgot to mention here.

Table of Content

Abbreviations

1, 2 and 3D	one-, two- and three-dimensional
Å	Angstrom
AA	amino acid
AFM	atomic force spectroscopy
APS	ammoniumpersulphate
ATP	adenosine triphosphate
BMRB	Biological Magnetic Resonance Data Bank
CD	circular dichroism
CMC	critical micellar concentration
CP	cross polarisation
CSA	chemical shift anisotropy
CW	continuous wave
Da	Dalton
DARR	dipolar-assisted rotational resonance
DNA	deoxyribonucleic acid
DDM	dodecyl-β-D-maltoside
E. coli	*Escherichia coli*
EM	electron microscopy
FID	free induction decay
GLB	gel loading buffer
GPCR	G protein coupled with receptor
Hz	Hertz
IPTG	isopropyl-β-D-thiogalactopyranoside
KDa	kilo Dalton
LDAO	lauryl-N,N-dimethydodecilamine-N-oxide
LPR	lipid-to-protein ratio
MAS	magic angle spinning
MP	membrane protein
NLP	nanolipoprotein particles
NMR	nuclear magnetic resonance
OD_{600}	optical density measured at 600 nm
OG	octyl-β-D-glucopyranoside
OmpG	outer membrane protein G

PAGE	polyacrylamide gel electrophoresis
pET	plasmid for expression, mediated by the T7 RNA polymerase
PCR	polymerase chain reaction
PDB	Protein Data Bank
PDSD	proton-driven spin diffusion
ppm	parts per million
REDOR	rotational-echo double-resonance
RNase	ribonuclease
Rf	radio frequency
ss	solid-state
SDS	sodium dodecyl sulphate
SH_3	Src-homology 3
SMFS	Single molecules force spectroscopy
S/ N	signal-to-noise ratio
SPINAL	small phase incremental alternation
TEDOR	transferred-echo double-resonance
TEMED	tetramethylethylendiamin
TPPM	two-pulse phase modulation
Tris	Tris (-hydroxymethyl-) aminomethan
TROSY	transverse relaxation-optimized spectroscopy
U	uniformly

Single- and three-letter amino acid code

Alanine	Ala	A
Arginine	Arg	R
Asparagine	Asn	N
Aspartate	Asp	D
Cysteine	Cys	C
Glutamate	Glu	E
Glutamine	Gln	Q
Glycine	Gly	G
Histidine	His	H
Isoleucine	Ile	I
Leucine	Leu	L
Lysine	Lys	K
Methionine	Met	M
Phenylalanine	Phe	F
Proline	Pro	P
Serine	Ser	S
Threonine	Thr	T
Tryptophan	Trp	W
Tyrosine	Tyr	Y
Valine	Val	V

1 General introduction

The most fascinating structures in biology are membrane proteins (MPs). They are sited at the interface between two compartments: cytoplasm and extracellular space, or mitochondrial matrix and intermembrane space, or else they make up most of the mass of the small vesicles involved in endocytosis, exocytosis or intracellular trafficking. For most of their life, they interact closely with both water and lipids in their environment, yet must be synthesised by the ribosome exactly like other proteins before moving to different membrane locations within the cell. This places unique and sometimes conflicting demands on MPs for folding, translocation and stability. Most MPs' functions are either transport, signalling or provision of the structural framework that shapes cellular compartments. In signalling, they provide both the sensory input and output, usually through direct or indirect involvement in the release of signalling molecules. Other MPs are key components of energy transduction and conversion. Chemical energy may be converted into electrical energy, whereas electrical energy may be converted into either mechanical energy or the synthesis of ATP, the universal energy currency of the cell. By observing an MP's structure it is possible to discover their orientation to the lipid bilayer. A lipid bilayer is a film of oil, thus structures immersed in it are relatively free to float about. For some membrane proteins, this is the case. For others, however, their mobility is limited. MPs do not work alone. The interaction with membrane lipids can be highly specific and is often important for full functional and structural integrity of the protein. Lipid molecules (figure 1) are arranged as a continuous double layer (phospholipid bilayer) formed by phospholipids, cholesterol and glycolipids. A great variety of membrane lipids exists.

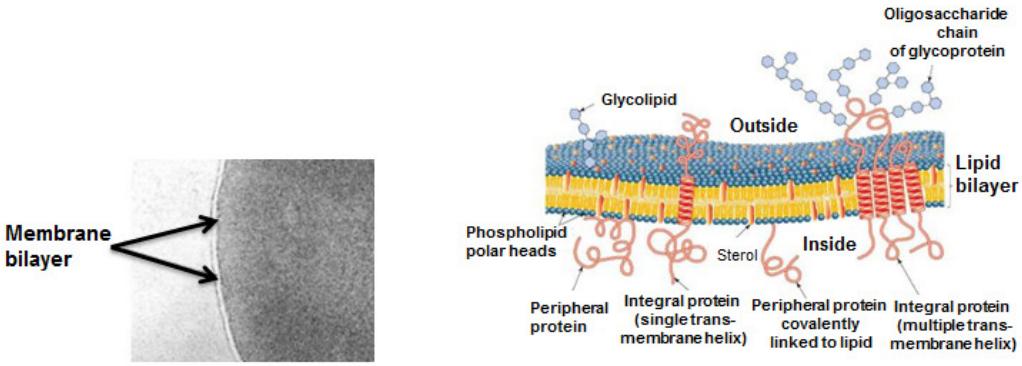

Figure 1.1 View of cell membrane. Left, electron micrograph of the plasma membrane after staining with osmium tetroxide. Right, three-dimensional model of a cell membrane and membrane components (Nelson and Cax, 2005).

To improve human and animal health, many targets of drugs are MPs involved in signalling or growth control at the cell surface. Over the last 20 years, there has been enormous progress in understanding membrane protein structure because MP mutations such as misfolding and malfunctioning are directly and indirectly involved in many diseases, for example cystic fibrosis, epilepsy, retinis pigmentosa and nephrogenic diabetes (Hubner and Jentsch, 2002; Schöneberg *et al.,* 2004). The number of unique membrane protein structures and multiple sets of coordinates deposited for many structures in the PDB in early 2011 is almost 270 (http://blanco.biomol.uci.edu/mpstruc/), which accounts for only ~ 1 % of all unique membrane protein structures deposited today. The number of solved MP structures is still lower than the number of solved structures of soluble proteins (~ 20000 structures of non-redundant protein sequences) deposited in the PDB since 1976 (Bermann *et al.,* 2000). When taking into account that the human genome consists of codes for ~ 36000 structural genes and that it is estimated that ~ 30 % of all eukaryotic proteins are MPs, it can be concluded that less than 1 % of the known protein structures are MP structures. Therefore, structure determination of MPs is of major interest not only in structural biology but also in pharmacology, especially for drug development.

1.1 Different techniques to study membrane proteins

Structural biology is developing universal tools for visualising biological processes in space and time at atomic resolution. This is possible because of the increasing availability of genome information due to the recombinant DNA technologies and the evolution of biochemical and biophysical understanding of MPs. The field has been built with established methodologies like X-ray crystallography, electron microscopy and solution NMR and is now incorporating new techniques like atomic force spectroscopy and solid-state magic-angle-spinning NMR.

These new techniques investigate non-crystalline, native-like biological materials and their development in structural characterisation studies is increasing the number of MP structures deposited in the PDB. Before being able to characterise the membrane protein structures it is necessary to express, isolate and purificate large amounts of the MPs of interest (tens or even hundreds of milligrams), as well as finding suitable sample conditions.

1.1.1 Expression, isolation, purification and (re)folding of membrane proteins

The first step in the preparation of MP samples suitable for structural studies is their expression. To express MPs means to accumulate sufficient amounts of chemically and conformationally homogenous protein for structural determination studies. With few exceptions, the natural abundance of MPs is very low, making it difficult to isolate sufficient material for structural studies. It is possible to try the extraction of MPs from the membrane with detergents. However, it is generally a harsh treatment, which leads to conformational aberrations. Thus, an efficient system for the heterologous expression of MPs is required to produce a sufficient amount of protein for structure analysis.

To overcome these problems, different expression systems were developed for prokaryotic and eukaryotic cells. In this introduction the main focus lies on the development of expression systems and the isolation, purification and (re)folding of MPs for prokaryotic cells (e.g. the outer membrane proteins called porins). Structure determination of MPs is a challenge. Classical methods for growing three-dimensional (3D) crystals have been successfully used to solve the structures of thousands of soluble proteins and protein complexes to atomic resolution, but these are more difficult to apply to MPs. The difficulty is the considerable amount of hydrophobic surfaces that an MP complex has at its interface with the surrounding lipid. While the MPs can be effectively solubilised with detergents that replace the lipid and keep the hydrophobic surfaces of the protein shielded from water, delipidation may destabilise the protein. In spite of the difficulties in growing 3D crystals, major progress has recently been made in structure determination of MPs. The archetype family of MP channels determined to atomic resolution by X-ray diffraction are the porins which form diffusional pores in the outer membrane of mainly Gram-negative bacteria. Numerous prokaryotes possess an outer membrane in addition to their cytoplasmic or inner membrane. Up to now, all established structures of integral bacterial outer membrane proteins contained β-pleated sheets but no trans-membrane α-helices. In all cases, these sheets formed circular β-barrels so that all polar atoms of the peptide bonds were buried, as in a trans-membrane α-helix. In contrast to the inner membranes, the outer membranes obviously function essentially as shields against mechanical and chemical stress and are permeable for small solutes. This may be the reason for the application of β-barrel proteins in this membrane because most of them contain a reasonably sized pore if they consist of more than about a dozen strands (Schulz *et al.,* 1993; Schulz *et al.,* 2002). However, there are a number of proteins with smaller β-barrels that form no pore, indicating that the β-barrel structure has been selected for a more general reason. The β-barrel residues are completely connected by main-chain hydrogen bonds and thus tend to form stable scaffold.

This is in contrast to the proteins of the inner membrane where the α-helices form bundles that are merely connected via side chain interactions and are therefore intrinsically less stable. This difference in stability is reflected in the number and resolution of the known membrane protein structures that are still dominated by outer membrane proteins. Outer membrane proteins are produced with an N-terminal signal sequence which directs the nascent polypeptide through the translocon in the inner membrane to the periplasmic space. The signal sequence is removed during translocation and the native protein is folded and inserted into the outer membrane. Overexpressed outer membrane polypeptides without a signal sequence usually end up in inclusion bodies.

The first X-ray crystal structure of outer membrane proteins were obtained with material extracted from the natural source, that is to say by native expression (Garavito *et al.,* 1980; Kreusch *et al.,* 1994). For this purpose, the growth conditions were optimised to enhance the expression of the outer membrane proteins of interest, most notably of specific porins (Cowan *et al.,* 1992; Meyer *et al.,* 1997). A higher degree of expression was obtained with plasmid-based systems. For example, the *Escherichia coli* maltoporin LamB was expressed using a plasmid carrying the lamB gene under control of the tac promoter (Stauffer *et al.,* 1989). To facilitate the purification process, an *E. coli* strain devoid of the abundant endogenous outer membrane proteins OmpF, OmpC and LamB was used. An *E. coli* strain with similar deletions was used for a plasmid-dependent overexpression of FhuA (Ferguson *et al.,* 1998). The most developed strain lacked the lamB, ompC and ompA genes, had the genomic ompF gene inactivated by an insertion, and produced OmpF under the control of a T7 promoter.

Furthermore, the protein isolation procedure was improved by adding an internal hexa-histidine tag for binding to a Ni-NTA column. Low protein expression levels render the subsequent purification more difficult. This procedure can be ameliorated by adding affinity tags to the protein. Such tags, however, are commonly considered crystallisation hazards and are therefore not popular. Improvements in purity can also be accomplished by using bacterial strains lacking the main outer membrane proteins.

Proteolysis is a further risk to the expressed protein. The protease-deficient strain *E. coli* BL21, or derivatives of it, were used in the expression of OmpF (Phale *et al.,* 1997), FhuA (Locher *et al.,* 1997) and TolC (Koronakis *et al.,* 1997).

The expression yield depends also on the cultivation temperature, which is usually 37 °C. The amount of the outer membrane protein OprM from *Pseudomonas aeruginosa*, however, increased threefold when the expression was performed at 28 °C (Dekker *et al.,* 1995).

For bacterial outer membrane proteins, the expression into inclusion bodies with subsequent solubilisation in denaturing buffer and in vitro (re)folding was surprisingly successful. The outer membrane phospholipase A (OmpLA) was accumulated into inclusion bodies, when

expressed without its signal sequence (Dekker *et al.,* 1995). The obtained inclusion bodies were then solubilised in urea and the protein (re)folded upon dilution into a buffer containing Triton X-100. The resulting fold was native as indicated by the enzymatic activity and by the gel electrophoresis migration behaviour, which differed for the unfolded and folded states. Moreover, the (re)folded protein yielded better crystals than the protein isolated from membranes (Blaauw *et al.,* 1995). In general, (re)folding from inclusion bodies is more difficult than the protein expression into the inclusion bodies itself. The procedure was successful for the small (ca. 17 kDa) outer membrane anchor proteins OmpA and OmpX (Pautsch *et al.,* 1999). Folding occurred upon dilution in an octylpoly-oxyethylenoxide (C8POE)-containing buffer, from which the protein was purified in a single ion-exchange chromatography step. The large 80-kDa outer membrane iron transporter FepA, however, was also produced in this way and then crystallised (Buchanan *et al.,* 1999). The 20-kDa outer membrane protease OmpT (Kramer *et al.,* 2000) and the 19-kDa outer membrane adhesion protein OpcA from *Neisseria meningitidis* were expressed into inclusion bodies, (re)folded and subsequently crystallised (Prince *et al.,* 2001; Vandeputte *et al.,* 2001). Two-dimensional crystalline arrays were obtained after the expression of *Comamonas acidovorans* outer membrane protein Omp21 into inclusion bodies (Baldermann *et al.,* 2000).
In most cases of outer membrane protein expression into inclusion bodies, the T7 promoter system together with the strain *E. coli* BL21(DE3) in standard culture media was used (Buchanan *et al.,* 1999; Schmid *et al.,* 1996; Charbonnier *et al.,* 2001, Dekker *et al.,* 1995, Pautsch *et al.,* 1999, Kramer *et al.,* 2000, Rogl *et al.,* 1998, Booth *et al.,* 2001).
In spite of the quite detailed knowledge about the structural properties of bacterial outer membrane proteins, no high-resolution structures of similar mitochondrial or plastid outer membrane proteins are known. The only two structures of mitochondrial outer membrane proteins described so far are that of the human voltage-dependent anion-selective channel (VDAC) as a low-resolution projection derived from two-dimensional crystals (Mannella *et al.,* 1997; Mannella *et al.,*1998) and that of human liver monoamine oxidase B (MAO-B) established by an X-ray analysis at atomic resolution (Binda *et al.,* 2002).
On the whole, the results with eukaryotic organellar proteins are much less spectacular than those with prokaryotic outer membrane proteins (Buchanan *et al.,* 1999). Until now, organellar outer membrane proteins were only expressed into inclusion bodies in *E. coli* (Rogl *et al.,* 1998; Linke *et al.,* 2000; Dolder *et al.*, 1999; Pohlmayer *et al.,* 1999).
Although outer membrane proteins are comparatively stable because they have to cope with the harsh external environment, stability is still one of the main considerations in crystallisation attempts (Rosenbusch *et al.,* 2001). It is probably an even more pronounced problem for the organellar outer membrane proteins as these contact the milder cytosol. It should be noted that protein stability is a multifaceted parameter. The stability of membrane

proteins should be differentiated in terms of heat, water-soluble denaturants and detergents (Booth *et al.,* 2001; Lau *et al.,* 1997). Because a large number of detergents with a broad range of properties have become available, an appropriate detergent can usually be chosen for any given application.

Functional overexpression into the outer membrane of *E. coli* was most successful with outer membrane proteins from *E. coli* itself (Stauffer *et al.,* 1989; Ferguson *et al.,* 1998; Phale *et al.,* 1997; Koronakis *et al.,* 1997; Smith *et al.,* 1997) and with ScrY of the closingly related *S. typhimurium* (Forst *et al.,* 1993). It failed, however, with the porin from *R. blasticus*, which is an α-proteobacterium and thus more distantly related to the γ-proteobacterium *E. coli* (Schmid *et al.,* 1996). Moreover, the authors do not know of any case of the expression of a eukaryotic organellar outer membrane protein into the *E. coli* outer membrane. In general, the functional expression systems are difficult to set up and most of them suffer from comparatively low yields. The main problem with non-functional expression into inclusion bodies is the in vitro (re)folding of the inactive polypeptide.

A low yield in the folding process can easily abolish the advantage of a high expression level. The success of the (re)folding procedure will therefore determine whether the inclusion body expression method finds a broader application (Booth *et al.,* 2001; Buchanan *et al.,* 1999). The (re)folding attempts of outer membrane proteins resulted in the following observations: the choice of the detergent is most important (Dekker *et al.,* 1995); the in vitro (re)folding into liposomes yields generally less native protein than folding into detergent micelles (Dekker *et al.,* 1995; Buchanan, *et al.,* 1999); the in vitro (re)folding requires the presence of micelles which means that the detergent concentration has to exceed the critical micelle concentration (CMC) (Kleinschmidt *et al.,*1999); the best results were obtained with zwitterionic detergents (Schmid *et al.,* 1996; Kramer *et al.,* 2000; Prince *et al.,* 2001; Dolder *et al.,* 1999) and with polyoxyethylene detergents (Dekker *et al.,* 1995; Pautsch *et al.,* 1999; Baldermann *et al.,* 2000; Linke *et al.,* 2000); a mixture of a zwitterionic detergent with SDS was also applied (Buchanan *et al.,*1999).

A quantitative assessment of the (re)folding efficiency as a function of the applied detergent was performed with OmpLA by monitoring its enzymatic activity (Dekker *et al.,* 1995) and within OEP16 by following the CD spectra (Linke *et al.,* 2000).

If the outer membrane protein is not an enzyme and if its CD spectrum cannot be easily determined, for instance because of spectral interference of detergents, electrophoretic assays should be tried.

At ambient temperatures, all bacterial outer membrane proteins examined assume two states with differing electrophoretic mobility in SDS-PAGE (Schmid *et al.,* 1996; Dekker *et al.,* 1995; Pautsch *et al.,* 1999; Prince *et al.,* 2001; Kleinschmidt *et al.,* 1999). No such difference in migration behavior has been reported for eukaryotic organellar outer membrane proteins.

For inclusion body expression of less stable membrane proteins, using a mild detergent to quickly remove the denaturant, adding stabilising agents (Schein *et al.,* 1990) and working at low temperatures is recommended. The mildest detergents (le Maire *et al.,* 2000) used for this procedure were Triton X-100 (Dekker *et al.,* 1995; Zhang *et al.,* 1999), C12E8 (octaethylene glycol monododecil ether) and C12M (dodecyl-β-D-maltoside, Linke *et al.,* 2000). If the protein is diluted in excess (re)folding buffer lacking the chaotropic agent, the denaturant concentration is lowered very quickly. The dilution is most efficiently performed by adding the protein solution drop by drop to the (re)folding buffer using, for instance, a peristaltic pump (De Bernadez-Clark *et al.,* 1999). In this way, the unfolded polypeptide is instantly dispersed and (re)folded, not having left much time for aggregation. The temperature during protein (re)folding should always be considered to be an important variable (Buchanan *et al.,* 1999; De Bernadez-Clark *et al.,* 1999; Chen *et al.,* 1997). A desirable expression system produces a large amount of protein and allows its purification and subsequent crystallisation.

While fusion protein approaches are becoming increasingly popular, only three of the structurally established outer membrane proteins were produced as fusion proteins. In all cases they were designated to be fused with a His-tag. These were FhuA (Ferguson *et al.,* 1998), VDAC (Dolder *et al.,* 1999) and Omp21 (Baldermann *et al.,* 2000). Among these, only FhuA with an internal affinity tag yielded three-dimensional crystals diffracting to high resolution.

Outer membrane proteins are often difficult to solubilise. Therefore, most purification protocols for native proteins involve selective membrane extractions in which other outer membrane proteins are separated according to their solubilisation properties in a given detergent. The target proteins were subsequently solubilised with LDAO (Forst *et al.,* 1993; Ferguson *et al.,* 1998; Chen *et al.,* 1997), C8POE (n-octyl polyoxyethylene Stauffer *al.,* 1989) or Triton X-100 (Koronakis *et al.,* 1997). Obviously, they should be stable enough to maintain their native conformation during the extraction procedure. All protocols for non-functional expression into inclusion bodies circumvent the membrane solubilisation step. Here, however, mild detergents and suitable buffer conditions have to be established for the folding process in order not to harm the protein. In general, purity and the ease of impurity removal vary appreciably among different proteins expressed into inclusion bodies. In numerous cases, the purification of (re)folded protein was not easier than a differential extraction from an outer membrane. Most inclusion bodies contain other outer membrane proteins, ribosomal proteins and sometimes even truncated versions of the plasmid-encoded target protein (Rinas *et al.,* 1992). Often these contaminants can be removed by washing, using a detergent-free buffer (Dekker *et al.,* 1995) or a buffer with detergents such as Triton X-100 (Buchanan *et al.,* 1999; Schmid *et al.,* 1996; Pautsch *et al.,* 1999; De Bernadez-Clark *et al.,*

1999) or LDAO (Prince *et al.,* 2001). It has been pointed out that extensive protein expression into inclusion bodies gives rise to morphological changes of the cell wall, which then calls for harsher procedures to isolate the inclusion bodies (De Bernadez-Clark *et al.,* 1999). With non-functional expression systems involving a His-tag (Baldermann *et al.,* 2000; Dolder *et al.,* 1999) the target protein can be purified in the fully or partially denatured state. Some proteins bind to an ion exchanger in the presence of high concentrations of urea (Schmid *et al.,* 1998; Schmid *et al.,* 1996; Pohlmayer *et al.,* 1997).

In general, however, the protein was purified after (re)folding by dilution. Gel filtration columns can be used to remove misfolded and aggregated unfolded protein due to their different hydrodynamic radii (Buchanan *et al.,* 1999; Prince *et al.,* 2001; Schiltz *et al.,* 1991). For the separation of different conformational and aggregation states, ion exchange columns were applied for several outer membrane proteins. In particular, unfolded FepA eluted at lower ionic strength than native FepA (Buchanan *et al.,* 1999), while unfolded OmpLA eluted at higher ionic strength (Dekker *et al.,* 1995) than its folded isoform.

Outer membrane proteins have been crystallised with lipids or lipopolysaccharides (Ferguson *et al.,* 1998), but more often without them. However, proteins isolated from membranes may require lipids for their stability, particularly if they contain strong lipid-binding sites (Kreusch *et al.,* 1994, Locher *et al.,* 1997). The introduction of crystallisation-enhancing mutations seems especially suited for proteins with a reasonably clear chain topology prediction (Pautsch *et al.,* 1999). Outer membrane proteins which cannot be sufficiently stabilised in an isolated state may form more stable complexes with other proteins and/ or low molecular mass compounds. A number of bacterial outer membrane proteins have been characterised with their substrates (Schirmer *et al.,* 1995; Locher *et al.,* 1998), substrate analogues (Weiss *et al.,* 1992; Meyer *et al.,* 1997; Ferguson *et al.,* 2001) or ligated lipids (Ferguson *et al.,* 2000). The structural analysis of a bacterial porin revealed, for instance, that it carried a periplasmic peptide ligand from its natural source (Zeth *et al.,* 2000). A co-expression of outer membrane protein complexes for structural studies has not yet been reported. The stabilisation of membrane proteins by designed mutations is being actively pursued (Lau *et al.,* 1997; Zhou *et al.,* 2000).

For structural studies by NMR spectroscopy the sample must be labeled with stable isotope such as ^{13}C and/or ^{15}N. *E. coli* is the primary expression system considering the lower cost for isotopically labelled amino acids and its cell cultures' rapid growth. Furthermore, expression protocols can be scaled up more easily when *E. coli* is used (Lian *et al.,* 2001). The development of the cell-free expression system allows the direct production of membrane proteins in membrane-mimetic environments (micelles or other hydrophobic environments) which may be suitable for NMR studies. Apart from strong expression yields, the advantage of the cell-free expression system is that the sample can be measured without

chromatographic protein purification and the direct incorporation of almost any combination of amino acids with very little metabolic scrambling. These advantages have allowed the development of a wide array of isotope labelling techniques which facilitate structural investigations of proteins that combined the reduction of spectral congestion and of broad line widths with a minimum number of samples for the identification of all cross-peaks (amino acid residue type) in solution-state spectra (Sobhanifar *et al.,* 2010).

1.1.2 Three-dimensional (3D) crystallisation and X-ray crystallography

Once an MP has been purified in a functional, stable and monodisperse state, 3D crystals may be relatively easily obtained, but MP crystals are often very small and disordered. The properties of the detergent and its final concentration are especially important (Ostermeier and Michel, 1997; Kühlbrandt *et al.,* 1988; Prive *et al.,* 2007). It is often necessary to screen a large number of crystallisation conditions and make frequent usage of synchrotrons. MPs solubilised in detergent micelles are flexible and dynamic complexes. The flexibility of a detergent micelle is strongly influenced by the polarity of the head group and the length of the alkyl chain of the detergent molecules (Ostermeier and Michel, 1997). However, any degree of flexibility in the crystal lattice is detrimental for growing high-resolution 3D crystals. (Ostermeier and Michel, 1997; Kühlbrandt *et al.,* 1988; Prive *et al.,* 2007). New strategies developed over the last ten years increase the probability of obtaining good diffracting crystals. Michel was the first to distinguish type I (stacks of 2D layers growing in the third dimension) from type II (involving contacts principally between hydrophilic parts of the protein) crystals (Michel *et al.,* 1983). With conventional vapour diffusion methods, type II crystals are more commonly observed because detergents form a belt around solubilised MPs and form small micelles that have been most successful in obtaining high-resolution structures with type II crystals. However, many proteins are stable only in detergents with large micelles, requiring different approaches. The key factor is the size of the protein in relation to the size of the detergent micelle. Dodecyl-β-D-maltoside has been used successfully to crystallise larger MP complexes, but only those with GPCRs (e.g. Cherezov *et al.* 2007). The availability of microfocus beams (1–10 mm diameter) allows scanning along the crystal to find particular areas that are better ordered as well as establishing a complete 3D data collection using tiny crystals. Various physiological processes are obtained by structural data of X-ray crystallography combined with additional biophysical investigations, like the sensory perception (smell, sight and taste), the transmembrane signalling, the control of the cytosolic Ca^{2+} concentration driven by the sarcoplasmic reticulum Ca^{2+}–ATPase (SERCA1) involved in skeletal muscle contraction, the renal water conservation, neuro-

homeostasis, digestion, regulation of body temperature and reproduction (Jaakola *et al.,* 2008, Cherezov *et al.,* 2007, Palczewsky *et al.,* 2000, Toyoshima, 2008, Sui *et al.,* 2001).

X-ray crystallography is a method which requires highly diffracting 3D crystals. If there is no diffraction, there is no possibility of solving the structure of the MP. However, X-ray crystallography provides high-resolution atomic structures of MPs (1–4 Å) and is the most successful technique used in this field. The instability in the detergent, the susceptibility to the protease and the flexibility of the MP can result in a lack of structural information. Although the research for the most suitable detergent was a critical step, lipids were added to stabilise the MP for the crystallisation of the Kv1.2/Kv2.1 chimera (Long *et al.,* 2005, Long *et al.,* 2007). Another example is the ADP/ ATP translocase which, in complex with an inhibitor carboxyatractyloside, has a higher stability in detergent micelles presumably by trapping the transporter in a single, relatively stable conformation. The structure of the ADP/ ATP translocase from bovine mitochondria crystallised in the presence of carboxyatractyloside showed the six transmembrane (TM) helical bundles with the helical hairpins related by a pseudo-threefold axis and revealed the transporter trapped in an outward facing conformation (Pebay-Peyroula *et al.,* 2003).

Different techniques to enhance the resolution of 3D crystals have been developed in the past few years, including the use of lipids to stabilise MPs, the use of antibody fragments to increase protein-protein interaction (Hunte & Michel, 2002), the use of either lipidic cubic phases or bicelles (Zhang *et al.,* 2003) or detergent-free crystallisation methods (Nollert *et al.,* 1999), or by addition of specific active-site ligands or inhibitors (Pebay-Peyroula *et al.,* 2003). Additionally, to test different buffer conditions and additives, crystallisation screens, for example the 'MembFac' from Hampton research, are commercially available.

1.1.3 Electron crystallography and two-dimensional (2D) crystallisation

Initially, electron crystallography was only used to study the structure of naturally occurring 2D crystals. It only matured into a generally applicable structure determination technique when atomic structures were determined using artificially produced 2D crystals, the first of which was obtained with the plant light harvesting complex 2 (LHC-2; Kühlbrandt *et al.,* 1994).

Other high-resolution maps of MPs were obtained and solved by electron crystallography of aquaporin 1 (Murata *et al.,* 2000; Ren *et al.,* 2001), torpedo ray nicotinic acetylcholine receptor (Miyazawa *et al.,* 2003; Unwin, 2003 and 2005), sheep aquaporin 0 (Gonen *et al.,* 2004; Gonen *et al.,* 2005), rat aquaporin 4 (solved using recombinant protein expressed in insect cells - Hiroaki *et al.,* 2006) and rat microsomal glutathione transferase 1 (Holm *et al.,*

2006). Currently, with a resolution of 1.9 Å, the structure of aquaporin 0 is the highest-resolution structure determined by electron crystallography, which revealed not only the structure of the protein but also water and lipid molecules (Gonen *et al.,* 2005).

One advantage of electron crystallography is that the phases can be directly obtained from the images, but collecting high-resolution images is much more challenging than recording high-resolution diffraction patterns. Therefore, adapting indirect phasing methods from X-ray crystallography may provide a faster way to determine structures than electron crystallography. It is notable that the X-ray crystallographic structures of bacteriorhodopsin have all been solved directly or indirectly from the original structures that were experimentally phased from electron microscope images. Structures that were determined using one technique can also be used to help solve or validate structures that were determined by another technique. EM can also assess structural differences observed in detergent micelles and in native lipid bilayers. The structure of the multidrug transporter EmrE differs significantly based on whether it was obtained by EM or X-ray (Tate *et al.,* 2006). Another example is the mitochondrial ADP/ ATP carrier, which shows a monomeric structure in detergent micelles. The same protein reconstituted into lipid bilayers exhibits a dimeric structure (Pebay-Peyroula *et al.,* 2003). The clear structural relationship between the acetylcholine receptor, determined by electron microscopy (EM), and the bacterial homopentameric GLIC and ELIC channels, determined by X-ray crystallography, validates the relevance of the bacterial structures to the pentameric ligand-gated channel family in general and confirms the correctness of the EM work. Electron microscopy is a valuable technique in other special cases as well, one of these being intransigent structures. It is notable that the structure of eukaryotic αβ-tubulin (Nogales *et al.,* 1997) has been determined only by electron crystallography of 2D zinc-induced sheets.

Another application is the investigation of functional changes in conformation that might disrupt a 3D, but not a 2D, lattice. The large structural change found in bacteriorhodopsin at the mid-point of the photocycle in the purple membrane of *halobacteria* appears either to be prevented by crystal packing forces in 3D crystals or to cause disorder, so that, up to now, the nature of the structural change could not be investigated by X-ray diffraction. Electron microscopy has been the only successful method in describing this key structural change at high resolution (Subramaniam and Henderson, 2000).

Numerous other structures have been determined to 5 to 9 Å resolution, which allows the architecture of α-helical membrane proteins to be determined (Henderson *et al.,* 2004). These low-resolution analyses are relatively quick and frequently very informative about secondary structure. By using other biochemical and evolutionary data in combination with hydrophobic moment calculations, these lower resolution maps can often be used to derive good working models of the structure, e.g. EmrE (Fleishman *et al.,* 2006). Detergent micelles

are an appropriate but imperfect substitution for the lipids surrounding MPs in situ although X-ray crystallography is the most frequently used method in structure determination of MPs. In particular, the structural integrity of an MP may depend on essential lipids. A new way to solve structures of MPs in a native-like environment is the reconstitution of MPs into artificial membranes to form two-dimensional crystals and their structural analysis by electron crystallography. The resolution of MP structures obtained by EM is lower than for X-ray crystallography but EM of MP in 2D crystals is not an all-or-nothing method like X-ray crystallography. Using poorly diffracting 2D crystals, it is at least possible to generate a molecular shape of the MP of interest.

Membrane proteins are generally considered as the most difficult to crystallise, mainly due to their amphiphilic character which implies the use of detergent for their solubilisation and their purification (Helenius *et al.,* 1975; le Marie *et al.,* 2000). Success in growing three-dimensional crystals in detergents is relatively rare, probably because of the difficulty in producing and/ or maintaining a crystal lattice through the sole interactions between extramembrane domains of the proteins, the hydrophobic domains being shielded by the detergent micelles (Garavito *et al.,* 1995; Ostermeier *et al.,* 1997). The bottleneck of 3D crystallisation has been addressed by Michel's group who has introduced a novel approach in which monoclonal antibody fragments are bound to the membrane complex with the idea of extending the hydrophilic domains of MPs (Ostermeier *et al.,* 1996). Therefore, due to the tremendous difficulty in 3D crystallisation, less than 25 original structures of membrane proteins have been solved by X-ray crystallography, a number which lags far behind that of soluble proteins. To help with this difficult problem, reconstitution of membrane proteins into artificial membranes to form crystals connected to two dimensions (2D crystals) has opened a new way to solve their structure into a native-like environment. Indeed, electron crystallography on 2D crystals is an excellent alternative and a complementary discipline to X-ray crystallography regarding the characterisation of membrane protein structures.

To date, the most employed strategy for 2D crystallisation relies on the general method of detergent-mediated reconstitution of membrane proteins into liposomes but at low lipid to protein ratios (Rigaud *et al.,* 1995). The strategy consists of starting with the purified protein and the suitable combination of lipids, both solubilised in detergent. In the next step, the detergent is removed from these lipid-detergent and lipid-protein-detergent micellar solutions, resulting in the progressive formation of lipid bilayers in which the proteins incorporate and eventually crystallise (figure 1.2). Several types of 2D crystals, which all contain a continuous lipid bilayer in which proteins have been incorporated, can be produced: vesicular crystals, tubular crystals (in which reconstituted proteins are helically ordered on the surface of a cylinder) and planar crystalline sheets (which in some instances can lead to thin 3D crystals upon the stacking of the 2D arrays).

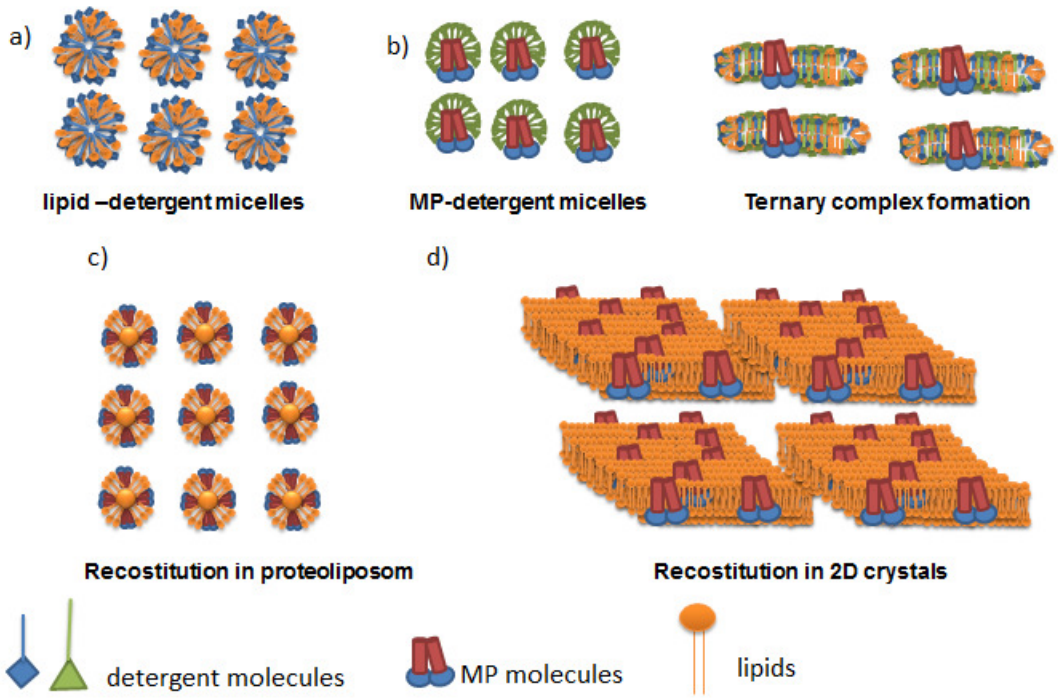

Figure 1.2 Reconstitution of MPs into proteoliposomes and two-dimensional crystallisation. (a) The starting mixture is composed of lipid-detergent micelles and MP-detergent micelles, (b) ternary micelles are formed upon equilibration in the starting mixture. After subsequent detergent removal different structures are formed: (c) at higher LPR the membrane protein is reconstituted into proteoliposomes. (d) At a sufficiently low LPR 2D crystals can assemble.

Whereas the intermolecular contacts in 3D crystals specifically involve the extra-membrane hydrophilic domains of the detergent-solubilised proteins, the intermolecular contacts in membrane-embedded 2D crystals also involve the intrinsic hydrophobic domains of the proteins. Thus, as opposed to proteoliposome reconstitution at high LPRs (in the range of 1 protein per 2000–10000 lipid molecules), 2D crystallisation at low LPRs (in the range of 1 protein per 10–50 lipid molecules) specifically involves more protein-protein and lipid-protein interactions. To favour protein arrangements in 2D crystals, these interactions should be considered in analogy to solvation interactions in crystallisation of soluble proteins. From such considerations, it is not surprising that the nature of both protein and lipid, the lipid to protein ratio, detergent concentration, temperature, pH and ionic strength are generally the most essential parameters in the 2D crystallisation of membrane proteins. However, the chosen LPR and the speed of detergent removal are critical. With an excess of lipid over protein, the protein is mainly incorporated into liposomes, similar to its native state. For crystal packing, the LPR must be as low as possible to ensure closing packing. However, an

excess of protein over lipid can also produce amorphous aggregates. Additionally, slow detergent removal results in the formation of large flat 2D crystals. Those crystals are often composed of a stack of 2D crystalline lamellae, which hampers the collection of images by EM and thus the construction of a 3D map of the MP. In contrast to that, rapid detergent removal promotes the formation of much smaller unilamellar 2D crystals, which are much better for the collection of images by EM. In most cases, however, the detergents in use were non-ionic mild detergents, and very few exceptions were ionic detergents. This could be related not to a crystallisation difficulty but to the fact that mild detergent with long alkyl chains and bulky head groups are advantageous for purifying and maintaining the activity of the protein, as compared to harsher ionic detergents. There are different strategies for detergent removal: dialysis is the most common used technique in 2D crystallisation trials (chapter 2, paragraph 2.2.11). The method of detergent removal by hydrophobic adsorption onto polystyrene beads is very efficient for proteoliposome reconstitution (Rigaud *et al.,* 1995; Lévy *et al.,* 1990). It has been demonstrated to be a powerful alternative to conventional dialysis for 2D crystallisation trials (Rigaud *et al.,* 1997). Another important advantage in the use of polystyrene beads was the possibility to vary and control the rate of detergent removal by controlling the amount of beads. This has been demonstrated to allow a possible identification and control of parameters critical to the formation of proteoliposomes (Rigaud *et al.,* 1997) and 2D crystals (Rigaud *et al.,* 1998; Lacapère *et al.,* 1998). The disadvantage of this technique is the difficulty in quantification of very small amounts of beads that would be needed for very slow detergent removal rates, comparable to those encountered in dialysis trials. 2D crystals of MPs can be produced by the induction of regular packing of a highly abundant MP in its native lipid bilayers. This can be achieved by incubating the isolated membranes with phospholipase A2 to remove excess lipids (Rigaud *et al.,* 2000). Reviews on 2D crystallisation of MPs are given by Kühlbrandt, Hasler and Rigaud (Kühlbrandt *et al.,* 1992; Hasler *et al.,* 1998; Rigaud *et al.,* 2000).

1.1.4 Atomic force microscopy (AFM) and Single molecule force spectroscopy (SMFS)

Atomic force microscopy and single molecule force spectroscopy are tools for imaging and manipulating membrane proteins in their native state. Images of native MPs have been recorded, enabling a quantitative interpretation of the data acquired. SMFS has been particularly successful to quantify the interactions and energies established between and within membrane proteins. Applied to membrane protein, SMFS provides a detailed insight into the nature of these interactions and, more importantly, locates and quantifies these interactions with an accuracy of ~ 4 AAs. Atomic force microscopes (AFMs) are tools to

address the surface structure and mechanics of single membrane proteins in their native environment, embedded in the lipid bilayer. Since some MPs are unstable when extracted by detergents, they are immersed in a physiological salt solution (Engel *et al.,* 2000) for solubilisation and purification and hence they are not accessible to NMR or X-ray crystallography. Not only are the surface structure, the supramolecular arrangement and the lateral organisation of the proteins revealed, but moreover individual proteins may be addressed and investigated in greater detail. They may be contacted by the AFM tip and subsequently extracted from the membrane (Oesterhelt *et al.,* 2000). The forces that keep the protein in the membrane as well as those that resist unfolding of the protein may thus be studied with unparalleled resolution and sensitivity (Kedrov *et al.,* 2007). The unfolding barriers may be localised in the sequence with an accuracy of a few amino acids, and the folding energy landscape can be analysed both in magnitude and in the dynamics of the response. The binding of individual ligands may be visualised and the alterations in the mechanics of the proteins may be detected and localised, again with the precision of a few amino acids. Not only unfolding processes may be followed, but also controlled refolding of the proteins into the membrane can be achieved. The unfolded polypeptide chain is gradually allowed to sink back into the membrane while the force at which it is pulled into its native environment is recorded. Unbalanced aspects of such folding/ unfolding cycles reveal details on kinetics and dynamics of the underlying processes. Images of rhodopsin (Müller *et al.,* 1995), photosynthetic membranes (Scheuring *et al.,* 2006) and mitochondrial outer membranes (Hoogenboom *et al.,* 2007) are detected by AFM. Membrane protein conformational changes induced by altering either the voltage or the pH were studied by SMFS (Damaghi *et al.,* 2010).

1.1.5 Solution and solid-state NMR

Solution NMR, as a method for protein and nucleic acid structure determination, has considerable impact, especially for smaller proteins or molecules with partially disordered regions that have inhibited crystallisation attempts. However, NMR of membrane proteins has been difficult. First, the surrounding detergent micelle frequently doubles the effective size of the protein so that the tumbling rate is lower and therefore the width of the spectral peaks is larger. The need for sharper spectral peaks is usually tackled by using an elevated temperature to increase the tumbling rate, but this is inapplicable for membrane proteins due to their thermal instability, particularly in the smaller detergents that make smaller micelles. Second, the chemical shifts for α-helical residues are concentrated in a smaller region of the spectrum so that peaks often overlap, increasing even more the need for sharper peaks. In contrast, β-barrel structures have proved to be easier to solve by NMR because of the

greater spectral dispersion. When embedded in lipid bilayers, membrane proteins are not amenable to solution NMR techniques since the tumbling of those systems is slow and highly anisotropic, which leads to unfavourable relaxation and hence very broad resonance lines. An alternative approach is the use of MPs in detergent or lipid micelles, which tumble fast enough on the NMR time-scale. In combination with the use of perdeuterated ^{13}C,^{15}N-labelled samples and TROSY-based triple resonance techniques, spectra of detergent solubilised MPs with reasonable line widths can be obtained by solution NMR (Liang & Tamm, 2006; Poget *et al.,* 2007). Complete or nearly complete backbone assignments have been obtained for several β-barrel MPs, e.g. for four α-helical MPs, outer membrane protein G (OmpG), PagP from *E. coli,* mistic from *Bacillus subtilis,* human pentameric phospholamban (PLB) and outer membrane protein X (Liang *et al.,* 2007; Oxenoid and Chou, 2005; Fernández *et al.,* 2004, Roosild *et al.,* 2005, Hwang and Kay, 2005).

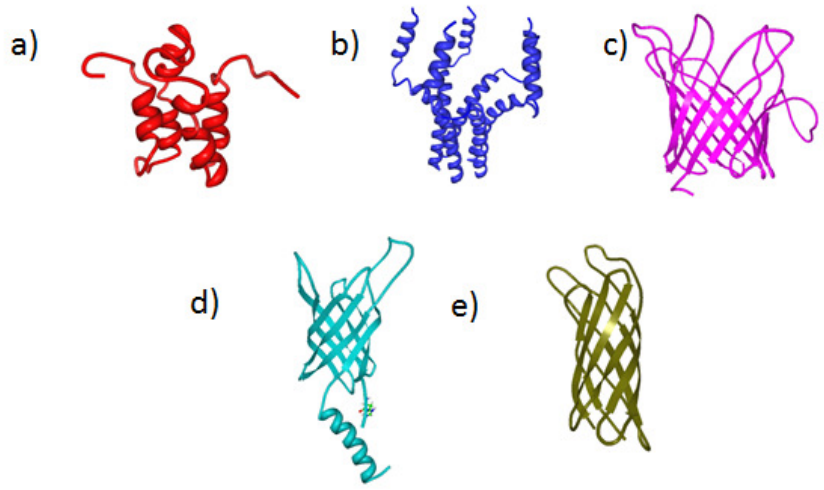

Figure 1.3 Solution NMR structures of MPs in detergent micelles. (a) Mistic (PDB code 1YGM), (b) Phospholamban (PDB code 1ZLL), (c) OmpG (PDB code 2JQY), (d) PagP (PDB code 1MM5) and (e) OmpX (PDB code 1Q9F).

Solid-state NMR (ssNMR) is an atomic-resolution spectroscopy used to study the structure and dynamics of molecules without isotropic mobility. The systems amenable to ssNMR include not only rigid solids but also anisotropically mobile molecules such as lipid membranes. Thus, membrane proteins, which have no long-range order and often exhibit anisotropic mobility, are ideal for ssNMR-based structure determination. Importantly, ssNMR allows membrane proteins to be studied in phospholipid bilayers, which represent biological membranes much more realistically than detergents do. SsNMR yields three-dimensional structural constraints by exploiting the interactions of nuclear spin magnetic moments with

static magnetic and radiofrequency fields and by detecting the effects of structurally sensitive nuclear spin interactions such as chemical shielding, dipolar coupling and quadrupolar coupling in the NMR spectra. Although these fundamental aspects of ssNMR are the same as solution NMR, ssNMR has the advantages of fully detecting the orientational dependence of these nuclear spin interactions to give precise information about protein orientation and dynamics. There are two major ssNMR approaches for studying membrane protein structures. The first involves orientational restraints of membrane-integrated peptides or proteins which derived from dipolar coupling and chemical shift measurements, so-called PISEMA experiments (Wu *et al.,* 1994). To align lipid bilayers on glass plates, lipids are dissolved in organic solvents followed by evaporation and lipid hydration (Opella and Marassi, 2004). Using this technique, structures of membrane-embedded peptides, for example Gramicidin, the M2 transmembrane segment of the nAChR, the M2 transmembrane domain from the M2 proton channel of the influenza A viral coat, the M6 transmembrane domain of the α-factor receptor from *Saccharomyces cerevisiae*, the Fd bacteriophage coat protein and the M2 transmembrane domain of the HI virus protein U (Vpu) were solved by solid-state NMR (figure 1.4 b-g) (Opella and Marassi, 2004).

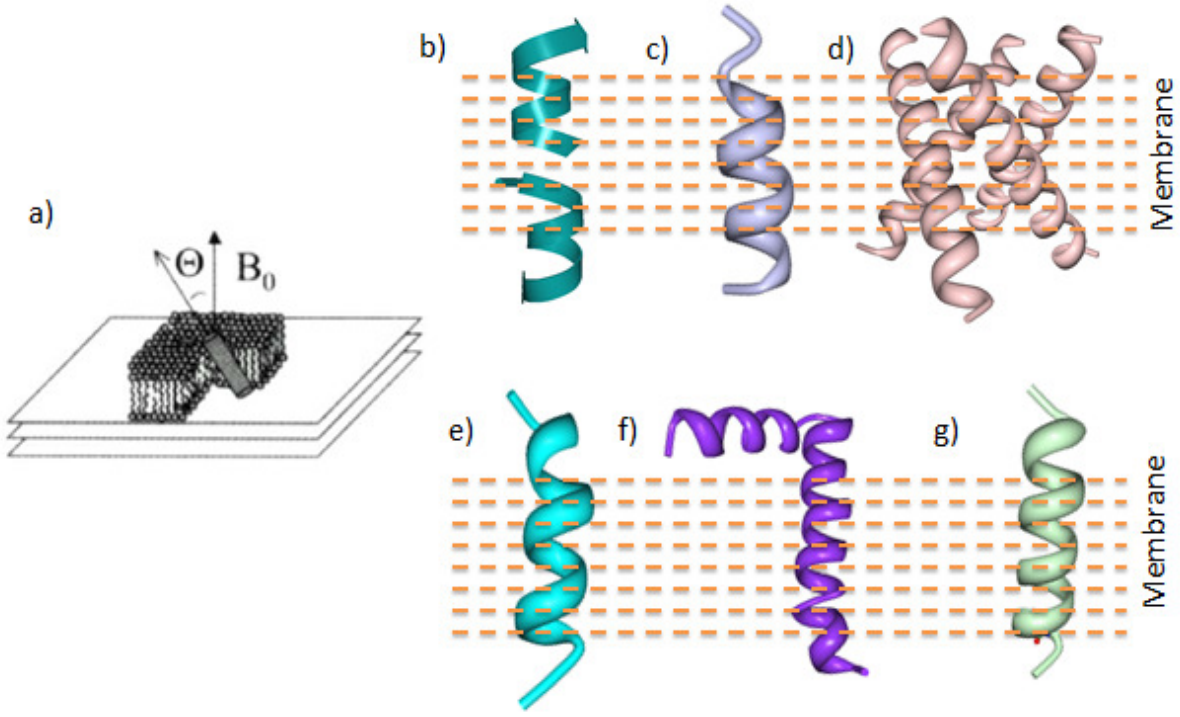

Figure 1.4 Structures determined by solid-state NMR in oriented lipid bilayers. a) Oriented lipid bilayers put on solid glass plates (Lange *et al.,* 2006). b) Gramicidin (PDB code 1MAG), c) the M2 segment of the nAChR (PDB code 1CEK), d) the closing-state structure of M2 proton channel (PDB code 1NYJ), e) the 6th transmembrane domain of the α-factor receptor (PDB code 1PJD), f) the Fd bacteriophage coat protein (PDB code 1MZT) g) the virus protein U (PDB code 1PJE) from the HIV-1 (Opella and Marassi, 2004).

The second ssNMR approach for studying membrane protein structures involves magic angle spinning (MAS) of the samples to obtain high-resolution spectra that reflect isotropic chemical shifts as well as recoupled, orientation-dependent (anisotropic), dipolar couplings and chemical shift anisotropy. MAS NMR provides a diverse array of structural information such as inter-atomic distances, backbone torsion angles, side chain conformations, and motional amplitudes and timescales. In the past ten years, solid-state MAS NMR underwent a rapid development in which a suite of 2D, 3D and 4D correlation techniques was invented to determine the full 3D structures of proteins (McDermott *et al.,* 2009). This development coincided with increasingly sophisticated molecular biology and biochemical methods to express, isotopically label and reconstitute proteins into lipid bilayers. These innovations resulted in the structure determination of ion channels and membrane-bound enzymes as well as non-membrane-associated globular proteins (McDermott *et al.,* 2004) and amyloid fibrils (Tycko, 2011). These MAS correlation techniques also stimulated site-specific studies of ligand binding to large membrane proteins such as G protein-coupled receptors (GPCRs; Smith *et al.,* 2010). In MAS NMR a randomly oriented sample rapidly spins around the so-called magic angle (θ=54.7°) in the static magnetic field (B_0). MAS, applied to randomly oriented samples, produces sufficiently resolved spectra and allows the detection of isotropic chemical shifts. This has important advantages for structural investigations by solid-state MAS NMR. To identify amino acids by their characteristic chemical shift pattern, well-established strategies for resonance assignment, known from solution NMR, can be implemented and chemical shift databases, compiled from solution NMR studies, can be accessed. The value of both (PISEMA and MAS) depends on the relative alignment of the molecule to the magnetic field (B_0). Additionally, bicelles have also been used to study aligned MPs by solid-state NMR (Nevzorov *et al.,* 2004; Sanders and Landis, 1995). Thus, solid-state MAS NMR spectra of solid protein preparations of soluble proteins, e.g. the α-spectrin SH3 domain (Pauli *et al.,* 2000 – Pauli *et al.,* 2001), amyloid fibrils systems, e.g. the Alzheimer β-amyloid fibrils (Petkova *et al.,* 2006) and MP-bound ligands, e.g. kaliotoxin bound to the KcsA - Kv 1.3 channel (Lange *et al.* 2006), have been fully or partially assigned. These studies were performed with numerous different sample preparations.

The lyophilised α-spectrin SH3 domain does not provide as sufficient a resolution as the microcrystalline ammonium-sulphate (Pauli *et al.,* 2000). The conformation of the side chains will be quite variable and each protein is in a different environment although the proteins might be properly folded in a lyophilised powder. Each molecule will then have a slightly different chemical shift for each side chain atom. Martin and Zilm (2003) show that nano-crystalline material far too small to be useful in X-ray diffraction studies is suitable for structural studies by solid-state MAS NMR. Solid-state MAS experiments have been carried out on lyophilised amyloid fibrils (Petkova *et al.,* 2002) and on fully hydrated amyloid fibrils

(Ferguson *et al.,* 2006*;* Heise *et al.,* 2005), but also by rehydrating the fibrils after lyophilisation (Petkova *et al.,* 2006). Hydrated samples exhibit narrower line widths, in particular for side chain resonances. The inhomogeneous broadening arising from static disorder in lyophilised samples is averaged out by molecular motions in hydrated samples (Tycko, 2006). The high spectral resolution of a ligand bound to a receptor or channel can be attributed to the defined ligand binding pocket (Lange *et al.* 2006). All these studies illustrate that solid-state MAS NMR requires homogeneous samples with a local order, although not necessarily as highly ordered crystalline samples as required for X-ray crystallography.

SsNMR experiments on MPs can theoretically be performed with numerous different sample preparation types, for example detergent solubilised MPs or nano-crystalline material originating from 3D crystallisation screens. MPs reconstituted into lipid bilayers (proteoliposomes) or 2D crystals allow the structural investigation of MPs in a near-native environment.

1.2 Basic elements for nuclear magnetic resonance

The Nuclear Magnetic Resonance (NMR) spectroscopy is an instrumental analytical technique that allows obtaining detailed information on the molecular structure of the test compounds. The NMR spectroscopy measures the absorption of electromagnetic radiation of radio frequency in molecules immersed in a strong magnetic field. This radiation causes the nuclear spin transitions in particular atoms (typically ^{1}H or ^{13}C). With NMR spectroscopy, information on the molecular structure is inferred from observing the behaviour of atomic nuclei. With the NMR technique, only the nuclei which possess a nuclear magnetic moment of spin are observable. They behave like the needle of a compass which can be orientated in an applied magnetic field. The nuclear magnetic moment of spin m is given by

$$\mu = \gamma I \frac{h}{2\pi}$$

where γ is the gyromagnetic ratio, I is the nuclear spin quantum number, h is Planck's constant. The nuclear spin is produced by the particles that make up the nucleus, protons and neutrons. These are in rotation (spin) around their axis and have spin 1/2. In many atoms (as in ^{12}C) all the spins are paired in opposition to each other, cancelling each other out. In this case, the atomic nucleus has a spin result I equal to zero. In some atoms (as in ^{1}H and ^{13}C) the nucleus has a spin with a result other than zero. The rules to determine the nuclear spin can be summarised as follows:

1) If protons and neutrons are both even, then the nucleus has spin zero.

2) If either protons or neutrons are equal to one and the other is odd, then the nucleus has spin half full (1/2, 3/2, 5/2... that is 1/2 + n) (spin 1/2 of the decoupled nucleon plus their orbitalic contribution).

3) If both are odd, then the nucleus has spin of any positive integer value (1, 2, 3... that is 1 + n) (1 spin of the two decoupled nucleons 1/2 + 1/2, plus their orbitalic contribution). Counted among the first case are ^{12}C and ^{16}O that have I=0 and therefore have no magnetic moment of spin and are not observable in NMR. Counted among the second case are ^{1}H, ^{13}C, ^{15}N, ^{19}F, ^{31}P that have I = 1/2 and therefore are observable in NMR. Counted among the third case are ^{2}H and ^{14}N which have I = 1, which are therefore also observable in NMR. When a nucleus with spin is immersed in a magnetic field, the core, like the needle of a compass, is subjected to a force couple, which makes it rotate to align with the external magnetic field. The possible orientations that the core can assume in a magnetic field are governed by the quantum number m which can take values from -I to +I (in increments of one unit). It therefore can assume 2I + 1 different values. In case of a nucleus with spin 1/2 (like ^{1}H) there are 2 possible orientations: one with m = –1/2 and one with m = +1/2. The nuclear magnetic moment m does not remain stationary, but continues to oscillate around the direction of the applied magnetic field B_0 making a precession motion similar to that of a spinning top (see figure 1.5).

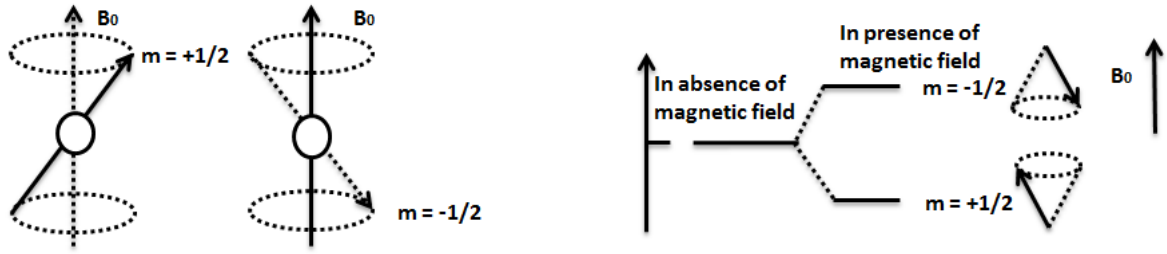

Figure 1.5 The two possible states of the nucleus. They have not the same energy, but the state with m = +1/2 (aligned with the field) is located to energy slightly lower than that with m = –1/2 (opposite to the field).

The precession of nuclear magnetic moments takes place with a frequency proportional to the energy difference between the two levels, said Larmor frequency, given by the formula:

$$\vartheta 0 = -\gamma \frac{B0}{2\pi} \text{ (in Hertz)}$$

where γ is the gyromagnetic ratio which depends on the nucleus in question. With increasing applied field B_0, the Larmor frequency and thus the energy difference between the two levels increases. However, since the energy difference between the two levels is very small, of the

dimension of 910.6 kcal mol^{-1}, the population of nuclei in the two states is almost identical with a very small prominence for the state at low energy, in line with the field. In the case of the hydrogen nuclei ^1H, at room temperature, in a magnetic field of 1.41 Tesla (n (^1H) = 60 MHz), there is one additional nucleus in the state of low energy every two hundred thousand cores. In a field of 7.05 Tesla (300 MHz) there are five additional nuclei in the state of low energy every two hundred thousand nuclei (figure 1.6). Yet it is precisely these few excess nuclei aligned with the magnetic field B_0 that allow generating the NMR signal. With a more intense magnetic field (7.05 T) there is a greater difference in energy between the levels, a higher Larmor frequency (300 MHz), a greater number of nuclei more aligned with the field (five out of 200.000) and thus a greater sensitivity in the analysis of e.g. ^1H NMR.

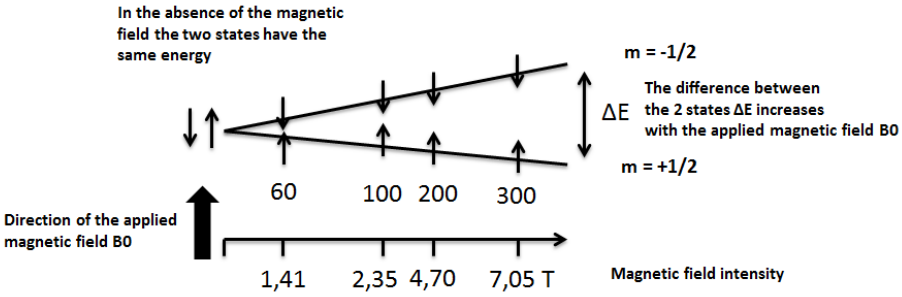

Figure 1.6 The difference between the two states ΔE versus the magnetic field B_0.

If the sample is irradiated with an electromagnetic radiation of frequency equal to the Larmor frequency, there is an interaction of the magnetic component of the radiation with the nuclear magnetic moments (these also oscillate at the Larmor frequency). The radiation energy can thus be transferred to the nuclei. All absorption of radiation leads to a change of orientation of the nuclear spin that rotate aligned with the field but in the opposite direction. When this spin transition occurs, it is said that the nuclei are in resonance with the applied radiation, hence the name nuclear magnetic resonance, NMR. In this case, in the state of maximum excitation, the population of nuclei in the two levels is approximately equal, given the very small energy difference between the levels. The excited state is only slightly more populated than the fundamental state with a reversed ratio of populations. In the first tools, NMR analysis was performed by irradiating the sample immersed in magnetic B_0 with a beam of radio waves of gradually increased frequency, in such a way as to excite in sequence all the nuclei in question to then record the amount of radiation absorbed. This technique was very slow and does not find any application anymore. In modern instruments FT-NMR signals are generated by the impulse method and Fourier transform. With this technique all nuclei of a species are excited simultaneously by a pulse of radio frequency which contains the entire range of frequencies necessary. The data are then processed to the computer using the technique of Fourier transform. To understand how the pulse of radiofrequency interacts with

the nuclei in question it is necessary to introduce a vector called macroscopic magnetisation M_0 which is the result of all nuclear magnetic moments. Given that there is a slight excess of nuclei that are aligned with the magnetic field B_0, M_0 is small and the vector aligned with the field. The direction of the magnetic field B_0 is called z-axis direction.

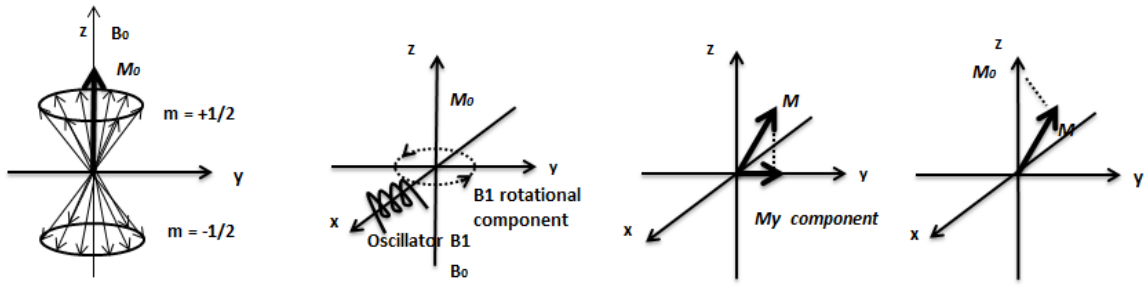

Figure 1.7 M_0 precession.

If now the sample is irradiated along the x-axis with a pulse of radiofrequency which contains also the Larmor frequency of the nuclei n under consideration (e.g.^{1}H), they absorb energy and undergo a transition of spin. At the macroscopic level it can be observed that the magnetisation vector macroscopic M_0 rotates from the z-axis to get closingr to the xy-plane starting a precession motion around the z-axis. At this point the pulse of radiofrequency emitted by the oscillator B1 stops along the x-axis, but the excited nuclei will continue to precess for a while until the weak signal frequency goes off in time, a kind of echo of the absorbed signal. To record this signal, a receiving circuit is placed along the y-axis. It has the purpose of measuring the oscillation, or the y component, of the vector *M*. The energy absorbed by nuclei is slowly transferred to the neighbouring atoms due to the phenomena of spin-lattice relaxation (with the dipoles of the surrounding molecules), which affects the component M_z, and of spin-spin (with the nuclei of hydrogen neighbours), which affects the component M_y. Due to this energy dissipation, the vector *M*, precession-spiralling around the z-axis, returns to the initial value M_0, a position for which the component M_y is nil (figure 1.7). The time required to recover the magnetisation M_z is 66 %. It is called relaxation time T1 and has a duration of about one second. In medicine, spin-lattice relaxation time T1 is indicative of the tissue in which is immersed the core under consideration. The duration t(i) of radio frequency pulses must be determined with precision in order to produce a strong NMR signal. If t(i) is such as to bend M_0 to 90°, then it produces the maximum of carrier M_y. In general, t(i) is a few microseconds long. The collected signal is an oscillating signal with a frequency n, the Larmor frequency of the nucleus in question, which fades over time. This is called free induction decay (FID).

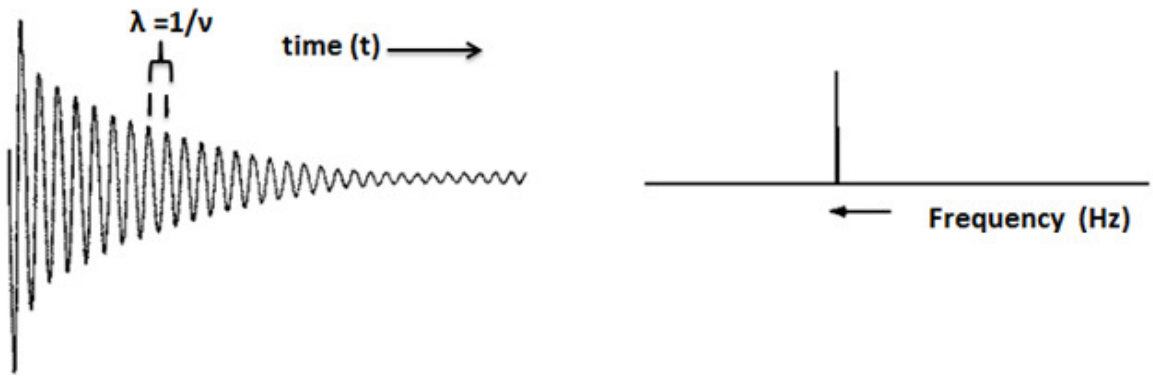

Figure 1.8 FID and Fourier transformed NMR.

In the figure 1.8 this frequency can be easily identified by measuring the wavelength (the distance between two successive crests and which represents the period of T wave) and by applying the formula:

$$\vartheta = \frac{1}{\lambda}$$

where ϑ is the frequency and λ the wavelength. From figure 1.8 as a function of time, the FID, it is possible to obtain a new graph as a function of frequencies, called NMR spectrum. If the sample contains nuclei with different resonance frequencies, these are all simultaneously excited by the impulse of radiofrequency and thus the signal FID is a complex curve, called interferogram, given by the combination of more FID samples, one for each frequency absorbed by nuclei. To be able to trace the individual frequencies which, combined with each other, have generated the FID complex, it is necessary to apply a mathematical procedure called Fourier transform. It allows passing from the graph as a function of time (the FID) to the graph as a function of frequency (the NMR spectrum). These informations were taken from Tonellato's booklet INTRODUZIONE ALLA SPETTROSCOPIA NMR.

1.2.1 Solid-state NMR

To understand why the NMR spectra of samples in solution and samples in the solid state have different widths of the spectral peaks, it is necessary to examine the individual interactions which makes the NMR signal rise (figure 1.9). The dipolar interaction is a direct interaction between nuclei. The chemical shift interaction is an indirect interaction (through electrons) between the static magnetic field (B_0) and nuclei.

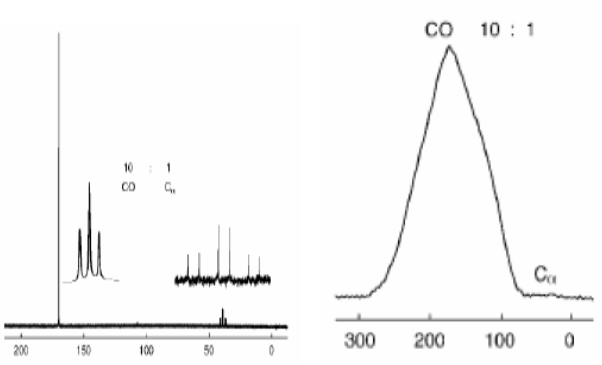

Figure 1.9 ^{13}C Spectrum of carbonyl region of Glycine in water solution (10mM) on the left and 90 mg of powder on the right (the figure was taken from: Manual solid state NMR - Minoia).

The scalar interaction J is an indirect interaction among the nuclei (through bonding electrons). The quadrupolar interaction is an interaction of the nuclei with field electric (only if the spins > ½). Some of those interactions depend from the spin orientation (figure 1.10).

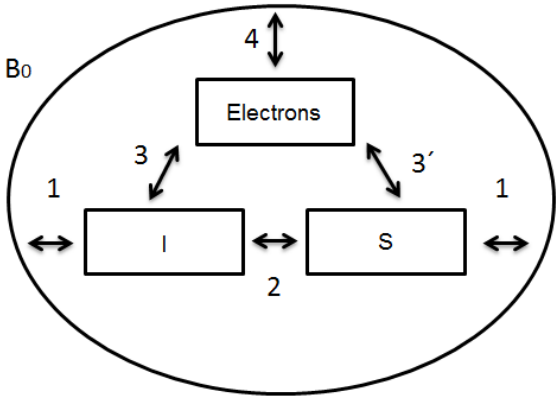

Figure 1.10 Different interactions in solid-state NMR. 1 Zeeman interaction, 2 dipolar interactions, 3-3' interaction J coupling, 3 interaction quadruple, 3–4 chemical shift. I and S are two different nuclei.

In solution, the Brownian motions, which are subject molecules, mediate the nuclei interaction with a static magnetic field (Zeeman interaction). The dipolar interaction in solution state is due to the molecular motions which mediate the non-isotropic components to 0. The chemical shift interaction in solution state is due to the average molecular motion in an isotropic value (chemical shift isotropy). In solid state the lack of motion (it has an influence on the spectral width) prevents this average, so there is chemical shift anisotropy. The scalar coupling (J coupling) is independent from the molecular motion, therefore there is no difference between solid and solution state. There are two alternatives to reduce the width of the spectral peak in solid-state NMR. The first is to take advantage of more information

given by CSA, the second is the use of dipolar (and quadruple) coupling to eliminate the unwanted effects, thus simplifying the reading of the measures and giving us back as much information as possible in the spectra of the liquid type. To obtain more narrow lines in NMR spectra, solid state spectra are generally acquired using MAS. The dipolar interaction, scalar interaction and chemical shift anisotropy have the same angular dependence: $3\cos^2(\theta)-1$ is the angle between the magnetic field and the internuclear vector. In a powder there are endless orientations for the same interaction. Rotating faster at an angle of θ = 54.7 reduces or eliminates these interactions. In this case side bands will be generated. To obtain a spectrum without spinning side bands requires that the speed of rotation is at least equal to the entity of the interaction to mediate. The current instrumentation allows up to 70 kHz; although most commonly the maximum speed of rotation is 15 kHz. This means that using MAS is hardly possible to mediate homonuclear proton dipolar interaction, while the technique is effective in reducing and/ or eliminating the scalar, CSA and heteronuclear dipolar interactions.

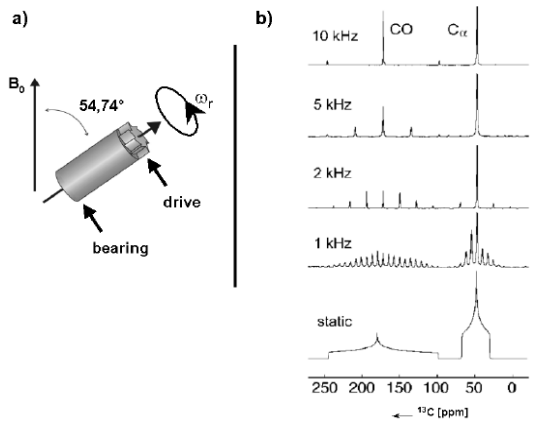

Figure 1.11 The solid-state MAS NMR technique. a) The rotor that contains the sample is tilted at 54.74°. By the combined application of bearing and driving pressures, the sample rotates around itself at the desired frequency. b) Solid-state MAS ^{13}C-NMR spectra of uniformly ^{13}C-labelled glycine powder sample at different spinning speeds. The figure was taken from Laws (Laws *et al.,* 2000).

1.2.2 Basic solid-state MAS NMR techniques

In solution NMR, the dipolar and *J*-couplings between ^{1}H spins in the molecule are used to define the structure. Low-γ nuclear spins, such as ^{13}C and ^{15}N, are employed to increase resolution of overlapping ^{1}H resonances, using multidimensional techniques. Protons do not only have a high gyromagnetic ratio but also high natural abundance. In an NMR experiment the sensitivity, or signal-to-noise ratio (S/ N), depends on both these parameters and, of all naturally occurring nuclei, the proton has the best sensitivity. In MAS NMR structural details

are primarily obtained from low-γ and dilute I=1/2 spins (^{13}C and ^{15}N). Protons are generally not the observed nuclei because they form a strongly dipolar coupled network of spins. In MAS solid-state NMR experiments the detection of low abundance ^{13}C and ^{15}N nuclei usually requires isotope labelling for sensitivity enhancement. To further increase the sensitivity and resolution of solid-state spectra, MAS is combined with high-power proton decoupling (Bloch *et al.,* 1958) and cross-polarisation (CP) (Pines *et al.,* 1972; Schaefer *et al.,* 1976). ^{1}H-decoupling is necessary to eliminate residual ^{1}H-^{13}C dipolar couplings and ^{1}H-^{13}C residual *J*-couplings under MAS. The decoupling is carried out analogically to the decoupling scale in solution although the size of the interactions is very different, making it necessary to use high powers. The dipolar constant can be up to 100 kHz. The simplest decoupling method involves continuous irradiation with Rf pulses of a fixed phase during the acquisition of the FID and is termed continuous wave (CW) decoupling (Bloch *et al.,* 1958). More sophisticated methods based on rapid phase switching, such as the TPPM (two-pulse phase modulation) or small phase incremental alternation (SPINAL) technique, have been introduced, which significantly improve the decoupling efficiency (Bennett *et al.,* 1995). The effects of the heteronuclear dipolar coupling are eliminated by the induction of transitions between the two states of hydrogen of a much higher frequency than that of the entity of the interaction: $\sqrt{}_{CH}$ ~ 30 kHz $\gamma_H B1_{DEC}$ ~ 100 kHz. At a pulse of 2.5 ms and hundreds of Watts the interaction cannot evolve. The decoupling is done with a single high power pulse, the high dipolar coupling ^{1}H-^{1}H therefore allows to transfer the decoupling to all hydrogens. The decoupling has no effect on the broadening of the signals due to CSA or a homonuclear dipolar interaction. Since the line width of the ^{13}C signal mainly depends on the heteronuclear dipolar interaction with less abundant nuclei, it is possible to get either a reduced or an enhanced signal. In ^{13}C or ^{15}N MAS spectra, CP between protons and low-γ nuclear spins can be used to greatly enhance the signal intensity (Pines *et al.,* 1972; Schaefer *et al.,* 1976). In a CP experiment, the field strengths in the rotating frame are set to the Hartmann-Hahn condition, as depicted in figure 1.12. Cross polarisation, in which magnetisation is transferred from abundant, high gyromagnetic-ratio nuclei to rare, low gyromagnetic-ratio nuclei via the dipolar couplings (Pines *et al.,* 1972), is a nearly ubiquitous procedure in solid-state NMR experiments. In practice, CP is most useful under magic angle spinning (Schaefer *et al.,* 1976), where it is well known that the cross polarisation intensity is modulated by the spinning frequency, giving rise to a sideband pattern where $|\omega_1 S \pm \omega_1 I| = n \omega r$, where $\omega_1 S$ and $\omega_1 I$ are the radio frequency fields applied to the *S* and *I* spins, and ω_r is the spinning frequency. At the magic angle, the $n = \pm 1$ and $n = \pm 2$ conditions dominate the matching profile and the center band is suppressed (Wind *et al.,* 1988; Wu *et al.,* 1993). The standard pulse programme of a CP experiment starts with a ^{1}H excitation 90° pulse (bringing the proton magnetisation into the xy-plane) where magnetisation is transferred from protons

to the low frequency channel (e.g. ^{13}C) by the matched pair of CP pulses. In the presence of molecular motion or with increasing spinning speed, problems in establishing and maintaining the Hartmann–Hahn matching condition can be encountered. The signal enhancement resulting from CP is due to two factors. First, the larger gyromagnetic ratio of protons (e.g. γH is four times larger than γC) creates a larger ^{1}H polarisation which is transferred to the low-γ nucleus. Second, the repetition time of the experiment is determined by the shorter ^{1}H relaxation time in relation to low-γ spins. Hence the experiment repetition rate can be increased. For typical ^{1}H-^{13}C CP experiments these two factors can easily result in a tenfold increase in sensitivity.

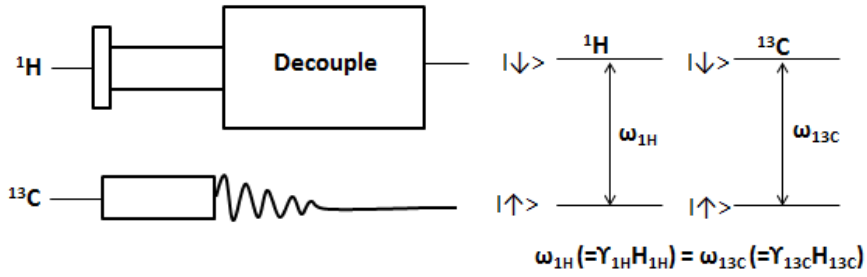

Figure 1.12 A simple 1D ^{13}C/CP MAS pulse sequence (left) and Hartmann-Hahn matching (right). The classic Hartmann-Hahn matching condition for a non-spinning sample that allows transfer of polarisation from ^{1}H to low-γ nuclei such as ^{13}C. For a spinning sample, the MAS frequency has to be taken into account and the matching condition becomes: $\omega^{1}H-\omega^{13}C = \pm n\,\omega r$.

1.2.2.1 Spin diffusion

Dipolar coupled spins exchange longitudinal magnetisation, which is therefore distributed among the coupled spins in a spin system. This process is termed spin diffusion. Under MAS it is generally attenuated and does not occur among ^{13}C or ^{15}N nuclei as their dipolar couplings are, on average, zero. However, strong couplings to a proton spin network broaden the signals of low γ nuclei and enable the exchange of magnetisation in an energy conserving way. This process is referred to as proton-driven spin diffusion (figure 1.13) (Szeverenyi *et al.,* 1982). By irradiating the protons at the rotary resonance condition (one or two times the MAS frequency) the magnetisation exchange can be accelerated. This technique is referred to as dipolar-assisted rotational resonance (Takegoshi *et al.,* 2001). The efficiency of the magnetisation transfer depends on the distance of the nuclei involved and can be used to correlate nuclei which are closed in space (e.g. up to 7–8 Å for ^{13}C). In figure 1.13 the pulse sequence of the standard 2D PDSD experiment is shown. The advantages of this technique are its robustness owing to its simplicity and aptness to be

implemented for very long mixing times. The main idea of this methodology for structure determination of proteins by solid-state MAS is based on the collection of a large amount of approximate distance restraints from spin diffusion experiments, in combination with extensive but reduced ^{13}C labelling. The dilute labelling is used to suppress dipolar truncation effects. In the PDSD magnetisation is transferred from hydrogen to ^{13}C nuclei. From here it is transferred to other ^{13}C nuclei which are closing in space. As the name of the experiment indicates, protons are involved in this transfer.

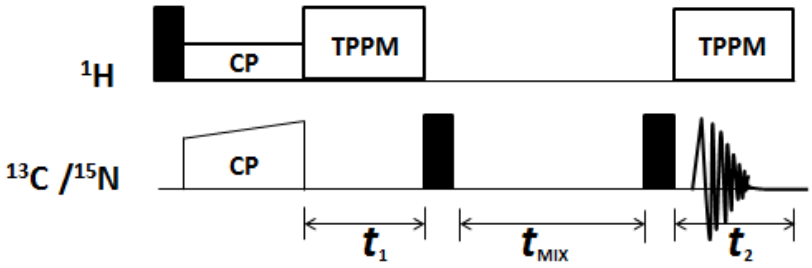

Figure 1.13 Pulse programme of a standard 2D homonuclear PDSD dipolar correlation experiment, applicable in the case of ^{13}C-^{13}C spectra. Following ^{1}H excitation, a ramped cross-polarisation between ^{1}H and ^{15}N or ^{13}C creates the initial ^{15}N/^{13}C magnetisation. Following the nitrogen or carbon evolution, a 90° pulse on the low-γ nucleus brings back the magnetisation along the z-axis. During the mixing time *t*MIX, proton decoupling is switched off and the polarisation transfer between ^{15}N or ^{13}C spins occur in the presence of ^{1}H-^{1}H and ^{1}H-^{15}N (or ^{1}H-^{13}C) dipolar couplings. During all evolution periods, proton decoupling is applied, using the two-pulse phase modulation technique (TPPM).

1.2.2.2 Recoupling techniques

The anisotropic interactions occurring in the solid state are averaged out by rapid MAS. However, these interactions contain valuable structural and dynamic information. This information can be brought back by employing recoupling methods to recover the anisotropic interactions lost during MAS. Different techniques have been developed for recoupling dipolar interactions, which function by the application of Rf pulses to counterbalance the effect of the sample rotation. These techniques can be separated in two general categories: techniques that recouple dipolar couplings between like spins, including RFDR (Bennett *et al.,* 1992) and techniques that measure dipolar couplings between unlike spins, for example REDOR (Gullion & Schaefer; 1989) and TEDOR (Hing *et al.,* 1992).

1.2.2.3 Assignment of solid-state MAS NMR spectra

The application of homonuclear dipolar correlation spectroscopy on uniformly ^{13}C labelled systems is important for assignment strategies in solid-state NMR. ^{13}C-homonuclear correlation experiments are used for the identification of amino acid side chains. To obtain site-specific information from NMR spectra, the observed isotropic chemical shifts have to be assigned to the nuclei in the protein. In solid-state MAS NMR spectroscopy complete assignment of small proteins has become possible only during the last decade, and is still not routine.

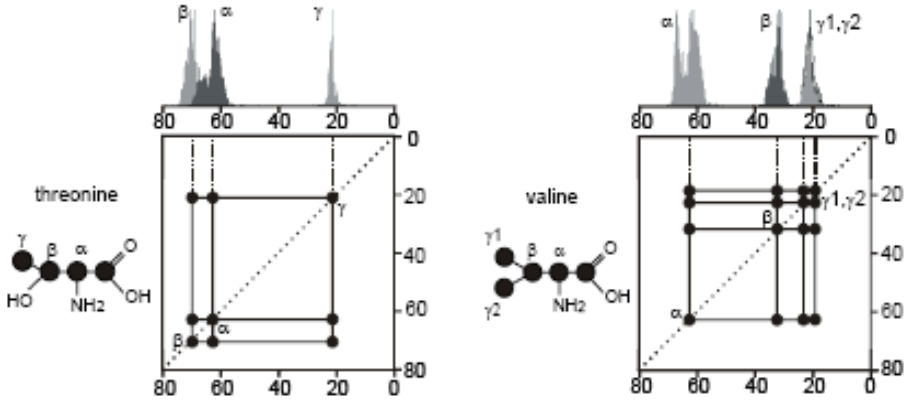

Figure 1.14 Illustration of the assignment of amino acid types in a protein. The illustrated schematic ^{13}C-^{13}C spectrum shows the typical correlation patterns of the amino acids alanine and threonine. The averaged chemical shift values for the C', Cα, Cβ and Cγ carbon atoms were taken from the BioMagResBank (BMRB). The figure was taken from Castellani's dissertation 2003.

In order to assign the signals to specific amino acid types, the averaged chemical shift values of C', Cα, Cβ and Cγ carbon atoms from the BioMagResBank (BMRB) can be used. In the first step of the resonance assignment procedure, ^{13}C homonuclear correlation experiments are recorded on uniformly or selectively labelled proteins. In these spectra, amino acid side chains can be identified due to characteristic correlation patterns formed by correlated peaks, which resonate in well-defined regions of the spectrum. In the second step, the amino acid spin systems need to be linked sequentially into a chain, which can then be matched to the protein sequence to yield sequence-specific assignments. This can be achieved using heteronuclear [^{13}C, ^{15}N] correlation experiments that correlate the backbone nitrogen either to the neighbouring Cα carbon atom of the same residue (i) or to the carbonyl carbon atom of the previous one (i–1) (figure 1.15). These experiments are referred to as NCA and NCO, which can be further extended to provide links not only to the Cα and C' atoms, but also to

the whole side chain in so-called NCACX and NCOCX experiments (Pauli *et al.,* 2001). Using this assignment procedure, near full assignments have been obtained for a number of small soluble proteins and amyloid fibrils, like the α-spectrin SH3 domain, ubiquitin, the non-crystalline amyloid fibrils of the HET-s prion protein and the amyloid fibrils of human CA150 WW2 (Pauli *et al.,* 2001; Igumenova *et al.,* 2004*;* Becker *et al.,* 2008*;* Siemer *et al.,* 2006).

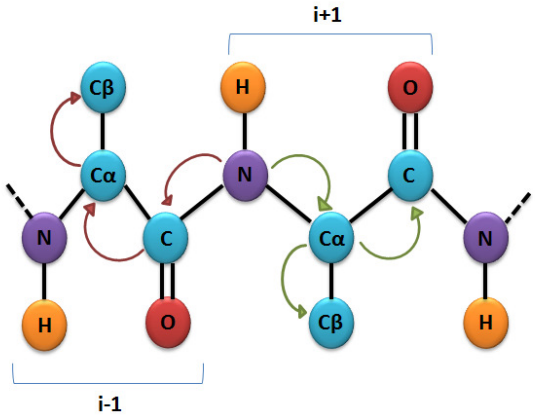

Figure 1.15 Illustration of the magnetisation transfer during an NCACX (green) and NCOCX (red) experiment. First, proton Rf fields are used to prepare ^{15}N polarisation via a broad band (^{1}H, ^{15}N) CP transfer. Second, a band selective ^{15}N-^{13}C CP step is used to transfer the magnetisation from ^{15}N to Cα or CO. Subsequently a ^{13}C-^{13}C PDSD mixing scheme can be used to transfer the magnetisation between Cα or CO and the side chain carbon atoms (CX).

1.3 Systems for membrane protein studies

The most commonly employed method to solubilise membrane proteins in aqueous solutions are micelle-forming detergent molecules (Prive, 2007), which are amphipathic molecules, consisting of a hydrophobic and a hydrophilic portion. At concentrations below their specific critical micellar concentration, molecules exist as detergent. Above the CMC, multimeric detergent micelles assemble that are in a highly dynamic equilibrium with detergent monomers. A large number of detergents with a wide range of chemico-physical properties are available. However, detergents are often not optimal for the activity and stability of a membrane protein (Tate *et al.,* 2010). Micelles are highly dynamic assemblies and their intrinsic instability can result in protein unfolding and aggregation. This is particularly problematic if the membrane proteins contain larger moieties that reach out into the aqueous extra-membranous space as detergents may destabilise or unfold those portions. Additionally, the lateral forces acting on a membrane protein in the roughly spherical detergent micelle are significantly different from those in the native planar membrane (van den Brink-van der Laan *et al.,* 2004; Cantor *et al.,* 1999). The search for a detergent that stabilises a functional conformation of a membrane protein is a highly empirical and time-consuming process.

1.3.1 Amphipols

One alternative to detergents are amphipathic polymers, abbreviated amphipols, which have been developed mainly by Jean-Luc Popot and colleagues (Breyton *et al.,* 2010). Amphipols consist of polymeric backbones that are covalently modified with a stochastic distribution of hydrophobic and hydrophilic groups. The use of amphipols as detergent-free membrane substitutes that conserve the membrane-protein function has been successfully shown in a number of cases, including the β-barrel proteins OmpA (Pocanschi *et al.,* 2006), FomA (Pocanschi *et al.,* 2006), and OmpX (Catoire *et al.,* 2010), as well as the α-helical protein diacylglycerol kinase (Gorzelle *et al.,* 2002), bacteriorhodopsin (Pocanschi *et al.,* 2006; Gohon *et al.,* 2008) and several G protein-coupled receptors (Dahmane *et al.,* 2009). The feasibility of studying amphipol-complexed membrane proteins by solution NMR spectroscopy has been demonstrated for the 171-residue transmembrane domain of the outer membrane protein A (tOmpA) (Zoonen *et al.,* 2005) and the outer membrane protein X (OmpX) from *E. coli* (Catoire *et al.,* 2010). A limitation of the currently mostly used amphipol A8–35 is its low solubility at acidic pH. Therefore, NMR studies using this amphipol are limited to a pH above 7, which can lead to exchange broadening and loss of signals from solvent exposed amide protons. Thus, amphipols that are pH-insensitive might be more suitable for NMR studies (Diab *et al.,* 2007).

1.3.2 Lipid bilayer systems

For many applications a membrane mimic comprising a lipid bilayer is preferable, as it may better maintain the structural integrity of a membrane protein. In the case of liposomes, the limited solubility, the formation of multilamellar vesicles and the inaccessibility of the vesicle interior may, however, interfere with functional investigations. Nevertheless, high resolution structural information of membrane proteins in liposomes may become accessible, predominantly by solid-state NMR techniques (Etzkorn *et al.,* 2010; McDermott *et al.,* 2009).

1.3.3 Bicelles

Bicelles are binary, water-soluble assemblies of lipids and detergents. The lipids form the central part and the detergents form the edge of a disc-shaped assembly so they can provide a roughly circular patch of a lipid bilayer in aqueous solution. There is a large distribution of shape, size and composition (Vold *et al.,* 1996). A disadvantage for their wide use in solution NMR experiments is their larger molecular weight compared to micelles, leading to broad

resonance lines. Recent reports have indicated that bicelle studies with NMR are well feasible (Poget *et al.,* 2008; Bocharov *et al.,* 2008). An example is given by the αII β3 integrin dimer, which consists of a lateral interaction of two transmembrane helices. This dimer is formed in bicelles, but not in micelles, and its structure could be determined by solution NMR in bicelles (Lau *et al.,* 2009). It was also shown that a β-barrel membrane protein in a bicelle is embedded in the central lipidic phase and is probably not in contact with the detergent surrounding the lipidic phase (Lee *et al.,* 2008). Limiting factors for bicelles include the constricted number of lipid-detergent combinations amenable to bicelle formation, their instability, and their size heterogeneity.

1.3.4 Nanolipoprotein particles

The introduction of nanolipoprotein particles, also referred to as nanodiscs or reconstituted high density lipoprotein particles (rHDLs), as membrane mimics has provided a novel tool for studying membrane proteins in a native-like membrane environment, a methodology pioneered by Stephen Sligar and colleagues (Bayburt *et al.,* 1998; Civjan *et al.,* 2003). NLPs consist of a non-covalent assembly of phospholipids arranged as a discoidal bilayer surrounded by amphipathic apolipoproteins. NLPs support protein stability and functionality of an incorporated membrane protein. The *in vitro* reconstitution of NLPs from purified lipids or membrane extracts offers the unique possibility to precisely mimic the native composition of a particular membrane and to probe the effect of selected lipids on membrane protein function. It is now well established that many membrane proteins require specific lipids for functional reconstitution, and specific lipid binding sites have been identified on several membrane proteins (Hunte *et al.,* 2008; Hiller *et al.,* 2008). The confinement of the lipids in NLPs is achieved by an integral number of apolipoproteins, resulting in a discrete particle size distribution (Denisov *et al.,* 2004). Currently, the process of NLP assembly cannot be controlled entirely, thus resulting in a distribution of NLPs with discrete diameters due to different copy numbers of the integrated apolipoproteins (Blanchette *et al.,* 2008). NLPs render membrane proteins water-soluble in the complete absence of detergent molecules. The confinement of the lipid bilayer by the amphipathic apolipoprotein increases the stability of NLPs when compared to other membrane mimicking systems. Restricting the lateral motion of NLP-embedded membrane proteins by the protein's aqueous edge further reduces potentially adverse protein-protein interactions, thus efficiently preventing protein aggregation. At the same time, NLPs are planar and of relatively small size, thus allowing simultaneous access to both the extracellular and cytoplasmic domain of an embedded membrane protein. These features make NLPs an ideal system for the application of functional enzyme assays that are often compromised by the presence of high concentrations of detergent.

1.3.5 Lanthanides in structural biology by NMR

Paramagnetic NMR spectroscopy has made spectacular advances in the understanding of the structural species involved in protein folding (Felitsky *et al.,* 2008) and the way in which proteins recognise proteins (Tang *et al.,* 2006; Volkov *et al.,* 2006), DNA (Iwahara and Clore, 2006) and small ligand molecules (Tang *et al.,* 2007). All these studies employed paramagnetic relaxation enhancements (PRE) from site-specifically introduced paramagnetic Tags (nitroxide radicals or Mn^{2+} chelates) to report on different conformational species in heterogeneous samples. This perspective emphasises other aspects of paramagnetism, mostly pseudocontact shifts (PCS) but also residual dipolar couplings (RDCs). The lanthanide tags offer significant scope for expanding the role of solution NMR spectroscopy in structural biology. Paramagnetism arises from unpaired electrons which in the case of the trivalent ions of lanthanides (Ln^{3+}) reside in chemically unreactive f orbitals. Since f orbitals are inner orbitals that are shielded from the ligand field and the interaction of lanthanide ions with ligands is mostly ionic in nature, the unpaired electrons do not nearly as readily delocalise to bound ligand molecules as the electrons of, e.g., paramagnetic heme-iron complexes. As a consequence, contact shifts (the paramagnetic equivalent of scalar couplings) are restricted to nuclei in the immediate vicinity of lanthanides. This leaves pseudocontact shifts (PCS) and paramagnetic relaxation enhancements (PRE) as the two most prominent effects caused by paramagnetic lanthanide ions in the NMR spectra of biological macromolecules. PCS are manifested by large changes in chemical shifts of the nuclear spins that are exposed to the paramagnetism of the metal ion. PCSs arise from through-space dipolar interactions with rapidly relaxing unpaired electrons. PREs depend on the nuclear spin and the distance from the paramagnetic centre (Otting *et al.,* 2008).

1.4 The outer membrane protein G (OmpG) from *E. coli*

The outer membrane of Gram-negative bacteria is a selective permeability barrier. It prevents uncontrolled exchange of solutes and nutrients such as sugars, nucleotides, amino acids and ions between the cell's exterior and interior. The uptake of these substances from the medium to the periplasm occurs through channel-forming integral MPs known as outer-membrane porins (Omps), which function as molecular filters. Omps are membrane-spanning β-barrels (surrounding an aqueous pore) with short turns extending into the periplasmic space and long flexible loops extending in the extra cellular space. Since the outer membrane of Gram-negative bacteria has no proton motive force, most proteins act as passive pores. Classical porins conform to a common pattern whereby three monomers

associate into trimers. This is their oligomeric state in 2D and 3D crystals, and also their functional state in lipid bilayers (Nikaido *et al.,* 2003). β-barrel membrane proteins dominate the outer membrane of Gram-negative bacteria (Dong *et al.,* 2006). A possible explanation for the large number of β-barrel observed in the outer membrane has been attributed to their less hydrophobic nature, which might aid in efficient transport across inner membrane and periplasmic space without the risk of aggregation. Crystallisation of β-barrel outer membrane proteins has been found to be much easier than α-helical TM proteins, largely due to their inherent stability. Numerous structures of β-barrel have been solved even with protein refolded from inclusion bodies (Gouaux *et al.,* 1998). The smallest β-barrel membrane protein structure known so far has eight strands while the largest has 24 (Remaut *et al.,* 2008). Porins such LamB and ScrY have 18-stranded β-barrels. They have more restricted pores and transport carbohydrates (Schirmer *et al.,* 1995). Some of them form non-selective channels such as OmpF and OmpC porins with 16-stranded barrels. They transport molecules of up to 600 Daltons and show a slight preference for cations (Cowan *et al.,* 1992; Basle *et al.,* 2006). It has also been shown that OmpF can transport unfolded polypeptides, a property utilised by colicins (Yamashita *et al.,* 2008). These classical porins form SDS stable homotrimers, each monomer having a separate translocation pathway. Maltoporins have a string of low affinity sugar binding sites lined with aromatic residues, termed the greasy slide, which allows the rapid uptake of oligosaccharides. Not all outer membrane proteins form pores. Some have evolved to perform other biological functions. Proteins with smaller barrels have no biological functions, one of which is the 14-stranded β-barrel OmpG. The opening/closing mechanism is regulated by pH function. It closes the interior of the barrel with an intricate hydrogen-bonding network (Yildiz *et al.,* 2006). Using the β-barrel as an anchor in the membrane, proteins have also evolved to carry out enzymatic reactions. OmpT, a protease whose catalytic centre protrudes from the 10-stranded β-barrel to the external medium, is involved in protein degradation (Vandeputte-Rutten *et al.,* 2001) and OmpLA, a phospholipase that cleaves lipopolysaccharides, forms a 12-stranded β-barrel (Snijder *et al.,* 1999). Proteins with smaller barrels such as OmpX (Vogt *et al.,* 1999) act as membrane anchors or for adhesion while OmpA, an abundant protein in *E. coli*, stabilises the outer membrane and has been used extensively to study protein folding (Pautsch *et al.,* 1999). All these examples demonstrate the great versatility of β-barrel Omps.

In *E. coli* the main porins for sugar uptake are LamB and ScrY (Szmelcman *et al.,* 1976; Schmid *et al.,* 1991). Thus, porin proteins are critical for bacterial growth. However, it was shown that porin deficient strains grow slowly and accumulate mutations that permit expression of new porin proteins. This finding led to the isolation of *E. coli* mutant strains that acquired the ability to synthesise new porin proteins (Nikaido *et al.,* 2003). The porin OmpG, for example, was discovered among mutants (*E. coli* RAM 194) that gained increased outer

membrane permeability in the absence of the classical porins OmpF and LamB (Misra and Benson, 1989). The novel porin is produced in response to a chromosomal mutation termed *cog-192* (for control of OmpG). Molecular characterisation of *cog-192* revealed that it is a large chromosomal deletion that placed the OmpG expression under the control of the *pspA* promoter (Fajardo *et al.,* 1998). OmpG, an outer membrane protein from *Escherichia coli*, is an unspecific porin, allowing the passage of ions and molecules up to 900 Da. OmpG consists of a 14-stranded β-sheet with long loops on the extracellular side and short turns on the periplasmic side. Only a small number of amino acids form a single α-helix in one of the extracellular loops. The biological function of OmpG is still unknown but it could be shown that it enables the diffusion of maltodextrins across the outer membrane in the absence of the LamB maltoporin.

An aromatic belt composed mainly of tyrosines exists, which has been previously shown to keep the structural integrity in the hydrophobic core of the lipid bilayers (Korkmaz *et al.,* 2008; Yildiz *et al.,* 2006). OmpG does not require oligomeric forms for its function as shown by activity and by structural studies (Conlan *et al.,* 2003). In contrast to the classical Omps, chemical cross-linking and two-dimensional electrophoresis suggested that OmpG is a monomer (Fajardo *et al.,* 1998). A projection map at 6 Å resolution obtained by cryo-EM of 2D crystals revealed a ring-shaped density indicative of a monomeric β-barrel, with no evidence of oligomer formation (Behlau *et al.,* 2001). A study with atomic force microscopy showed dimers and monomers for OmpG reconstituted into native *E. coli* lipids (Mari *et al.,* 2010). However, there is no evidence regarding the stability or biological relevance of these dimers. Growth and uptake experiments showed that OmpG displays a porin-like activity. Thus, OmpG seems to function as a rescue porin. The gene for OmpG encodes a polypeptide with 301 amino acids, which show all features of an Omp: a signal sequence of 21 amino acids at its N-terminus, which is cleaved during export into the outer membrane, absence of long hydrophobic stretches, lack of cysteine residues and a C-terminal phenylalanine, which is important for membrane insertion. Circular dichroism spectroscopy of detergent-solubilised OmpG indicated that, like other outer-membrane porins, it consists largely of β-sheet secondary structure with little α-helix content. Proteoliposome swelling assays have shown that OmpG is a non-selective channel for mono-, di- and trisaccharides, with an unusually large limiting pore diameter of around 2 nm. Initial secondary structure predictions of OmpG suggested 16 β-strands (Fajardo *et al.,* 1998). However, it was estimated to be 14, which would better agree with the diameter of the β-barrel in the projection map (Behlau *et al.,* 2001; Conlan *et al.,* 2000). The high resolution X-ray structures of OmpG revealed that OmpG is closing below pH 6 and opening at above pH 7.5, which was later confirmed by different spectroscopic techniques (Yildiz *et al.,* 2006; Liang & Tamm, 2007; Mari *et al,* 2010; Korkmaz-Ozkan *et al.,* 2010). Mutation studies as well as the crystal

structures showed that the opening/closing of the protein is controlled by two histidines (His 231 and His 261) (Yildiz *et al.,* 2006; Korkmaz-Ozkan *et al.,* 2010). At low pH the imidazole side chains of these histidines are protonated and hence repel each other causing the loop L6 to fold towards the channel entrance. This considerably restricts the channel permeability at acidic pH. At high pH, the histidines are deprotonated and form H-bonds with Ser 218 and Asp 267, which in turn cause the loop L6 to stand in upright position with respect to the channel entrance and leave the channel completely opening for passive diffusion (Korkmaz-Ozkan *et al.,* 2010). Single molecule force spectroscopy revealed that β-hairpins establish interactions that lead to a stable structure, independent of the pH (Damaghi *et al.,* 2010). On the other hand, the interaction stabilising β-hairpin VI (β-strands S11 and S12) is at the periplasmic surface at neutral pH. At acidic pH, it shifts L6 to an extracellular loop. It was also shown that the interactions among β-strands S11 to S13 change with environment in a pH-dependent manner. While the β-strands S11 and S12 establish 14 interactions at neutral pH, they establish eight interactions at acidic pH. Using an ATN-FTIR study, Korkmaz demonstrates that the opening/closing of OmpG channels remains essentially unchanged and most of the changes are located in the side chain moiety (Korkmaz *et al.,* 2012). In addition to the histidines, other charged AAs (Asp, Glu and Arg) play an active role interacting each other inside the pore lumen mainly at acidic pH (this is also claimed by Damaghi *et al.,* 2010). They suggest a closure of the channel via changing the electric potential inside the lumen due to the AAs' different states of charge. There are also changes in the Tyr moiety due to either a variation in protein-micelle interaction located in the aromatic girdle or the buffer changed at different pH's.

However, it is known that OmpG exhibits spontaneous gating behaviour (switching between the opening/closing state at neutral pH), which interferes with the application of the pore as a biosensor. It was found out by molecular dynamics simulations that the flexibility of L6 and β12 are responsible for most of the spontaneous gating activity (Chen *et al.,* 2008). An OmpG mutant was generated to stabilise the position of β12 and L6 in the opening state. First, a disulphide bond was created between β12 and β13 by introducing cysteine residues at position G231 and D262, which are located at the extracellular ends of β12 and β13. Second, D215 was deleted to optimise the hydrogen bonding between β11 and β12. Chen has shown that the monomeric OmpG is well suited as a stochastic sensing pore (Chen *et al.,* 2008). It was possible to detect ADP by using this OmpG double mutant in combination with a molecular adapter.

The crystal structure of OmpG was solved by two groups (Subbarao and Van den Berg, 2006; Yildiz *et al.,* 2006). For one of these studies OmpG was extracted from native membranes with lauryl-*N*,*N* dimethyldodecylamine-*N*-oxide. During the purification step the detergent was exchanged against tetraoxy-ethylene-mono-*n*-octylether (C8E4) and the

subsequent crystallisation was performed at pH 5.5 (Subbarao and Van den Berg, 2006). In contrast to that, Yildiz expressed OmpG without its signal sequence, extracted and purified the protein from inclusion bodies and subsequently refolded the protein into detergent micelles. Using octyl-β-D-glycopyranoside and LDAO as detergent, two different crystal forms, at pH 5.6 and pH 7.5 respectively, were obtained (Yildiz *et al.,* 2006).

The three structures show similar structural features typical for β-barrel porins (figure 1.18). OmpG forms a monomeric 14-stranded (β1-β14) β-barrel with six short turns (T1-T6) extending into the periplasmic space and seven large loops (L1-L7) extending into the extracellular space. Loop 4 contains a short α-helix. The average angle between the β-strands and the membrane plane is around 43°– 60°.

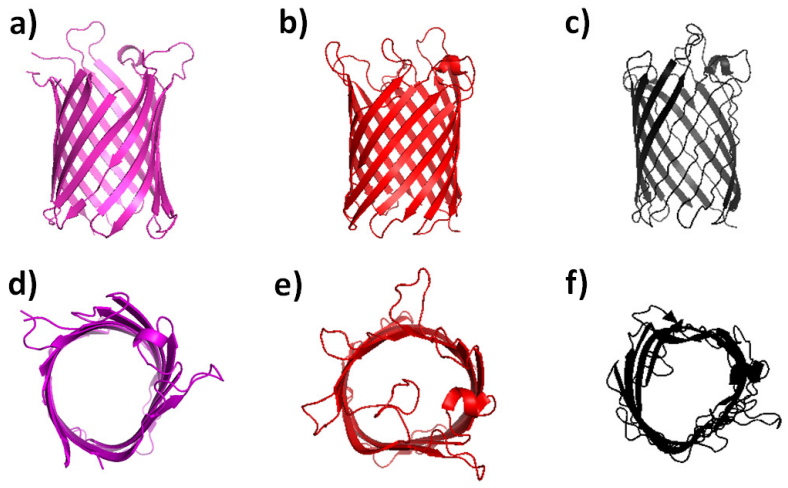

Figure 1.16 Crystal structures of OmpG in the opening/closing state. a) and d) OmpG in the opening state at pH 5.5 (PDB code 2IFC). b) and e) OmpG in the closing state at pH 5.6 (PDB code 2IWW). c) and f) OmpG in the opening state at pH 7.5 (PDB code 2IWV). The images were rendered by PyMOL.

In all crystal structures the side chain densities were well defined except for the loop residues 20–27, 58–62, 220–231 and 261–266, indicating a degree of flexibility in L1, L2, L6 and L7. The pore diameter measured between Cα atoms of opposite β-strands is ~ 25 Å or ~ 13 Å when taking side chains into account. The entry of disaccharides into the pore is facilitated by a line of aromatic residues (also termed an aromatic slide) adjusted parallel to the barrel axis (figure 1.18; Subbarao and Van den Berg, 2006; Yildiz *et al.,* 2006). The authors suggested that the OH groups in the aromatic slide might function as a guide rail for incoming substrates. Additionally, the pore is lined by charged and polar residues (mainly Glu and Arg), which might create an electrostatic barrier that prevents ions and charged compounds from entering the channel. These data are consistent with the assumption that

OmpG could be needed for the transport of large oligosaccharides under very specific growth conditions (Fajardo *et al.,* 1998). As mentioned above, Yildiz obtained two different crystal structures by crystallisation of OmpG at pH 7.5 and pH 5.6.

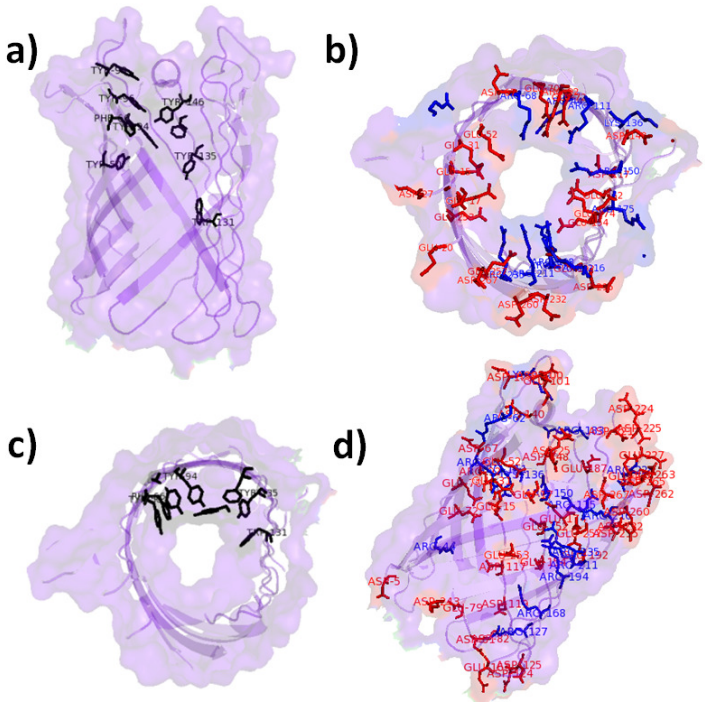

Figure 1.17 Stereo views of the arrangement of aromatic and positively and negatively charged residues in the OmpG pore. a) and c) Lines of aromatic residues ('aromatic slides') leading from the extracellular channel entrance to the pore interior. b) and d) Top view of positive charged side chains in the pore (mostly Arg, blue) and negatively charged residues (mostly Glu, red) on opposite sides of the barrel wall. The images were rendered by PyMOL.

The latter shows closing conformations in which loop 6 folds into the pore (figure 1.16, b and e). The authors postulate that the pH-induced conformational change of loop 6 is induced by the protonation of two solvent-exposed histidine residues (His 231 and His 261) located at the C-terminal end of loop 6 and the N-terminal end of loop 7. At pH 7.5 the distance of the imidazole rings is 4.9 Å, whereas at pH 5.6 this distance increases to 13.7 Å. The unzipping of the hydrogen bond between His 231 and His 261 results in the increasing length of loops 6 and 7. Loop 7 and the adjacent loop 1 move outward to make room for the reorientation of loop 6 into the pore (Yildiz *et al.,* 2006).

These findings are consistent with electrophysiological channel gating measurements with OmpG (Conlan *et al.,* 2003). At neutral and basic pH the OmpG channel was opening, but it was closing at acidic pH below pH 5.0. At pH 6.0, OmpG fluctuated between the opening/closing state. Additionally, the projection map obtained from 2D crystals also shows

restricting loops in the middle of the pore. This might be due to the fact that the 2D crystals were stained with uranyl acetate (pH ~ 4.0) immediately before the EM investigation. So far, OmpG is the only Omp for which pH-depending gating has been demonstrated and structurally validated by EM and X-ray crystallography (Behlau *et al.,* 2001; Conlan *et al.,* 2000; Yildiz *et al.,* 2006). Surprisingly, the Subbarao crystal structure resembles the opening state and not the closing state of the Yildiz structure, even though both crystals were formed at nearly the same pH (pH = 5.5 and 5.6 respectively; Subbarao and Van den Berg, 2006; Yildiz *et al.,* 2006). The reason for this discrepancy is presently unresolved. A third OmpG structure determined by solution NMR was published (Liang and Tamm, 2007). Deuterated ^{13}C, ^{15}N labelled OmpG sample was expressed as inclusion bodies. The protein was purified under denaturing conditions (8M urea) and subsequently refolded into OG detergent micelles. In a last step, the detergent was exchanged against dodecylphosphocholine (DPC) and NMR datasets were recorded at pH 6.3. The structure was determined with an RMSD of 1.43 ± 0.3 Å for the backbone of the β-barrel residues, 1.67 ± 0.29 Å for the backbone of the turn residues and 7.37 ± 1.29 Å for the backbone of the residues located in the loops (figure 1.18. The structure is in good agreement with both crystal structures in the β-barrel region, although the barrel is a little shorter. Additionally, the extra cellular loop region indicates high flexibility. This might be due to the pH value (pH 6.3) at which the protein may undergo conformational exchange between the opening/closing conformation on the microsecond to millisecond time scale.

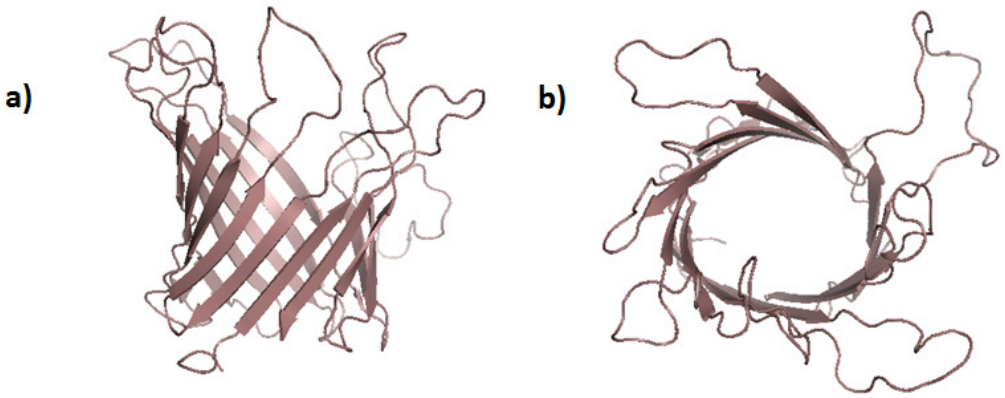

Figure 1.18 Solution structure of OmpG at pH 6.3. Lowest-energy conformer of the 10 NMR structure ensembles calculated from nuclear Overhauser effect (NOE), dihedral angle and hydrogen bond restraints. The images were rendered by PyMOL.

Because of their robustness, pore forming β-barrel proteins have considerable potential in biotechnology as stochastic sensors for single molecule detection and for covalently attached chemical modification (Chen *et al.,* 2008, Grosse *et al.,* 2010, Bayley and Cremer, 2001; Rhee and Burns, 2007). The ionic current flowing through a pore under an applied potential

is altered when an analyte binds to the lumen of the pore. Measurement of the frequency of occurrence of binding events allows the determination of the analyte concentration.

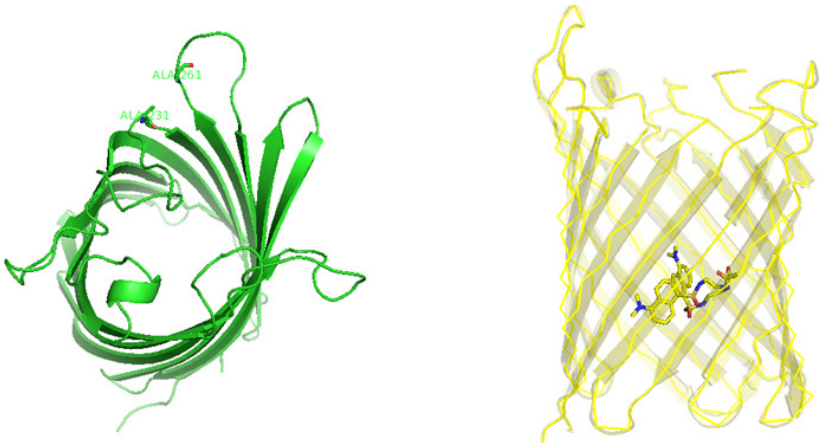

Figure 1.19 X-ray structures of OmpG mutated in positions 231 and 261 with 2 Ala (on the left side, PDB code 2X9K) and OmpG mutated in position 209 with a Cys covalently bound to a dansyl group (on the right side, PDB code 2WVP). The images were rendered by PyMOL.

1.5 Overview of the thesis

The thesis describes the development of different labelling strategies for structural characterisation of large MPs by solid-state MAS NMR. The labelling strategies were chosen to investigate different regions of the 281 residues OmpG. The labelling approach used for the thesis provides complementary informations for the ambiguous identification of the assignment's starting point of OmpG.

The paragraph 3.1 of the chapter 3 describes the preparation of the labelled sample to investigate the dynamics of OmpG at different pH's. The *E. coli* BL21(DE3) expression system used allows the production of a sufficient amount of labelled OmpG sample. It was refolded and reconstituted in a planar lipid bilayer (2D crystals) at three different pH's (7.5, 7.0 and 5.6). The 2D crystals are analysed by solid-state MAS NMR to characterise the different conformation states of the OmpG channel in a lipid environment, especially to identify the AAs involved in the pH gating. Furthermore, this paragraph describes the biophysical problems with the preparation of 2D crystals at acid pH and how they are prepared to get NMR spectra with sufficient resolution. The resolution of the spectra at different pH's demonstrates how the preparation of labelled OmpG is very important to achieve solid-state MAS NMR data.

In the paragraph 3.2 a labelled OmpG sample was prepared to characterise the region of the protein involved in the sugar coordination. To get a sufficient amount of OmpG protein and to minimise isotope dilution due to transaminase respectively, an excess of unlabelled AAs and some inhibitors to get enough level were used (Tong *et al.,* 2008). The expression system used is *E. coli* BL21(DE3). After the refolding and reconstitution of the protein in a lipid bilayer, 2D crystals were obtained. Solid-state MAS NMR analysis is confirmed by the spectral resolution of this sample and the intraresidual assignment of labelled OmpG.

The results of the paragraphs 3.1 and 3.2 further demonstrate that a homogeneous sample with a high degree of local order is required for solid-state MAS NMR studies in contrast to the X-ray crystallography, for which a crystalline sample is required for high resolution structural investigation. Thus solid-state MAS NMR can be a helpful tool for the structural investigation of MPs, which do not easily form 3D or 2D crystals.

In the paragraph 3.3 it is shown how vast the amount of mixing time in the pulse sequence can be to get interresidual correlations for the sequential assignment. This experiment was applied to the samples at different pH's described in the paragraph 3.1. For a better understanding of the difference in terms of chemical shift one should also consult the other new peaks that appear in the spectra which should represent the interresidual correlations necessary for the sequential assignment. In the paragraph 3.4, the importance of the use of

NMR buffer systems in the NMR study, especially in solid-state MAS NMR, is described. The buffer systems help to keep the pH at a particular value but the concentration of the ions and their mobility can influence the resolution of the spectra. To improve the resolution of the spectra, some easily prepared buffers are used. These demonstrate an enhancement of the sensitivity (S/ N ratio). A 2D NCO spectrum was recorded using labelled OmpG samples. Some peaks were assigned but for the fully interresidual assignment other double or triple resonance experiments are necessary.

2 Material and methods

2.1 Material

All chemicals, if not indicated otherwise, were purchased from Merck (Darmstadt, Germany), Sigma-Aldrich (Munich, Germany), Roth (Karlsruhe, Germany), Biomol (Hamburg, Germany) and VWR International (Darmstadt, Germany), based in the highest available purity. The detergents were of Glycon Biochemicals (Luckenwalde, Germany).

2.1.1 *E. coli* expression and cloning strain

Strain	Genotype	Company
BL21(DE3)	F^-, ompT, $hsdS_B$ ($r_B^- m_B^-$) gal, dcm (DE3)	Merck Biosciences Germany

Table 2.1 *E. coli* expression and cloning strain. This table lists the genotypes of strain commonly used for cloning and expression with the pET System in our laboratory for this project.

2.1.2 Expression plasmid

The pET OmpG plasmid was a gift from Prof. W. Kühlbrandt from the MPI for Biophysics (Frankfurt am Main, Germany). With an N-terminal methionine but without the signal sequence, the DNA of the mature form of OmpG (280 amino acids) was cloned into the pET-26b plasmid (Novagen, Merck Biosciences, Germany) using the *NdeI* and *SacI* restriction sites. The coding sequence for OmpG was amplified from chromosomal DNA (D2001) of *E. coli* strain B (SIGMA, Deisenhofen, Germany) using the following primers:
forward: 5'-GATCTCGGTTGGGCTGGCTTCTGTCTCCCT;
reverse: 5'-CCGACGCAGGAGTTAGGTCAACAAAGCTGCG.
To introduce the restriction sites for *NdeI* and *SacI*, the product was used in a second PCR using the following primers:
forward: 5'-GGCCTGCGCACATATGGAGGAAAGGAACGAC;
reverse: 5'-CGGATAAGGAGCTCGCGCCGCATCC).
The amplified DNA was digested with *NdeI* and *SacI* and cloned into a pET-26b expression plasmid from Novagen (Bad Soden, Germany).

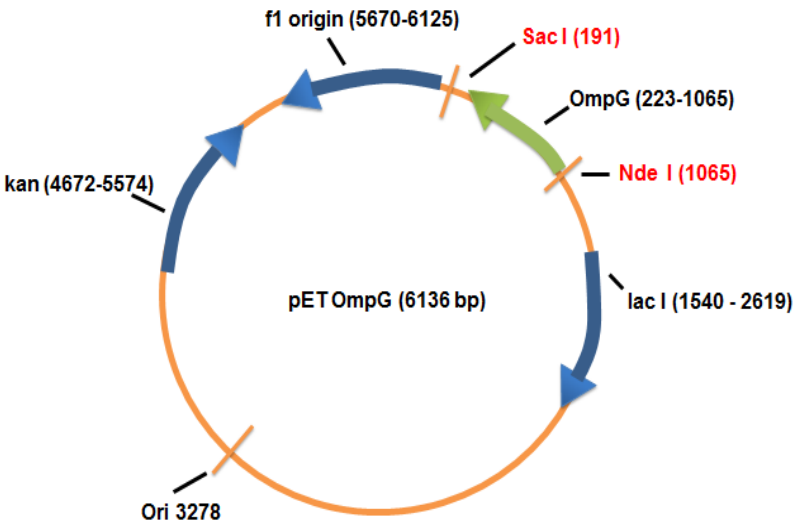

Figure 2.1 Plasmid map of the pET OmpG construct.

2.1.3 Isotopically labelled substances

All labelled substances were purchased from Cambridge Isotopes Laboratories Inc. (Andover, Massachusetts, USA) and Sigma-Aldrich/ ISOTEC (Munich, Germany).

2.1.4 Accessories and devices

The accessories for the protein crystallisation come from the Hampton Research (Aliso Viejo, California, USA). For cell harvesting and protein purification the centrifuges by Beckman Coulter, Brea, CA were used with the rotors Avanti® J25.50 and JLA10.500 and Optima™ TLX ultracentrifuge with the rotor TLA 45. Additional devices are added in the appropriate section.

2.2 Methods

2.2.1 Preparation of Competent cells

For the preparation of competent cells, the $CaCl_2$ - *E. coli* strains were plated onto an LB Agar plate (Sambrook *et al.,* 1989). From this agar plate a start culture was inoculated and incubated at 37 °C. It was shaken at 180 rpm overnight. Then the main culture was inoculated to an OD_{600nm} = 0.1 at 37 °C, then shaken at 160 rpm. After the culture had reached OD_{600nm} of 0.3, the cells were incubated for 30 min on ice and centrifuged at 4.800 rpm for 10 min at 4 °C. The pellet was resuspended in 1/10 of the initial volume in 0.1 M $CaCl_2$ and incubated for 30 min on ice. The mixture was then pelleted at 4.800 rpm for 10 min at 4 °C, then the cells were dissolved in 1/20 of the starting volume in 0.1 M $CaCl_2$ and 15 % (v/v) glycerol. The competent cells were transformed directly or stored at –80 °C.

2.2.2 Transformation of pET26 in *E. coli* BL21(DE3)

For the transformation of *E. coli* with plasmid DNA Sambrook's $CaCl_2$ method was used (Sambrook *et al.,* 1989). 100 µl of competent cells were mixed with 1µl of plasmid DNA (100 ng/ µl) and incubated for 30 min on ice. This was followed by a heat shock at 42 °C for 90 seconds. The mixture was placed on ice for 5 min and subsequently treated with 1 ml of LB medium. After one hour of incubation at 37 °C, 100 µl of the mixture were put on an LB plate with the appropriate antibiotic (kanamycine) and incubated at 37 °C overnight.

2.2.3 Test expression of OmpG fragment in *E. coli* BL21(DE3) pET26

From the LB agar plates, nine transformed colonies are picked up and transferred in 3 ml of LB medium plus 3 µl kanamycin (the original cultures) until the concentration is OD_{600nm} = 0.6. Simultaneously, nine other test tubes containing 3 ml LB medium plus 3 µl kanamycine are incubated and prepared for 5–6 hours at 37 °C and at 180 rpm. They will be used to prepare glycerol stocks of the best clone. The original cultures are used to induce the expression of the OmpG fragment. After adding IPTG to a final concentration of 1 mM to each culture, they were incubated for another three hours at 37 °C and 180 rpm. From each culture were taken and centrifuged 100 µl at 5.000 rpm for 5 min at room temperature. After discarding the supernatant, the cells were resuspended with 9 µl of H_2O, 1 µl of SDS (20 % w/v) and 10 µl of GLB 2X. Then the sample was incubated for 10 min at 90 °C. In general, there will be used 5 µl from each sample to analyse the protein content in the cells (especially the recombinant protein). After analysing the experiment, a glycerol stock from

the best clone should be prepared and stored at – 80 °C. The glycerol stock's final concentration is 15 % (v/v).

2.2.4 SDS gel electrophoresis for the separation of proteins

Purified proteins and cell lysis samples were analytically separated by SDS polyacrylamide gel electrophoresis as described by Laemmli in 1970. The polyacrylamide gels had a separation length of 6 cm. Electrophoresis was performed with the system of the company Mighty Small SE250 Hoefer (San Francisco, California, USA) at a voltage of 150 V. The electrophoresis buffer consisted of 250 mM Tris-Base, 1.9 M glycine and 1 % SDS. The stacking gel consisted of 30 % acrylamide, 0.625 M Tris/ HCl (pH 6.8) and 20 % SDS, and the separating gel of 30 % acrylamide, 0.75 M Tris HCl pH 8.8, 20 % SDS and H_2O. For the polymerisation TEMED and APS were used. The protein samples were mixed prior to electrophoresis with 4 % (w/v) SDS, 25 % stacking gel, 20 % (v/v) glycerol, 0.01 % (w/v) bromophenol blue and 0.05 % (v/v) mercaptoethanol. After electrophoresis, the gels were fixed with 50 % ethanol and 10 % acetic acid. In the next step, the proteins were stained with 0.025 % Coomassie brilliant blue (G 625) and then fixed with 10 % acetic acid. Subsequently the excess was removed with 10 % acetic acid (Schägger and von Jagow, 1987). The molecular weight marker was purchased from Fermentas GmbH (St. Leon-Rot, Germany).

2.2.5 Main media

LB medium consisted of 1 % tryptone, 0.5 % yeast extract, 1 % NaCl and NaOH, of which was added until the pH value reached 7.3 (Miller *et al.,* 1992). The LB plates contained additional 1.5 % of agar-agar. In 1 ℓ of M9 minimal medium were contained: 760 ml H_2O, 20 ml of trace element solution (500 ml: 2.5 mg of EDTA, 0.25 g $FeSO_4$, 25 mg $ZnCl_2$, 5 mg $CuSO_4$, pH 7.5 to 7.7), 200 ml of 10 × M9 salt (80 g Na_2HPO_4 × 2 H_2O, 20 g K_2HPO_4, 5 g NaCl), 1 ml $MgSO_4$ (1 M), 0.3 ml $CaCl_2$ (1 M), 1.5 ml thiamine-HCl (1 mg/ ml), 15 ml biotin (0.1 mg/ ml), 10 ml glucose (20 % w/v), 2 ml NH_4Cl (5 g/ 20 ml) and 1 ml kanamycine (30 mg/ ml). For the production of the uniformly [^{13}C, ^{15}N]-labelled OmpG were added ^{13}C glucose (2 g/ ℓ) and $^{15}NH_4CL$ (0.5 g/ ℓ). For the production of [^{13}C, ^{15}N]-labelled GALVSHF$_{\alpha,\beta}$Y$_{\alpha,\beta}$-OmpG uniformly [^{13}C, ^{15}N]-labelled AAs were added to the medium (100 mg/ ℓ). For the production of [^{13}C, ^{15}N]-GENDPQASR-OmpG some inhibitors were added (15 min before IPTG induction) using the following concentration: 180 mg/ ℓ L-methionine sulfone, 45 mg/ ℓ Na-succinate, 45 mg/ ℓ Na-maleate, 45 mg/ ℓ aminooxyacetate and 45 mg/ ℓ DL-malate and an excess of unlabelled AAs (1 g/ ℓ) and an excess of both unlabelled and labelled AAs (100 mg/ ℓ). All media for plasmid selection

antibiotics were added according to the resistance of the plasmids used in the following final concentrations: carbenicillin, 60 mg/ ml and kanamycin, 30 mg/ ml.

2.2.6 Determination of protein concentration

The protein concentration was determined by measuring the absorbance of the protein solution at a wavelength of 280 nm on the spectrophotometer. According to the Lambert-Beer Law

$$A_{280} = C \times d \times \text{Ɛ}$$

C is the unknown protein concentration c [mol × l^{-1}], A is the absorbance at 280 nm, d is the cell length [cm], and Ɛ is the molar extinction coefficient of the investigated protein/ complex [ℓ × mol × cm^{-1}]. The molar extinction coefficient based on the protein sequence was established with the support of the ProtParam protocol (www.expasy.ch).

2.2.7 Expression of labelled and unlabelled OmpG in *E. coli* BL21(DE3)

2.2.7.1 Isotopically labelled supplements for different labelling schemes

Unlabelled OmpG was expressed in LB medium. Labelled OmpG was expressed in standard M9 minimal medium. The standard expression protocol was done using shaking flasks. The amounts of sole carbon and nitrogen sources for uniformly and site-specifically labelled OmpG samples are listed below (Table 2.2).

Labelling scheme	sample	Labelled source	amount [g/ ℓ]
Uniform ^{13}C- and ^{15}N-labelling	u-[^{13}C, ^{15}N]-OmpG	u-[^{13}C]-glucose [^{15}N]-NH_4Cl	2 0.5
Site-specific ^{13}C- and ^{15}N-labelling	[^{13}C, ^{15}N]-GALVSHF$_{\alpha,\beta}$Y$_{\alpha,\beta}$-OmpG [^{13}C, ^{15}N]-GENDPQARS-OmpG*	u-[^{13}C, ^{15}N]-AAs	0.1

Table 2.2 Amounts of sole carbon and nitrogen sources for labelled growth media

* In this case the amount of labelled AAs was added twice.

Selectively labelled OmpG samples were prepared using the modified procedures by forward labelling. The amounts of labelled and unlabelled supplements used are listed separately.

2.2.7.2 Standard expression protocol

An overnight LB culture of *E. coli* BL21(DE3) transformed with pET OmpG was used to inoculate 1 ℓ of LB or M9 minimal medium culture. Cells were shaken at 37 °C and 180 rpm until an optical cell density of ~ 0.6, measured at 600 nm, was reached. The expression of OmpG was induced by the addition of 1 mM IPTG. After three hours of expression, cells were harvested by centrifugation (5.000 g, 10 min at 8 °C). Cells were resuspended and washed with an ice cold 0.15 M NaCl solution and centrifuged again. The amount of biomass was determined and cells were cooled down to –80 °C for long time storage or –20 °C for short time storage.

2.2.7.3 Modified expression protocol (Marley *et al.,* 2001)

A 4 ℓ pre-culture (LB medium) was inoculated with an overnight culture. The pre-culture was shaken at 37 °C and 180 rpm up to an OD_{600nm} of 0.5. Cells were harvested by centrifugation (5.000 g, 10 min at 8 °C) and washed with 200 ml of ice cold 0.15 M NaCl. Cells were harvested again and subsequently resuspended in 1 or 2 ℓ of M9 minimal medium, depending on the type of carbon source in the medium. If glucose was used as the carbon source, cells from a 4 ℓ LB culture were resuspended in 1 ℓ of M9 minimal medium supplemented with the indicated amounts of carbon and nitrogen sources (Table 2.2). For selective amino acid labelling a forward labelling strategy was used. Cells from a 4 ℓ LB culture were resuspended in 2 ℓ of M9 minimal medium containing all amino acids (100 mg/ ℓ) in unlabelled or labelled form, 2 g of unlabelled glucose and 0.5 g of unlabelled NH_4Cl. Cells were then shaken at 37 °C and 180 rpm for one hour for recovery of growth and clearance of unlabelled metabolites. Then protein expression was induced by the addition of 1 mM IPTG. After three hours of incubation, the cells were harvested and stored at either –80 °C or –20 °C. For the expression of the [^{13}C, ^{15}N]-GENDPQARS-OmpG a further modified expression protocol was used.

2.2.7.3.1 Expression protocol of [^{13}C, ^{15}N]-GALVSHF$_{\alpha,\beta}$Y$_{\alpha,\beta}$-OmpG

The expression protocol for the production of [^{13}C, ^{15}N]-GALVSHF$_{\alpha,\beta}$Y$_{\alpha,\beta}$-OmpG started with the preparation of a pre-culture consisting of five ml of LB and five µl of kanamycine, which was then inoculated with the glycerol stock *E. coli* BL21(DE3)-pET26-OmpG, incubated for three hours and shaken at 180 rpm and 37 °C. After the pre-culture, an overnight culture was prepared (100 ml LB + 100 µl kanamycine + 1 ml of the pre-culture), to be incubated overnight and shaking at 180 rpm and 37 °C. To obtain the main culture, 8 ℓ of LB containing kanamycine (30 µg/ ml) + glucose 20 % (w/v) were inoculated with the overnight culture until an optical density, measured at 600 nm = 0.1, was reached. The culture was incubated at 180 rpm and 37 °C until the cells reached an OD_{600nm} of 0.5–0.7. Cells were sedimented by centrifugation at 5.000 g, 15 min, at 8 °C and the resulting pellet was washed with ice cold NaCl solution (0.15 M). The cell pellet was resuspended into 2 ℓ of standard M9 minimal medium supplemented with [^{13}C, ^{15}N]-GALVSHF$_{\alpha,\beta}$Y$_{\alpha,\beta}$ (100 mg/ ℓ culture) used as the sole carbon and sole nitrogen sources and unlabelled glucose (2 g/ ℓ culture) and ^{14}N-ammonium chloride (0.5 g/ ℓ culture) were used for coenzyme production. After one hour, the expression of OmpG was induced by isopropyl-β-D-thiogalactopyranoside (1 mM). A 1 ml sample was taken before induction of the expression to check the protein content of uninduced cells by SDS-PAGE. Cells were further incubated for three hours at 37 °C. After induction a 1 ml sample was taken once per hour to check the protein expression by SDS-PAGE. All SDS-PAGE samples were normalised to an OD_{600nm} = 1. These samples were centrifuged at 5.000 rpm for 10 min. The supernatant was discarded and the cell pellet was resuspended with 9 µl H_2O, 1 µl SDS (20 % w/v) and 10 µl gel loading buffer 2X (GLB 2X). After three hours of IPTG induction the cell pellet was collected by centrifugation at 5.000 g for 15 min at 4 °C. The pellet was washed with 500 ml ice cold NaCl solution (0.15M) and stored at –80 °C.

2.2.7.3.2 Expression protocol of [^{13}C, ^{15}N]-GENDPQASR-OmpG

The expression and purification of [^{13}C, ^{15}N]-GEQNDPASR-OmpG was done as described by Tong (Tong *et al.,* 2008). A pre-culture (5 ml of LB + 5 µl of kanamycine) was inoculated with the glycerol stock BL21(DE3)-pET26-OmpG and incubated for three hours at 180 rpm and 37 °C. An overnight culture (100 ml LB +100 µl kanamycine + 1 ml of the pre-culture) was incubated overnight at 180 rpm and 37 °C]. The main culture was prepared (4 ℓ LB + kanamycine (30 µg/ml) + Glucose 20 % (w/v)), which was then inoculated with the overnight culture until an optical density measured at 600nm = 0.1 was reached. The resulting culture was incubated at 180 rpm and 37 °C until the cells reached an OD_{600nm} of 0.5–0.7. Cells were sedimented by centrifugation at 5.000 g, 15 min, at 8 °C and the resulting pellet was washed

with ice cold NaCl solution (0.15 M). The suspension was subdivided into two parts and centrifuged again. Each cell pellet was resuspended into 500 ml of standard M9 minimal medium and in 500 ml of modified M9 minimal medium (Protocol A). After one hour, protein expression was induced by the addition of IPTG (1mM). A 1 ml sample was taken before induction of the expression to verify the protein content of uninduced cells by SDS-PAGE. After induction a 1 ml sample was taken once per hour to check the protein expression by SDS-PAGE. After four hours the complete cell suspension was harvested by centrifugation at 5.000 g, 15 min, at 8 °C. All SDS-PAGE samples were normalised to an $OD_{600nm} = 1$. These samples were centrifuged at 5.000 rpm for 10 min. The supernatant was discarded and the cell pellet was resuspended with 9 µl H_2O, 1 µl SDS (20 % w/v) and 10 µl GLB 2X. Protocol A consists of the resuspension of the cells in modified M9 minimal medium consisting of standard M9 minimal medium, unlabelled amino acids (0.1 g/ ℓ), L-methionine sulfone (1 g/ ℓ), Na-Succinate (0.25 g/ ℓ), Na-Maleate (0.25 g/ ℓ), aminooxyacetate (0.25 g/ ℓ) and DL-malate (0.25 g/ ℓ). In a third test series a modified M9 minimal medium with an excess of unlabelled AAs (1 g/ ℓ) and labelled AAs (100 mg/ ℓ) was used. In this case an overnight culture was used to inoculate the modified M9 minimal medium. Fifteen minutes before induction of the protein expression an excess of AAs (H, F, Y, C, K, L, M, T, I, W and V at 1 g/ ℓ and G, N, D, Q, R, E, P, A and S at 0.1 g/ ℓ) was added to the culture. Additionally, inhibitors were added using the following concentration: 180 mg/ ℓ of L-methionine sulfone, 45 mg/ ℓ of Na-Succinate, 45 mg/ ℓ of Na-maleate, 45 mg/ ℓ of aminooxyacetate and 45 mg/ ℓ of DL-malate.

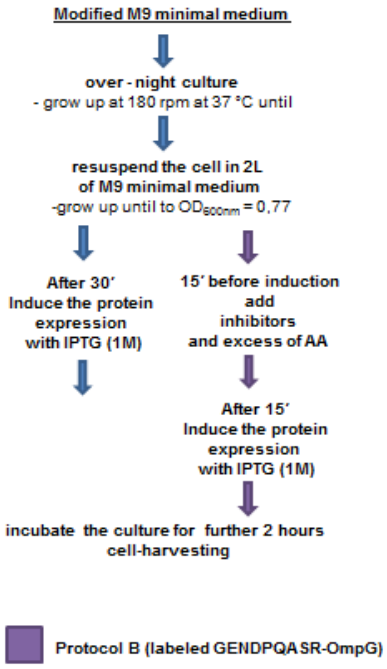

Figure 2.2 Schematic protocol of the labelled GENDPQASR-OmpG

All other steps, henceforward called Protocol B, were the same as described before. Protocol B will be used for the expression of the [^{13}C, ^{15}N]-GENDPQASR-OmpG (Figure 2.2).

2.2.8 Protein purification from inclusion bodies

OmpG purification was carried out in a similar manner to that described by Conlan (Conlan *et al.,* 2000). Cells (1 g biomass) were broken by using a homogenisator, then resuspended in 200 ml of buffer A containing 10 mM Tris-HCl at pH 8.0, a protease inhibitor cocktail (four tablets of complete™ by Roche), 1M $MgSO_4$ and benzonase 10 µl/ 50 ml. The cell homogenate was centrifuged at 60.000 g and 8 °C for 30 min. The resulting insoluble fraction was washed first in 200 ml washing buffer A containing 1 % (w/v) triton X-100, 1 M urea and then in 200 ml washing buffer B containing 1 M urea. It was centrifuged after each washing step at 60.000 g for 30 min at 8 °C. The resulting inclusion body pellet was resuspended in 200 ml solubilisation buffer containing 8 M urea and protease inhibitor cocktail (1 tablet of complete™ by Roche) and incubated overnight in a rotating system at 8 °C. The following day the resulting solution was centrifuged at 60.000 g and 8 °C for 30 min. The solubilised inclusion body fraction was then loaded on a Q Sepharose® Fast Flow column with a bed volume of 180 ml. The column was washed with three column volumes of buffer A containing urea (8 M). OmpG was eluted with a linear gradient of NaCl (0–1 M). The final concentration was determined by measuring the absorbance at 280 nm in buffer A containing urea (8 M) with an extinction coefficient Ɛ of 85060 M^{-1} cm^{-1} (Gill *et al.,*1989).

2.2.9 OmpG refolding

OmpG was refolded by rapid dilution in the presence of detergent micelles. Typically, denatured protein was diluted into buffer-containing detergent up to a protein concentration of 50 µg/ ml. The concentration of detergents in refolding buffer was set ten times higher than their critical micelle concentration. Refolding of OmpG (100 mg denatured protein) was done by rapid dilution and agitation into 2 ℓ of refolding buffer containing 1 mM DDM and 0.6 M L-arginine at 8 °C using a peristaltic pump with a flow rate of 0.1 ml/ min. The refolded protein was concentrated and washed with buffer-free L-arginine containing 1 mM DDM to a final concentration of 1–2 mg/ ml in an ultra-filtration chamber (Millipore GmbH, Schwalbach am Taunus, Germany) with a membrane cut-off of 30 kDa. The refolding efficiency was monitored by differential migration of the folded (28 kDa) and unfolded (34 kDa) form of OmpG in the SDS-PAGE gel (Fajardo *et al.,* 1998).

Detergent concentration in the refolded OmpG sample was reduced by using a second anion-exchange chromatography column (6 ml Resource™ Q, GE Healthcare, Germany). The protein was bound to the column and subsequently washed with three column volumes of buffer A' containing 0.4 mM DDM. OmpG was eluted at 300 mM NaCl in buffer B' containing 0.4 mM DDM. To enrich the folded form of OmpG all fractions were analysed by SDS-PAGE. Fractions containing folded OmpG were pooled and concentrated using a centrifugal filter device (Ultrafree-15, cut-off 50 kDa, Millipore) to a final concentration of around 3 mg/ ml.

2.2.10 Vivapure ion exchanges spin columns (Sartorius)

Vivapure ion exchange spin columns accomplish the separation on the basis of the selective, reversible adsorption of charged molecules (OmpG negative charged) to anion exchange group of the opposite charge (diethyl amino group in solution is positively charged). The rapid purification protocol based on membrane absorbers allows the parallel separation of proteins with high yield in less than twenty minutes (see chapter 3, paragraph 3.2.5). This is achieved in a 50 ml centrifuge tube for the Vivapure Maxi spin columns. Vivapure IEX columns replace time-consuming and expensive chromatographic methods for many protein applications. The exchanger used to separate the charged biomolecules (20 ml volume-medium binding capacity) is Vivapure IEX D-Diethylamine (D) R-CH_2-NH^+-$(CH_2H_5)_2$, a weak basic anion exchanger with a working pH between 4 and 10 and an ionic group of 9.5 pKa.

2.2.11 Reconstitution into lipid bilayers and two-dimensional crystallisation

Refolded OmpG was reconstituted into lipid bilayers. For this purpose, an *E. coli* total lipid chloroform extract (20 mg) was dried in a nitrogen stream and subsequently overnight in a vacuum pump. The resulting lipid film was resuspended in a solution containing Tris HCl 10 mM pH 8 and 34 mM octyl-β-D-glycopyranoside and sonicated for 20 min to destroy the vesicles. Aliquots of this lipid solution and refolded OmpG (~ 3 mg/ ml) were mixed to yield a lipid to protein ratio of 1:2 (w/w). For 2D crystallisation, the detergent was removed by dialysis (dialysis tube molecular weight cut-off 25 kDa, Roth, Karlsruhe, Germany) at 20 °C against 5 ℓ of different crystallisation buffers 1X at different pH's (7.5, 7.0 and 5.6) containing 20 mM Tris-HCl, pH 7.5 (or pH 7.0) or 20 mM Na-citrate at pH 5.6, 150 mM NaCl, 25 mM $MgCl_2$, 3 mM NaN_3. At the beginning of the dialysis procedure were added 10 mg of Bio-Beads™ (Bio-Rad, Munich) (to improve the removal of the detergent and to facilitate the reconstitution procedure), suspended in 10 ml of crystallisation buffer (the air inside the Bio-

Beads™ was removed by vacuum pump). The dialysis buffer was changed every five days instead. The dialysis tube was exchanged one time during this procedure to increase the removal of the detergent. 2D crystals were observed after seven days. To ensure complete removal of the detergent the crystal solution was dialysed for four additional weeks.

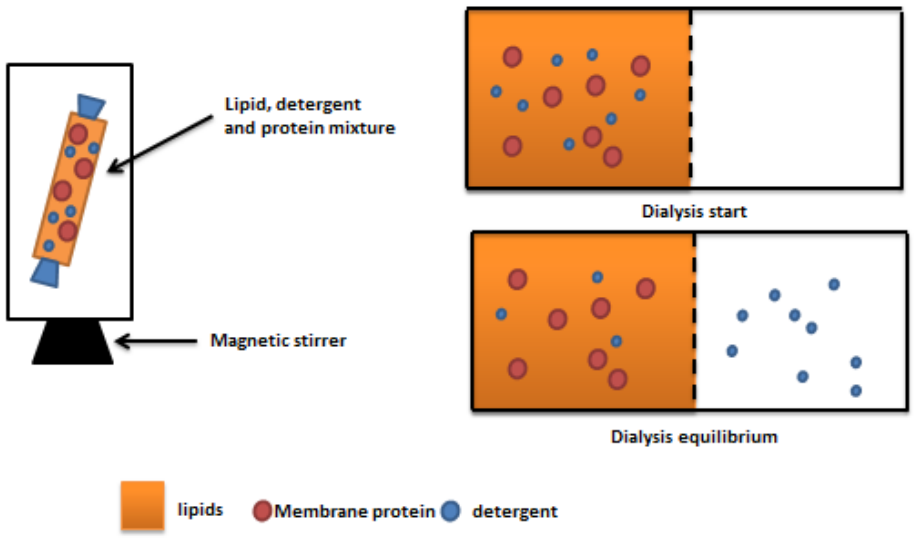

Figure 2.3 Dialysis procedure. Dialysis tube on the left and dialysis procedure on the right.

2.2.12 Electron microscopy analysis

The crystallised samples (5 µl) were applied to a carbon-coated Quantifoil® grid (200 Mesh size, copper/ rhodium) from Quantifoil Micro Tools GmbH (Jena, Germany) and incubated for 15 s. The grid was stained with 5 µl of uranyl acetate solution (1 % w/v) for 10 s and residual solution was removed with filter paper. The grids were washed two times with 5 µl water for 10 s. Images were recorded on a CM12 electron microscopy (Philips) at an accelerating voltage of 120 kV with an electron dose of 10 e-A-2 on Kodak SO-163 film at 1µm magnification.

2.2.13 Solid-state MAS NMR spectroscopy

Before using samples for solid-state MAS NMR investigations, the buffer was exchanged to a phosphate buffer (20 mM, pH 7.5, 7.0 and 5.6 containing 50 mM NaCl and 3 mM NaN_3). Samples were centrifuged at 14.000 rpm for 30 min and the resulting pellet was resuspended in phosphate buffer three times. 2D crystals of OmpG were finally sedimented in an ultracentrifuge at 235.000 g overnight and at 8 °C. Afterwards, samples were transferred into

a 3.2 mm or 4 mm MAS rotor (Bruker, Karlsruhe, Germany) by centrifugation in a table top centrifuge. All NMR measurements were performed on AVANCE-900 and AVANCE-700 spectrometers (Bruker), equipped with a 3.2 mm or 4 mm triple-resonance MAS probe (Bruker). During these measurements typical standard parameters are recorded. For the 1D ^{13}C-CP/MAS, 1D ^{15}N-CP/MAS, 2D ^{13}C-^{13}C PDSD and 2D NCO experiments magnetisation was transferred from ^{1}H to ^{13}C or ^{1}H to ^{15}N with a ramped CP with a contact time of 1500 µs (Metz *et al.,* 1994). Spin lock field strengths of ~ 55 kHz for ^{1}H, ~ 70 kHz for the ^{13}C and ~ 45 kHz for ^{15}N were used. For the 2D ^{13}C - ^{13}C experiments PDSD mixing times between 20 - 700 ms in combination with dipolar assisted rotational resonance (DARR) were chosen (Takegoshi *et al.,* 2001). For the 2D NCO experiment during the evolution of nitrogen, adiabatic CP was employed to selectively transfer magnetization from ^{15}N to ^{13}C with RF powers of ~ 15 and 23 kHz, respectively. The amide signals and the C' signals were irradiated on-resonance. During the acquisition time of these experiments proton decoupling was applied. For this the two-pulse phase modulation (TPPM) or the small phase increment alteration technique (SPINAL 64) with a proton RF field of ~ 90 kHz was used (Bennett *et al.,* 1995; Fung *et al.,* 2000). 256 scans per increment were collected, with an effective evolution time of ~ 6 ms (for the 2D ^{13}C-^{13}C experiments) and 2.6 ms (for the 2D NCO experiment) in the indirect dimension. The 2D ^{13}C-^{13}C data were recorded in 2-5 days, depending on the length of the PDSD mixing time and the 2D NCO data was recorded in 12 hours.

2.2.13.1 1D ^{13}C- and ^{15}N-CP/MAS experiments

One-dimensional (1D) CP/MAS NMR spectra were recorded by Dr. Matthias Hiller on a 700 MHz wide-bore or on a 900 MHz narrow-bore spectrometer at an MAS frequency (wR/2ρ) of 11 kHz or 18 kHz.

1D ^{13}C solid-state MAS NMR spectra of [GALVSHF$_{\alpha,\beta}$Y$_{\alpha,\beta}$, ^{15}N]-OmpG 2D crystals at pH 7.5 and pH 5.6 were recorded with 1024 scans, with a proton-decoupling power of 80 kHz and a spinning frequency of 11 kHz at 280 K on a 700 MHz wide-bore spectrometer.

1D ^{15}N-CP solid-state MAS NMR spectra of [GALVSHF$_{\alpha,\beta}$Y$_{\alpha,\beta}$, ^{13}C]-OmpG 2D crystals at pH 7.5 and pH 5.6 were recorded with 4096 scans, with a proton-decoupling power of 80 kHz and a spinning frequency of 11 kHz at 280 K on a 700 MHz wide-bore spectrometer.

1D ^{15}N-CP solid-state MAS NMR spectra of [GALVSHF$_{\alpha,\beta}$Y$_{\alpha,\beta}$, ^{13}C]-OmpG 2D crystals at pH 7.5 and pH 5.6 were recorded with 4096 scans on a 900 MHz narrow-bore spectrometer with a spinning frequency of 18 kHz at 280 K.

1D ^{13}C-CP/MAS [^{13}C, ^{15}N]-GENDPQARS-OmpG was recorded on a 900 MHz spectrometer with an MAS frequency of 18 kHz at 280 K.

2.2.13.2 2D ^{13}C-^{13}C PDSD experiments

2D ^{13}C-^{13}C spectra of OmpG were recorded by Dr. Matthias Hiller on a 700 MHz wide-bore or 900 MHz narrow-bore spectrometer at an MAS frequency (wR/2ρ) of 11 or 13 kHz, using the proton-driven spin diffusion (PDSD) mixing scheme (Szeverenyi *et al.,* 1982).

2D ^{13}C-^{13}C PDSD solid-state MAS NMR spectrum of [GALVSHF$_{\alpha,\beta}$Y$_{\alpha,\beta}$, ^{15}N]-OmpG 2D crystals at pH 7.5 was recorded at 700 MHz, 280 K, with a PDSD mixing time of 50 ms and an MAS frequency of 11 kHz (data not shown in chapter 3).

2D ^{13}C-^{13}C PDSD solid-state MAS NMR spectrum of [GALVSHF$_{\alpha,\beta}$Y$_{\alpha,\beta,}$ ^{15}N]-OmpG 2D crystals at pH 5.6 was recorded at 900 MHz, 280 K, with a PDSD mixing time of 50 ms and an MAS frequency of 13 kHz.

2D ^{13}C-^{13}C PDSD NMR spectra of the [GALVSHF$_{\alpha,\beta}$Y$_{\alpha,\beta}$, ^{15}N]-OmpG at pH 7.5 and at pH 5.6 were recorded at 900 MHz, 280 K, with a PDSD mixing time of 50 ms and an MAS frequency of 13 kHz. Successively 2D ^{13}C-^{13}C PDSD NMR spectra of the [GALVSHF$_{\alpha,\beta}$Y$_{\alpha,\beta}$, ^{15}N]-OmpG at pH 7.5 and at pH 4.7 were recorded with a mixing time of 50 ms and an MAS frequency of 18 kHz.

The spectrum of the [GANDSH, ^{15}N]-OmpG sample at pH 7.5 was recorded with a mixing time of 20 ms and an MAS frequency of 13 kHz on a 900 MHz machine at 280 K.

2D ^{13}C-^{13}C PDSD spectrum of [GENDQPASR,^{15}N]-OmpG at pH 7.5 was recorded at 900 MHz, 280 K, with a PDSD mixing time of 20 ms and an MAS frequency of 18 kHz.

2.2.13.3 2D NCO experiment (Baldus *et al.,* 1998)

2D NCO spectrum of 2D crystals of [^{13}C, ^{15}N]-GALVSHF$_{\alpha,\beta}$Y$_{\alpha,\beta}$-OmpG was recorded by Dr. Hiller on a 700 MHz spectrometer at 13 kHz MAS frequency at 280 K.

2.2.13.4 NMR Data processing and analysis

All NMR data were processed with TOPSPIN, version 2.1 (Bruker, Germany). The spectra images were analysed with Coreldraw® 10 (Corel Corporation, Ottawa, Ontario, Canada). The data were analysed using CCPNmr analysis (Vranken *et al.,* 2005). The images of protein structures were performed with the software PyMOL (DeLano scientific LLC, San Francisco, California, USA).

3 Results and discussions

In this work, different labelling approaches and different solid-state MAS NMR methods are described to investigate the pH-dependent structural rearrangement and substrate-binding of the outer membrane protein G (OmpG, 281 residues) from *E. coli*. OmpG is a 14-stranded β-barrel with six periplasmic turns (T1-T6) and seven extracellular loops (L1-L7) (Yildiz *et al.,* 2006). It has been shown that the entrance of the channel is gated in a pH-dependent manner (Conlan *et al.,* 2003; Yildiz *et al.,* 2006). At pH 7.5 the channel is opening, allowing the substrate uptake, whereas at pH 4.7 loop 6 folds into the pore and constricts the channel entrance. This structural rearrangement may be triggered by two solvent-exposed residues (His 231 and His 261) (Yildiz *et al.,* 2006). Within the pore, sugar molecules are coordinated by hydrogen bonds to residues Trp 131, Tyr 135, Glu 152, Glu 154, Arg 168, Tyr 196 and Glu 253. To study the pH gating mechanism and the substrate uptake by solid-state MAS NMR were prepared two specifically [^{13}C, ^{15}N]-labelled samples: GALVSHF$_{\alpha,\beta}$Y$_{\alpha,\beta}$-OmpG (to investigate the pH gating mechanism) and GENDQPASR-OmpG (to investigate substrate binding). Both samples were expressed, purified as described earlier (Hiller *et al.,* 2005), crystallised, analysed by electron microscopy and subsequently packed into NMR rotors. To study the pH gating mechanism 1D ^{13}C-^{15}N and 2D ^{13}C-^{13}C solid-state NMR spectra of the [^{13}C, ^{15}N]-GALVSHF$_{\alpha,\beta}$Y$_{\alpha,\beta}$ sample were recorded at different pH values (pH 7.5 and pH 4.7). To characterise the labelling scheme of the [^{13}C, ^{15}N]-GENDQPASR sample a 2D ^{13}C-^{13}C spectrum was recorded. The starting point was the work of Dr. Hiller (2009). In that work samples were prepared in which the backbone nitrogen atoms of all 20 amino acids are ^{15}N-labelled. This was achieved by growing *E. coli* cultures on M9 medium containing ^{15}N-NH_4Cl and uniformly ^{13}C-labelled glucose or glycerol supplemented with unlabelled amino acids, whose ^{13}C-labelling is been suppressed. This strategy is called reverse labelling. Another possibility that was used for this research is the forward labelling strategy where the growth of *E. coli* cultures on M9 minimal medium was supplemented with labelled and unlabelled amino acids as sources of carbon and nitrogen. These samples have to be planned carefully, as several amino acids are building blocks for the synthesis of other amino acids, and isotope dilution to other amino acids can occur. The labelling scheme proposed in this thesis was chosen in a way to minimise isotope dilution, to decrease spectral overlap and to provide complementary information for the ambiguous identification of the assignment's starting point of OmpG. Each labelled sample was purified and reconstituted into 2D crystals as described in paragraphs 3.1 and 3.2.

3.1 Protein labelling strategy: [^{13}C, ^{15}N]-GALVSHF$_{\alpha,\beta}$Y$_{\alpha,\beta}$-OmpG

According to the X-ray Crystallography (Yildiz Ö *et al.,* 2006), OmpG at pH 7.5 is in the opening conformation, allowing the incoming of the sugars, and is in a closing conformation at pH 5.6. Looking for a pH-sensitive switch that can trigger the opening/closing mechanism the authors found two His (His 231 and His 261) that are involved in this different rearrangement at different pH's. When the channel is in the opening conformation at pH 7.5 His 231 (on loop 6) forms an H-bond with Ser 218 (on β-strand 11) and His 261 (on loop 7) forms another H-bond with Asp 267 (on β-strand 14). At pH 5.6, when the channel is in the closing conformation, the imidazoles of His 231 and His 261 are protonated and repeal each other, as there is an electrostatic interaction. This repulsion folds loop 6 inside the pore of the channel, thus blocking the channel in a closing conformation (figure 3.1). The pH gating is also confirmed by other studies: Conlan *et al.,* 2003; Chen *et al.,* 2008; Damaghi *et al.,* 2010; Mari *et al.,* 2010; Korkmaz *et al.,* 2012.

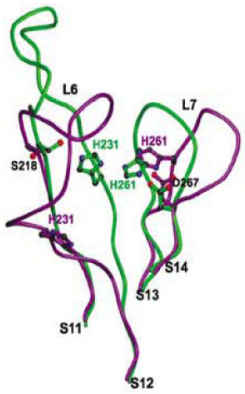

Figure 3.1 Loops L6 and L7 in the opening (green) and closing (purple) conformation. His 231 in L6 and His 261 in L7 combined act as a pH-sensitive switch, with the protonated side chains repelling one another at low pH. In the opening conformation, L6 is stabilised by hydrogen bonds from His 231 to Ser 218 and from His 261 to Asp 267. This image was taken from Yildiz (Yildiz *et al.,* 2006).

The first objective of this work is the investigation of this different rearrangement of OmpG at different pH's by solid-state MAS NMR. To study the movement of L6 and L7 between the opening and the closing state, a sample of OmpG was prepared which is specifically [^{13}C, ^{15}N]-GALVSHF$_{\alpha,\beta}$Y$_{\alpha,\beta}$ labelled. The following AAs were labelled (figure 3.2) in OmpG on the one hand to reduce overlapping signals in the spectra and on the other hand to assign them

at different molecular states (especially His signals). The mature form of OmpG contains 280 amino acids. It was expressed without the signal sequence, but with an N-terminal methionine. It will be discussed later.

```
1-   MEERNDWHFN IGAMYEIENV EGYGEDMDGL AEPSVYFNAA NGPWRIALAY YQEGPVDYSA-60
                            L1                                    L2
61-  GKRGTWFDRP ELEVHYQFLE NDDFSFGLTG GFRNYGYHYV DEPGKDTANM QRWKIAPDWD-120
                                                  L3
121-VKLTDDLRFN GWLSMYKFAN DLNTTGYADT RVETETGLQY TFNETVALRV NYYLERGFNM-180
                          L4
181-DDSRNNGEFS TQEIRAYLPL TLGNHSVTPY TRIGLDRWSN WDWQDDIERE GHDFNRVGLF-240
     L5                                                   L6
241-YGYDFQNGLS VSLEYAFEWQ DHDEGDSDKF HYAGVGVNYS F-281
                          L7
```

Figure 3.2 OmpG protein sequence. Loops 1, 2, 3, 4, 5, 6 and 7 are indicated and underlined by blue letters. The labelled amino acids are indicated by red letters.

To understand the labelling strategies adapted to prepare this specific labelled OmpG sample it is very important to consider the metabolism of the AAs in *E. coli* (figure 3.3).

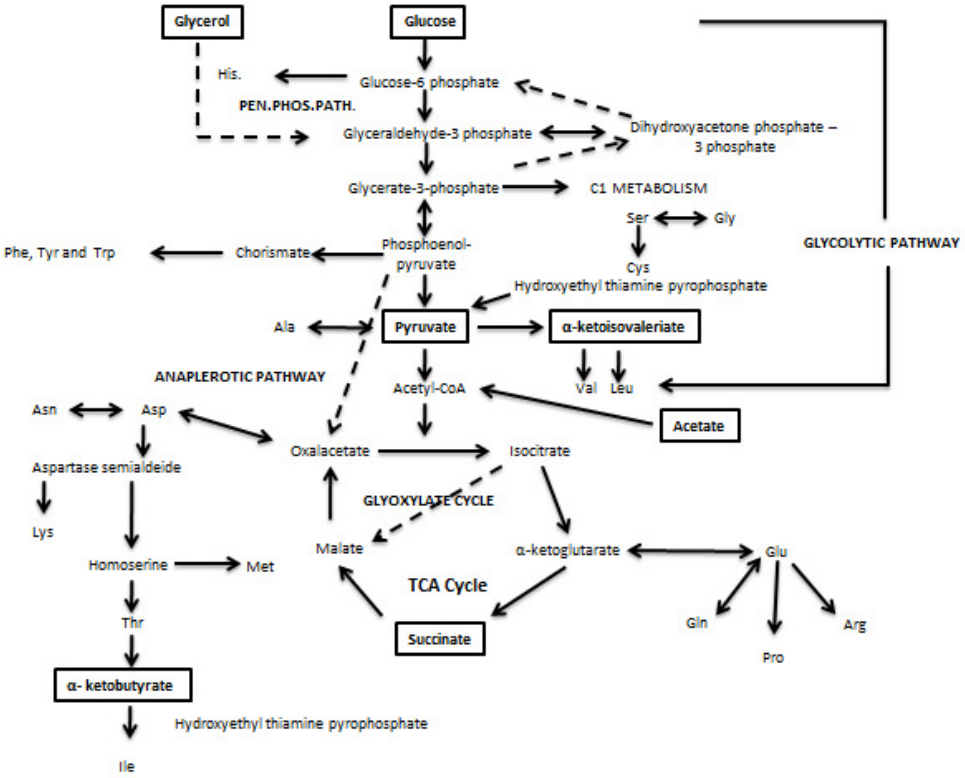

Figure 3.3 Schematic of amino acid biosynthesis in *E. coli*. Amino acid biosynthetic pathway in bacteria, utilising glycerol and glucose as the sole carbon source. The precursory compounds of the twenty amino acids are shown.

To avoid an overlapping signal in the aromatic region Trp was not labelled as it has almost the same chemical shift as His. The indole carbons of Trp have chemical shifts similar to the imidazole carbons of His in the region between 140–120 ppm in the 2D ^{13}C-^{13}C spectrum (which also applies to the Cα and Cβ of Trp and His). To avoid the overlapping of the signal in the aromatic region of the His' imidazole carbons with the phenyl and phenol carbons of the Phe and Tyr, these were, as well, labelled in α and β positions respectively. Leucine and valine were labelled to increase the signal of the latter (figure 3.4).

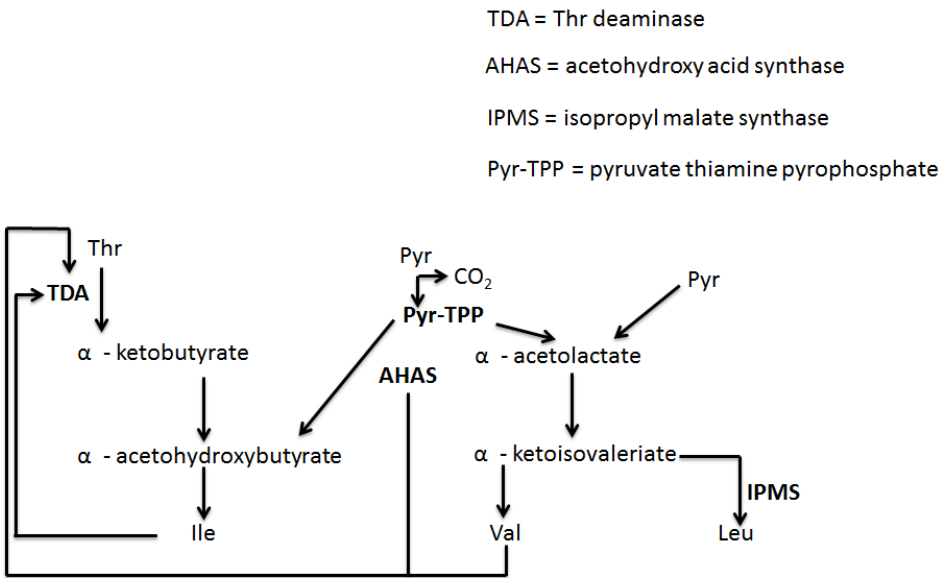

Figure 3.4 Biosynthetic pathways of the branched AA side chains in *E. coli* K12 (Yang *et al.*, 2005, www.expasy.ch).

In addition were labelled serine, alanine and glycine to increase the signal of the serine and glycine necessary for the sequential assignment, always considering the biochemical pathway of these AAs in *E. coli* (figure 3.5).

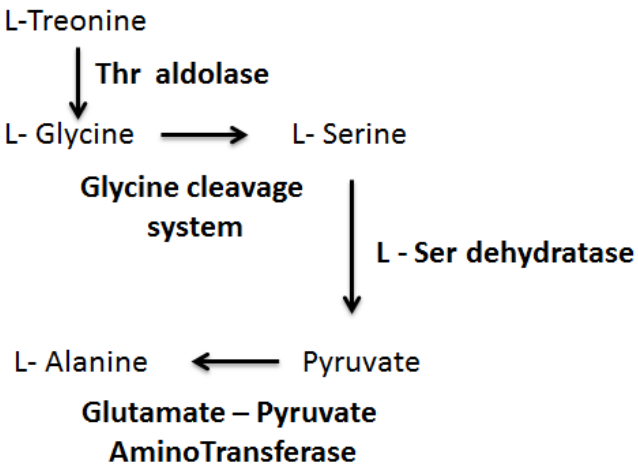

Figure 3.5 Biosynthetic pathways of Ser, Gly and Ala in *E. coli.*

3.1.1 Expression and purification of the [^{13}C, ^{15}N]-GALVSHF$_{\alpha,\beta}$Y$_{\alpha,\beta}$-OmpG and U-[^{13}C, ^{15}N]-OmpG.

The availability of high amounts (>10 mg) of a homogeneous isotopically labelled protein sample in terms of purity and conformation is an essential pre-requisite for structural analysis of proteins by NMR. OmpG was expressed without the leader peptide causing the formation of non-functional cytoplasmic inclusion bodies. The expression of OmpG in inclusion bodies was favoured for the following reasons: the cultures must be grown in M9 minimal media with the addition of isotopically labelled AAs, which represent carbon and nitrogen sources. For the native expression, this would result in high costs even for 10 mg of labelled protein; the expression of inclusion bodies is like a purification step containing the over-expressed protein (>95 %) in denatured form; other outer membrane proteins have been refolded with high yield, so inclusion bodies provide a successful strategy to express recombinant protein, which can be adapted for OmpG (Bannwarth *et al.,* 2003).

OmpG was expressed without the signal peptide but with an N-terminal methionine (starting with M-EERNDWH…) in *E. coli* BL21(DE3) (Miroux and Walker, 1996). NMR samples were prepared as described with the following exception (Hiller *et al.,* 2005). Using LB medium for cultivation after the inoculation of the overnight culture, the BL21(DE3) easily achieved a cell density of 0.7. The curve in figure 3.6 describes the growth of the *E. coli* BL21(DE3) in exchanged media using the protocol of Marley (Marley *et al.,* 2001). After one hour of incubation in M9 minimal medium to recover the growth and clearance of unlabelled

metabolites, the recombinant protein was induced with 1mM IPTG. At this point the optical density measured at 600 nm was 4.5–5.

The labelled and unlabelled AAs implemented in M9 minimal medium represent the carbon and nitrogen sources for the *E. coli* BL21(DE3) strain. After three hours of IPTG induction, the *E. coli* BL21(DE3) strain reached optical density of 6.7–7 and the cells were harvested. The bio wet mass obtained using this protocol was 15.4 g, considering that 8 ℓ of LB for cell production were used and the cell pellet was resuspended in 2 ℓ of M9 minimal medium implemented with 200 mg of labelled AAs (GALVSHF$_{\alpha,\beta}$Y$_{\alpha,\beta}$) and 200 mg of unlabelled AAs (TIQDENKPMWRC).

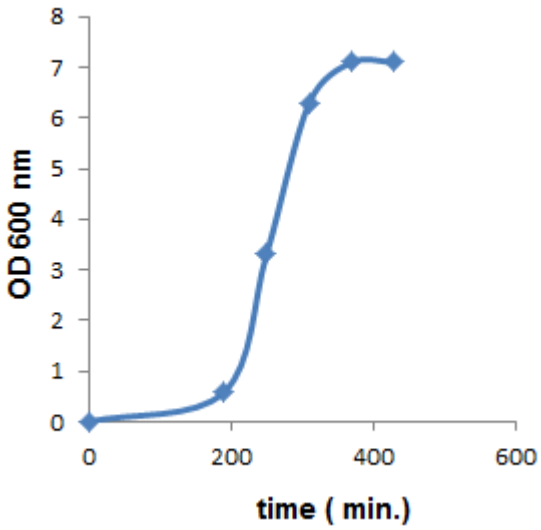

Figure 3.6 Growth curve of *E. coli* BL21(DE3) cells in exchanged medium implemented with uniformly labelled AAs according to the modified protocol expression of Marley (Marley *et al.*, 2001).

The protein content of uninduced cells one hour before the IPTG (1mM) induction and once per hour afterwards was analysed with SDS-PAGE taking a 1 ml sample. All SDS-PAGE samples were normalised to an OD_{600nm} = 1 (figure 3.7). After three hours the complete cell suspension was harvested by centrifugation at 5.000 g for 15 min at 8 ℃.

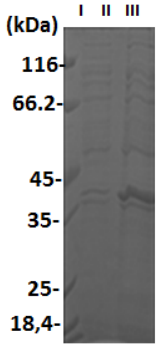

Figure 3.7 SDS-PAGE analysis of [^{13}C, ^{15}N]-GALVSHF$_{\alpha,\beta}$Y$_{\alpha,\beta}$-OmpG. Lane I = molecular weight marker (Fermentas); lane II and III = OmpG samples one hour before and three hours after induction with IPTG 1mM. These samples were centrifuged at 5.000 rpm for 10 min. The supernatant was discarded and the cell pellet was resuspended with 9 µl H_2O, 1 µl SDS (20 % w/v) and 10 µl gel loading buffer 2X (GLB 2X).

For the preparation of uniform [^{13}C, ^{15}N]-OmpG were additionally used 8 ℓ of LB medium for cells production. The cells were harvested when their growth reached an OD_{600nm} = 0.7. The cell pellet was resuspended in 3 ℓ of M9 minimal medium. The carbon and nitrogen sources were represented by ^{13}C glucose (2 g/ ℓ) and ^{15}N NH_4CL (0.5 g/ ℓ). After one hour of incubation in M9 minimal medium to recover the growth and clearance of unlabelled metabolites, the recombinant protein was induced with 1 mM of IPTG. At this point the OD_{600nm} was almost 2.5. After three hours of IPTG (1 mM) induction the cells reached an OD_{600nm} = 3.5 and were harvested. The bio wet mass obtained using this protocol was almost 10 g/ 3 ℓ culture.

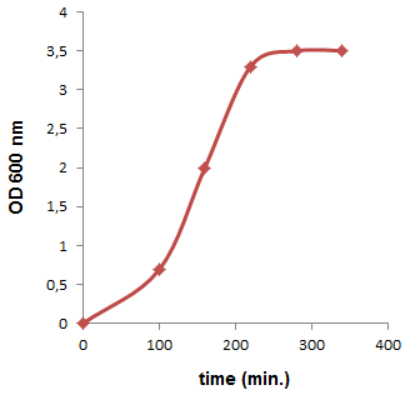

Figure 3.8 Growth curve of *E. coli* BL21(DE3) cells in exchanged medium implemented with uniformly labelled glucose and $^{15}NH_4Cl$ according to the modified protocol expression of Marley (Marley *et al,* 2001).

The protein content of uninduced cells one hour before the IPTG (1mM) induction and once per hour afterwards was analysed with SDS-PAGE taking a 1 ml sample. All SDS-PAGE samples were normalised to an OD_{600nm} = 1 (figure 3.9). After three hours the complete cell suspension was harvested by centrifugation at 5.000 g for 15 min at 8 ℃.

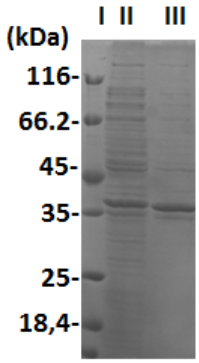

Figure 3.9 SDS-PAGE analysis of U-[^{13}C, ^{15}N]-OmpG. Lane I = molecular weight marker (Fermentas); lanes II and III = OmpG samples one hour before and three hours after induction with IPTG 1 mM. These samples were centrifuged at 5000 rpm for 10 min. The supernatant was discarded and the cell pellet was resuspended with 9 µl H_2O, 1 µl SDS (20 % w/v) and 10 µl gel loading buffer 2X (GLB 2X).

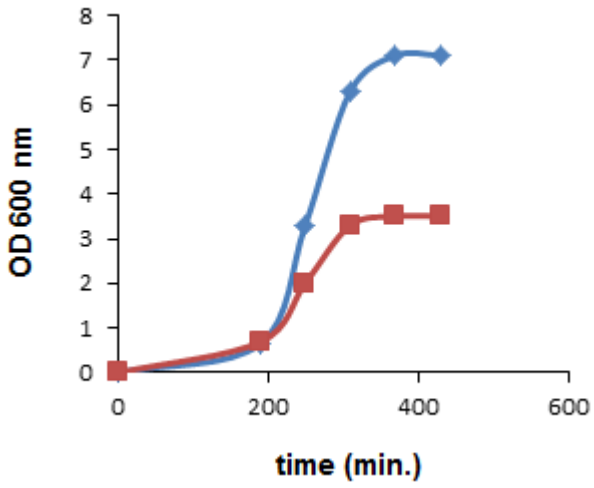

Figure 3.10 Overlay of the growth curves of *E. coli* BL21(DE3) cells in exchanged medium, implemented with uniformly labelled glucose and $^{15}NH_4Cl$ (red), and *E. coli* BL21(DE3) cells in exchanged medium, implemented with uniformly labelled AAs (blue), according to the modified protocol expression of Marley (Marley *et al,* 2001).

From other experiments it is known that the target protein (OmpG) is expressed as insoluble inclusion bodies (Bannwarth *et al.,* 2003). After the solubilisation of the inclusion bodies, 212

mg of protein in denatured form were yielded because the inclusion bodies, which contain OmpG in denatured form, were dissolved with 8 M urea, a chaotropic agent. The denatured protein was not perfectly pure so it needed purification. Therefore a first anion exchange chromatography (Source Q Column, figure 3.11 from lane VIII to XIX) was performed to separate the pure denatured protein from the residual lipids DNA and RNA that co-precipitated with the insoluble part of the protein (inclusion bodies). This procedure yielded up to 155 mg of [^{13}C, ^{15}N]-GALVSHF$_{\alpha,\beta}$Y$_{\alpha,\beta}$-OmpG from the 212 mg obtained from the solubilisation of the inclusion bodies. The anion exchange chromatography was chosen due to the calculated number of positive (22) and negative charges (50) at the isoelectric point of OmpG (4.28) using *Protparam www.expasy.ch.* The protocol applied is shown in the methods chapter and it was performed in our laboratory following the purification procedure of Conlan (Conlan *et al.,* 2000). OmpG started to elute when the concentration of NaCl was almost 300 mM. However, the 155 mg of OmpG were denatured and had to be refolded in detergent micelles.

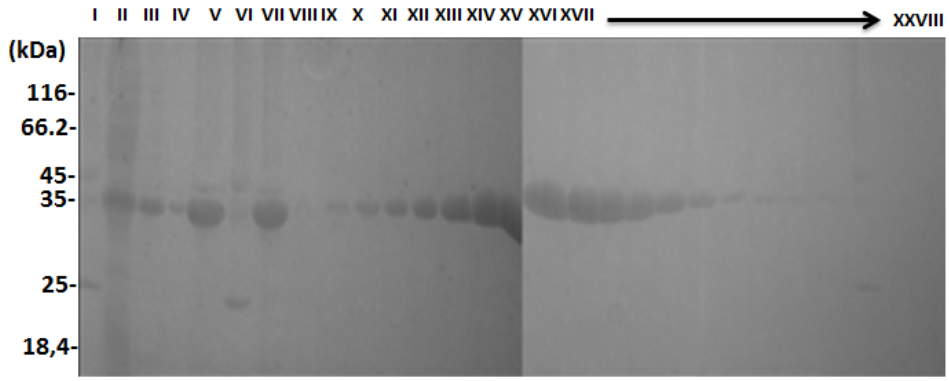

Figure 3.11 Solubilisation of the inclusion body fraction and purification by anion exchange chromatography of [^{13}C, ^{15}N]-GALVSHF$_{\alpha,\beta}$Y$_{\alpha,\beta}$-OmpG. Lane I = molecular weight marker (Fermentas); Lane II = soluble protein fraction after homogenisation; Lane III = supernatant after first inclusion bodies washing step; Lane IV = supernatant after second inclusion bodies washing step; Lane V = inclusion bodies fraction after solubilisation with 8 M urea; Lane VI = molecular weight marker (Fermentas); Lane VII = inclusion body fraction before loading onto the column; Lanes VII to XXIII = OmpG eluate at 300 mM NaCl.

The cell growth to express U-[^{13}C, ^{15}N]-OmpG as insoluble inclusion bodies followed the same procedure as before, yielding 374,7 mg of not completely pure denatured OmpG from 3 ℓ of culture after the solubilisation of the inclusion bodies (figure 3.12).

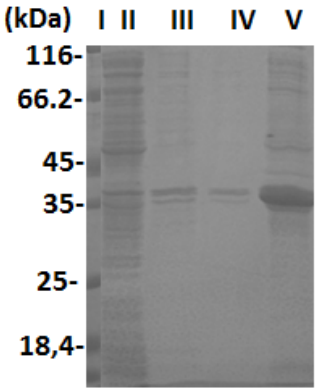

Figure 3.12 Solubilisation of the inclusion body fraction of U-[^{13}C, ^{15}N]-OmpG. Lane I = molecular weight marker (Fermentas); Lane II = soluble protein fraction after homogenisation; Lane III = supernatant after first inclusion bodies washing step; Lane IV = supernatant after second inclusion bodies washing step; Lane V = inclusion bodies fraction after solubilisation with 8 M urea.

After the purification by a first anion exchange chromatography the total yield of denatured pure protein was 179.7 mg from 3 ℓ of culture (figure 3.13).

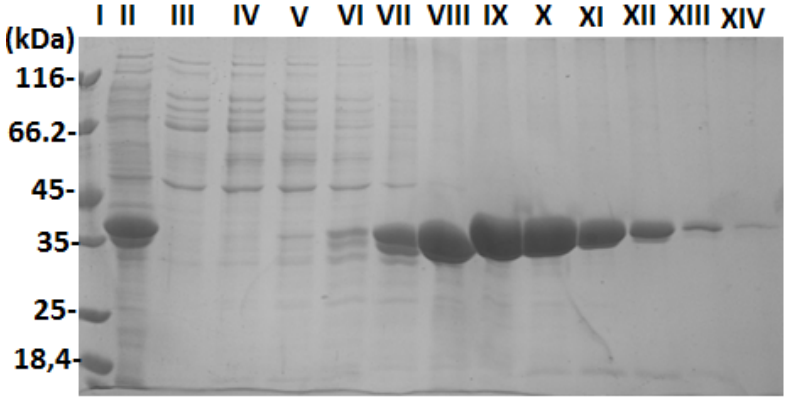

Figure 3.13 Purification by anion exchange chromatography of U-[^{13}C, ^{15}N]-OmpG. Lane I = molecular weight marker (Fermentas); Lane II = inclusion body fraction before loading onto the column; Lanes III to XIV = OmpG eluate at 300 mM NaCl.

However, the 155 mg of [^{13}C, ^{15}N]-GALVSHF$_{\alpha,\beta}$Y$_{\alpha,\beta}$-OmpG and the 179.7 mg of U-[^{13}C, ^{15}N]-OmpG were denatured and had to be refolded in detergent micelles.

3.1.2 A modified protocol expression (Marley *et al.,* 2001)

To improve the yield of isotopically labelled protein a modified expression protocol based on normal shaking flasks was tested. Marley (Marley *et al*., 2001) introduced a procedure for the production of isotopically labelled proteins that permits high yields of labelled protein reducing significantly the cost in both isotopes and production time (figure 3.14). First, the cell mass is predominantly produced in unlabelled rich media (LB media) allowing fast growth to high cell densities. Following their growth in LB media, cells are exchanged into M9 minimal media with labelled carbon and nitrogen sources. During this step, cells can be concentrated by centrifugation and resuspension in a smaller volume of isotopically labelled M9 minimal medium. After one hour of incubation to recover the growth and clearance of unlabelled metabolites, the protein expression can be induced (figure 3.13).
This method was followed, so as to produce high amounts of recombinant isotopically labelled OmpG. The results for a [GALVSHF$_{\alpha,\beta}$Y$_{\alpha,\beta}$]-OmpG sample in which only the amino acids Ala, Gly, Leu, Val, Ser and His were uniformly [^{13}C, ^{15}N]-labelled and the amino acids phenylalanine and tyrosine were labelled only in positions 2 and 3 are shown in table 2.2. In summary, a number of OmpG samples has been expressed with different sole carbon sources using the modified expression protocol. The improvement of protein yields reduces the costs for isotopically labelled sources. It has to be mentioned here that isotopic incorporation rate could not be determined by mass spectrometry for the labelled OmpG samples. This might be due to the strong hydrophobicity of the protein. Marley (Marley *et al*., 2001) described an isotopic incorporation rate of 95 % for ^{13}C and 90 % for ^{15}N nuclei. It was shown that this reduced isotope incorporation has no significant influence on the sensitivity of the recorded NMR experiments. Thus, the method offers an alternative to fermenter cultivation, which requires additional set-up time and specialised equipment. The time required to prepare isotopically labelled samples using this method is slightly longer than that using the standard expression protocol. However, the initial growth on unlabelled rich media is time-saving in comparison to the standard protocol, which requires significantly longer time spans to reach cell densities suitable for the induction of protein expression.

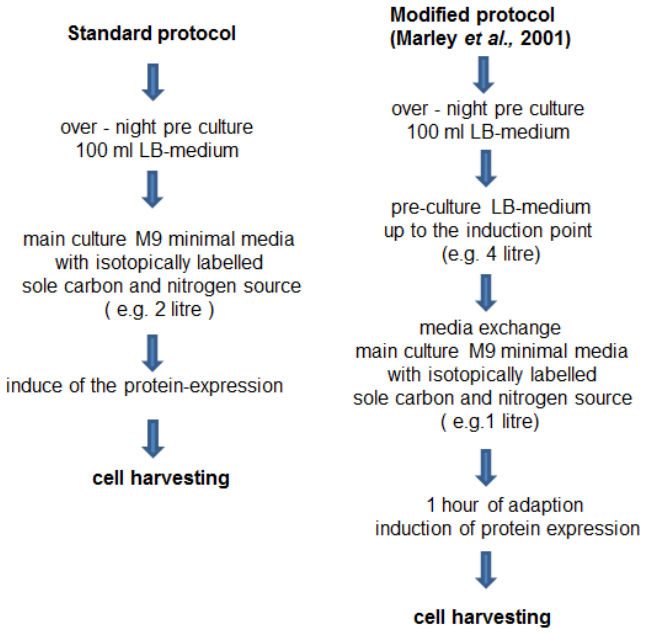

Figure 3.14 Schematic representation of the standard and the modified cultivation protocols.

3.1.3 Refolding of [^{13}C, ^{15}N]-GALVSHF$_{\alpha,\beta}$Y$_{\alpha,\beta}$-OmpG and U-[^{13}C, ^{15}N]-OmpG

Typically, denatured OmpG was diluted into buffer up to a protein concentration of 50 µg/ ml. The refolding buffer contains 1mM of DDM and 0.6 M of L-Arg. The refolding efficiency was monitored by SDS-PAGE (figure 3.15). The CMC of DDM is almost 0.17 mM and its aggregation number is 98.

OmpG refolding was screened by dilution of the denatured form in different detergents with different chain lengths at concentration above their CMC (Conlan *et al.,* 2000). The refolding efficiency was monitored and compared by differential migration of the folded and unfolded form of OmpG on SDS-PAGE gels, which depends on whether the sample was heated before analysis or not (Beher *et al.,* 1980). The denatured form of OmpG in urea migrates at an apparent molecular weight of 34 kDa, whereas the refolded form runs at around 28 kDa (figure 3.15, Fajardo *et al.,* 1998).

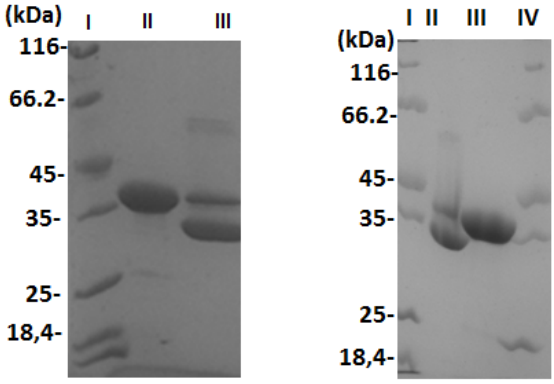

Figure 3.15 [^{13}C, ^{15}N]-GALVSHF$_{\alpha,\beta}$Y$_{\alpha,\beta}$-OmpG on the left and U-[^{13}C, ^{15}N]-OmpG on the right refolded by rapid dilution into a detergent containing buffer. On the left [^{13}C, ^{15}N]-GALVSHF$_{\alpha,\beta}$Y$_{\alpha,\beta}$-OmpG: Lane I = molecular weight marker (Fermentas); Lane II = denatured protein; Lane III = refolded protein. On the right U-[^{13}C, ^{15}N]-OmpG: Lane I = molecular weight marker (Fermentas); Lane II = refolded protein; Lane III = denatured protein; Lane IV = molecular weight marker (Fermentas).

The gels were run at 4 °C to prevent heat denaturation. 70 % refolding was observed with DDM. To improve the refolding efficiency achieved by DDM, L-arginine was used as an additive in the refolding buffer. The addition of 0.6 M of L-arginine improves the refolding efficiency up to more than 90 %. Arakawa (Arakawa *et al.,* 2007) showed that L-arginine increases the yield of folded protein by suppressing protein aggregation during the refolding reaction. It has intermediate properties between guanidine HCl (salting-in agent) and betaine (protein stabiliser). The refolding procedure yielded up to 155 mg of [^{13}C, ^{15}N]-GALVSHF$_{\alpha,\beta}$Y$_{\alpha,\beta}$-OmpG/ 2 ℓ of culture and 179.7 mg/ 3 ℓ of culture for U-[^{13}C, ^{15}N]-OmpG. From the purification of the solubilised inclusion bodies to the refolding, the needed concentration of OmpG is exactly the same for the two differently labelled samples. This demonstrates the efficiency of the applied refolding procedure (figure 3.15).

Usually an excess of detergent is normally employed when OmpG is solubilised from native membrane, to ensure complete dissolution of the membrane and to provide a large number of micelles with one protein molecule each. A second anion exchange chromatography was used after the refolding procedure to reduce the detergent concentration from 1 mM DDM to 0.4 mM DDM (to reconstitute the protein in lipid bilayer and to separate the 10 % of the unfolded protein). At the end of the second anion exchange chromatography the yield of the protein is almost 80 mg/ 2 ℓ of culture for [^{13}C, ^{15}N]-GALVSHF$_{\alpha,\beta}$Y$_{\alpha,\beta}$-OmpG and 78.1 for U-[^{13}C, ^{15}N]-OmpG/ 3 ℓ of culture. In this case a portion of the protein was lost during the

refolding procedure, but the obtained amount was enough for solid-state MAS NMR studies (figure 3.16).

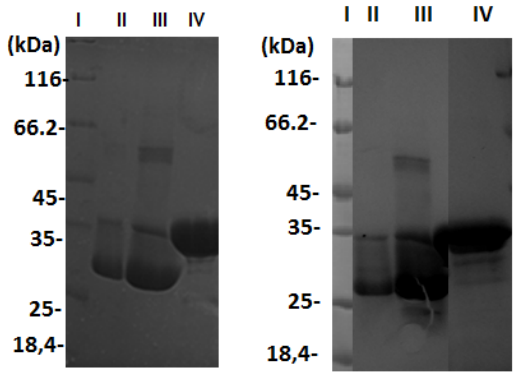

Figure 3.16 [^{13}C, ^{15}N]-GALVSHF$_{\alpha,\beta}$Y$_{\alpha,\beta}$-OmpG on the left and U-[^{13}C, ^{15}N]-OmpG on the right refolded after second anion exchange chromatography. Lane I = molecular weight marker (Fermentas); Lane II = control used to test the refolded protein; Lane III = refolded OmpG; Lane IV = unfolded OmpG.

3.1.4 2D crystals of reconstituted [^{13}C, ^{15}N]-GALVSHF$_{\alpha,\beta}$Y$_{\alpha,\beta}$-OmpG

With membrane proteins different preparation types are possible. In our case labelled OmpG was reconstituted into lipid bilayers to reproduce the natural biological condition. Solid-state MAS NMR experiments were performed using 2D crystals of [^{13}C, ^{15}N]-GALVSHF$_{\alpha,\beta}$Y$_{\alpha,\beta}$-OmpG at pH 7.5, 5.6 and pH 4.7 as well as [^{13}C, ^{15}N]-GENDQPASR-OmpG at pH 7.5. OmpG in its native lipid environment can be prepared with a high degree of homogeneity. This homogeneity is reflected in the resolution achievable in the electron microscopic projection maps of the reconstituted protein structure as well as in the [^{13}C, ^{13}C] correlation spectra, which are of exceptional quality and comparable to the spectra of a microcrystalline protein preparation (Linser *et al.,* 2011). 2D crystallisation of OmpG solubilised and purified from native membrane led to crystalline sheets (up to about 300 nm diffracting to 6 Å resolution) (Behlau *et al.,* 2001). These observations additionally confirmed that OmpG refolded from inclusion bodies had attained its native structure. The projection maps showed a circular molecule indicative of a β-barrel (diameter of 25 Å × 27 Å) and some strong central density, possibly reflecting the presence of loops covering the barrel opening (figure 3.17).

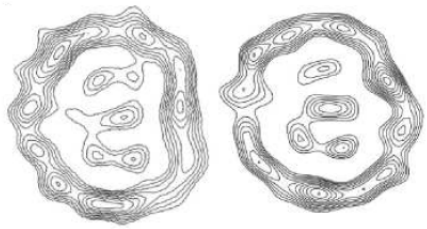

Figure 3.17 Comparison of projection density maps of 2D crystals from recombinant refolded OmpG (left) and native OmpG (right) at 8 Å resolution.

To crystallise OmpG at different pH's were used the crystallisation condition shown in table 3.1.

pH 7.5	pH 7	pH 5.6
Tris-HCl 20mM pH 7.5	Tris-HCl 20mM pH 7.0	Na-citrate 20mM pH 5.6
NaCl 150 mM	NaCl 150 mM	NaCl 150 mM
$MgCl_2$ 25 mM	$MgCl_2$ 25mM	$MgCl_2$ 25mM
NaN_3 3mM	NaN_3 3mM	NaN_3 3mM

Table 3.1 Composition of crystallisation buffers at different pH's.

Before the EM analysis the samples with different pH's were SDS-PAGE-analysed to check if the protein was still refolded in the lipid bilayer (figure 3.18). The SDS-PAGE analysis confirms us the stability of our sample at different pH's in lipid bilayers.

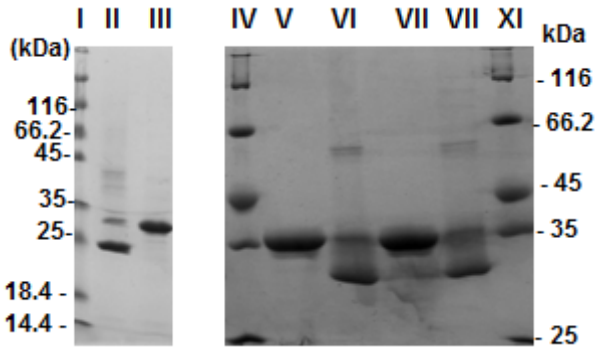

Figure 3.18 SDS-PAGE analysis of 2D crystals of OmpG at different pH's. SDS-PAGE on the left side: I = molecular weight marker (Fermentas); II = refolded protein at pH 7; III = denatured protein at pH 7. SDS-PAGE on the right side: IV = molecular weight marker (Fermentas); V = refolded protein at pH 7.5; VI = denatured protein at pH 7.5; VII = refolded protein at pH 5.6; VIII = denatured protein at pH 5.6; IX = molecular weight marker (Fermentas).

The obtained crystals were analysed by electron microscopy (figure 3.20).

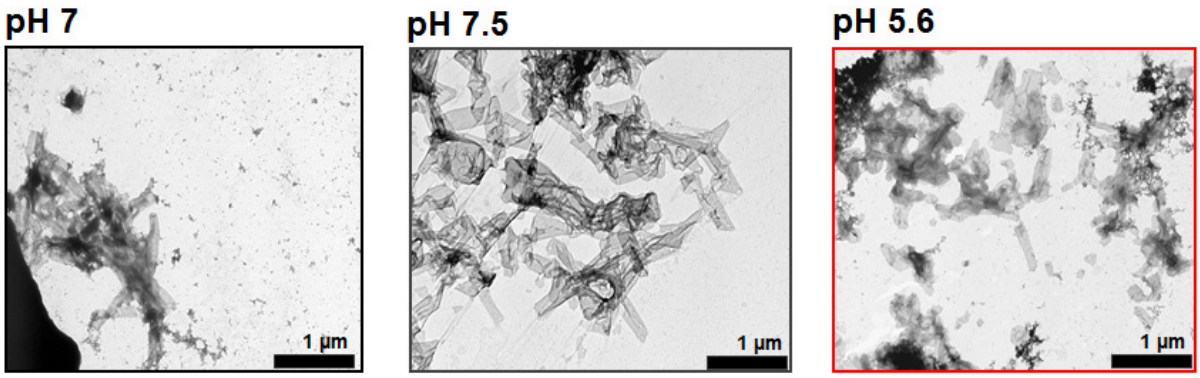

Figure 3.19 2D crystals of [^{13}C, ^{15}N]-GALVSHF$_{\alpha,\beta}$Y$_{\alpha,\beta}$-OmpG at pH 7.5, 7.0 and 5.6 (from left to right).

After the EM analysis were used the standard procedure to load the NMR sample in the 4 mm rotor: centrifugation at 14.000 rpm for 5 min at room temperature, resuspension of the 2D crystal pellets in phosphate buffer (the composition will be shown later) at different pH's and ultracentrifugation at 235.000 g, 8 °C overnight. During this procedure the labelled sample at pH 5.6 seems to show instability at acid pH. After the overnight ultracentrifugation the colour of the crystal pellets changed from the characteristic yellow to white (data not shown).

3.1.5 Solid-state MAS NMR characterisation: [^{13}C, ^{15}N]-GALVSHF$_{\alpha,\beta}$Y$_{\alpha,\beta}$-OmpG

The solid-state MAS NMR characterisation starts with the recording of the 1D ^{13}C-CP/MAS of the labelled sample at pH 7.5 and at pH 5.6.

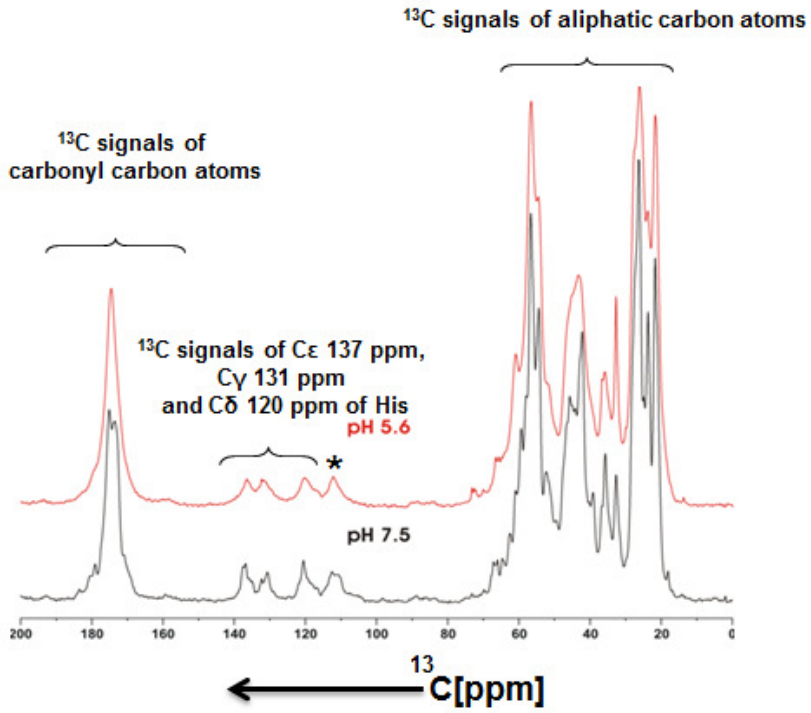

Figure 3.20 1D ^{13}C solid-state MAS NMR spectra of [GALVSHF$_{\alpha,\beta}$Y$_{\alpha,\beta}$, ^{15}N]-OmpG 2D crystals at pH 7.5 (black) and pH 5.6 (red). 1D ^{13}C spectrum was recorded with 1024 scans, with a proton-decoupling power of 80 kHz and a spinning frequency of 11 kHz at 280 K on the 700 MHz wide-bore spectrometer.

In figure 3.20 it is possible to see the signals of our labelled sample in different regions. In this spectrum there are the ^{13}C signals of aliphatic carbon of the side chain of all labelled AAs between 80–10 ppm. In the aromatic region there are the ^{13}C signals of Cε1 (137 ppm), Cγ (131 ppm) and Cδ2 (~ 120 ppm) of the His' imidazole without the aromatic signals of the phenyl and phenol of Phe and Tyr because these AAs were labelled only in α and β position. There was no overlapping in this region. The signals of the imidazole are evident and their chemical shift is in agreement with the values reported in www.bmrb.wisc.edu. The asterisk indicates the side band generated at 11 kHz MAS frequency. The spectrum at pH 7.5 shows

better (sharper) peaks than the spectrum at pH 5.6. This suggests a different conformation of the sample at these two different pH's.

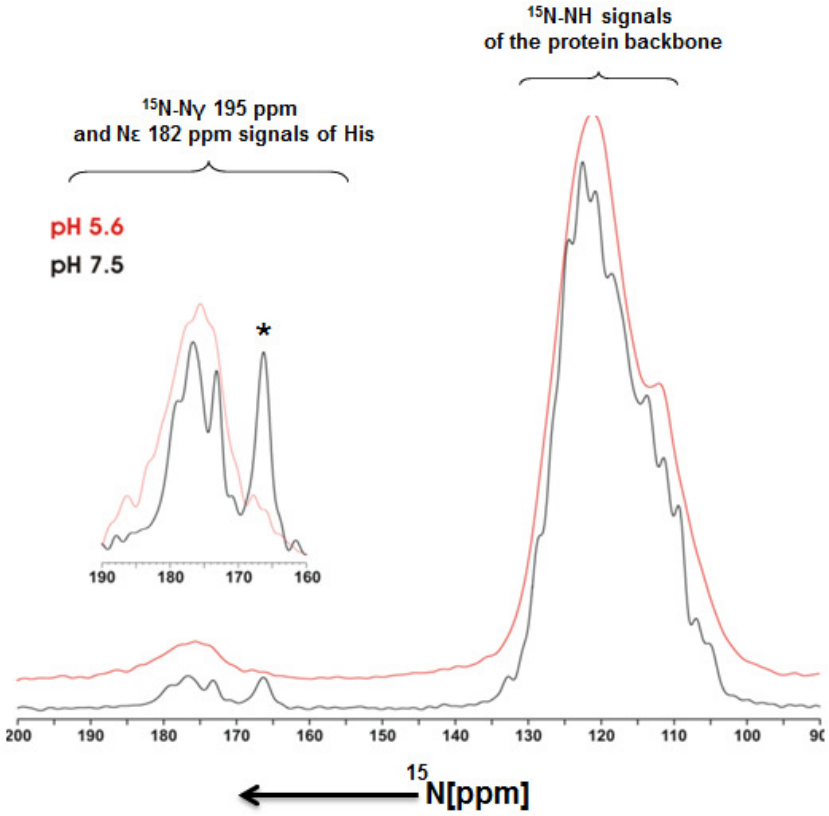

Figure 3.21 ^{15}N-CP solid-state MAS NMR spectra of [GALVSHF$_{\alpha,\beta}$Y$_{\alpha,\beta}$, ^{13}C]-OmpG 2D crystals at pH 7.5 (black) and pH 5.6 (red). The 1D ^{15}N spectrum was recorded with 4096 scans, with a proton-decoupling power of 80 kHz and a spinning frequency of 11 kHz at 280 K on a 700 MHz wide-bore spectrometer.

The ^{15}N-CP solid-state MAS NMR spectra (figure 3.21) of [GALVSHF$_{\alpha,\beta}$Y$_{\alpha,\beta}$,^{13}C]-OmpG 2D crystals at pH 7.5 show us a better resolution than the spectrum at pH 5.6. The peaks of the ^{15}N-NH amidic (around 120 ppm) of the protein backbone are much sharper in the spectrum at pH 7.5 than those at pH 5.6. In the region of the His' imidazole ring between 190–160 ppm some signals that appear at pH 7.5 disappear at pH 5.6 (it is indicated by the asterisk). The chemical shifts of the nitrogens were taken from BMRB website. This could maybe reinforce our hypothesis that the channel could change in conformation at different pH's, considering the different protonation state of the imidazole at different pH's.

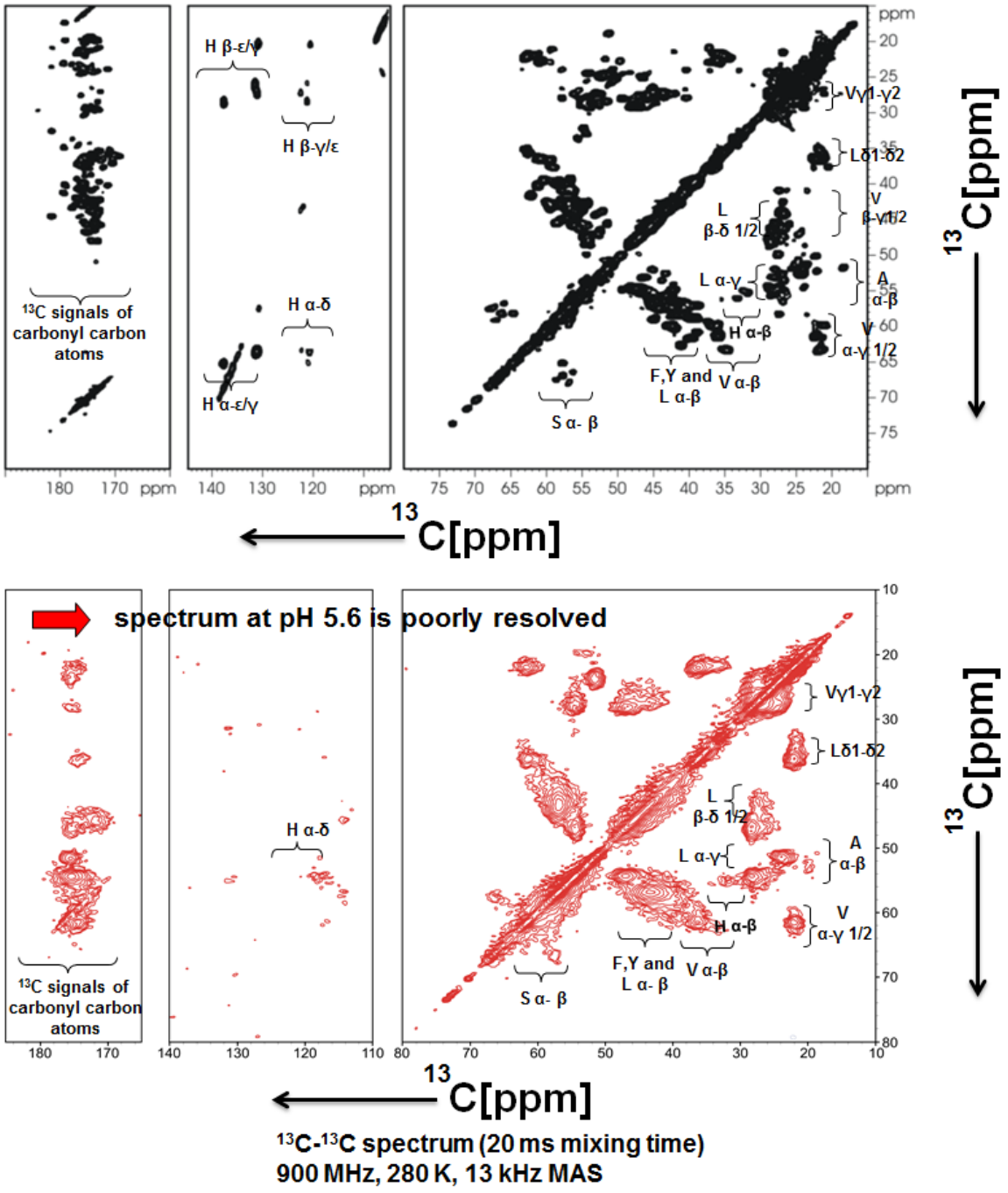

Figure 3.22 2D ^{13}C-^{13}C PDSD NMR spectra of the [GALVSHF$_{\alpha,\beta}$Y$_{\alpha,\beta}$]-OmpG at pH 7.5 (black) and at pH 5.6 (red). The spectra were recorded at 900 MHz, 280 K, with a mixing time of 50 ms and an MAS frequency of 13 kHz.

2D ^{13}C-^{13}C homonuclear correlation spectra of tubular OmpG 2D crystals were acquired by using the PDSD technique (Bloembergen, 1949; Suter and Ernst, 1985). In the 2D ^{13}C-^{13}C PDSD spectrum at pH 7.5 (shown in black in figure 3.22) are visible the complete side chain signal patterns for Ala, Gly, Phe, Tyr, Leu, Ser and Val. In addition, signals in the range of 50–60 ppm and 30–40 ppm are visible along with correlations to the imidazole region. These signals are in the typical chemical shift range of Cα and Cβ correlations of His residues. In the aromatic region it is possible to visualise the intraresidual correlations between the carbons of the imidazole and the histidine's aliphatic side chain. The only problem here is the overlay of the side bands with these intraresidual correlations. To see these signals better the spin should be increased to shift the side band at higher ppm. The strong diagonal signals arise from ^{13}C-labelled sites in OmpG and from the lipids' background, whose ^{13}C is naturally abundant. The unlabelled lipids do not give rise to detectable cross peaks due to the low abundance of adjacent ^{13}C nuclei. The first impression observing the spectrum at pH 5.6 (shown in red in the figure 3.22) was in the aliphatic region. The intraresidual correlations of the aliphatic side chain of all labelled AAs are broadened. This could suggest a fluctuation between the opening/closing conformations at pH 5.6. This consideration was similar to Conlan's (Conlan *et al.,* 2003) with single channel recording at the same pH. These fluctuations could generate broadened signals. In the aromatic region of the imidazole ring system some intraresidual correlations are lost, probably due to the channel's changes in conformation. The partial conclusion was that with the ^{13}C- and ^{15}N-CP/MAS NMR and 2D ^{13}C-^{13}C PDSD spectra at pH 7.5 and the same spectra at pH 5.6 it is possible to highlight changes that could be reflected in conformation changes of [GALVSHF$_{\alpha,\beta}$Y$_{\alpha,\beta}$]-OmpG 2D crystals at different pH's. 2D ^{13}C-^{13}C PDSD spectrum at pH 7.5 could confirm the opening state of the OmpG channel, but the spectrum at pH 5.6 might suggest the presence of fluctuations between opening/closing states at this pH (Conlan *et al.*, 2003). This could mean that it is necessary to prepare the same labelled sample at a lower pH to get the channel's spectrum in the closing state.

3.1.5.1 Going back to the preparation of the labelled sample at pH 5.6?

To understand if the labelled sample at pH 5.6 shows broadened signals either because it fluctuates between the opening/closing conformation or because there are problems in the preparation of the sample at pH 5.6 (in this case the 2D ^{13}C-^{13}C spectrum of the labelled sample at pH 5.6 shows a lower resolution, and not broadened signals, in comparison to the

labelled sample at pH 7.5), the labelled sample at pH 5.6 was removed from the 4 mm rotor, resuspended in PPi at pH 5.6 (20 mM phosphate buffer pH 5.6, 50 mM NaCl and 3 mM NaN_3) and loaded on the SDS-PAGE at different dilution states in gel loading buffer 2X. 1/10, 1/20 and 1/50 are the different dilution states. These three different diluted samples were compared with two different references (I and II) showing ~ 50 % of unfolded protein (figure 3.23).

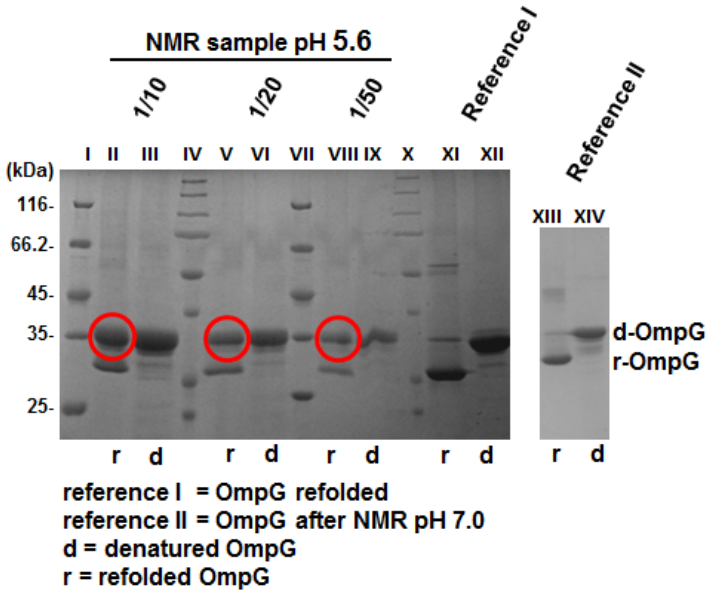

Figure 3.23 Analysis of OmpG sample at pH 5.6 after NMR measurement in comparison to two different references. Lane I = molecular weight marker (Fermentas); Lane II = partially unfolded OmpG at pH 5.6 (diluted state 1/10); Lane III = denatured OmpG at pH 5.6 (diluted state 1/10); Lane IV = molecular weight marker; Lane V = partially unfolded OmpG at pH 5.6 (diluted state 1/20); Lane VI = denatured OmpG at pH 5.6 (diluted state 1/20); Lane VII = molecular weight marker (Fermentas); Lane VIII = partially unfolded OmpG at pH 5.6 (diluted state 1/50); Lane IX = denatured OmpG at pH 5.6 (diluted state 1/50); Lane X = Marker; Lane XI = folded OmpG (reference I); Lane XII = denatured OmpG (reference I); Lane XIII = folded OmpG (reference II); lane XIV = denatured OmpG. r and d mean refolded and denatured.

The different references I and II are two samples of OmpG refolded with high efficiency. The first reference is an unlabelled refolded OmpG, the second reference is a labelled sample of OmpG reconstituted in a lipid environment at LPR 0.5 and pH 7 after NMR measurement (figure 3.23). In comparison, the three shown diluted samples of 2D crystals OmpG at pH 5.6 are still in their unfolded form. After NMR measurements OmpG at pH 5.6 is partially

unfolded. The unfolding could be triggered by the ultracentrifugation or by the spinning of the 4 mm rotor at MAS frequency 13 kHz. According to the X-ray crystallographers crystallising OmpG at pH 5.6 is difficult. The OmpG is in orthorhombic bipyramidal form but it does not show any trace of the crystal lattice. This does not explain how the monomer is generally able to assemble to a crystal lattice in orthorhombic bipyramidal form at pH 5.6. Instead, Conlan (Conlan *et al.,* 2003) showed by electrophysiological methods that OmpG at pH 5.6 fluctuates between the opening/closing conformation, as shown in figure 3.24.

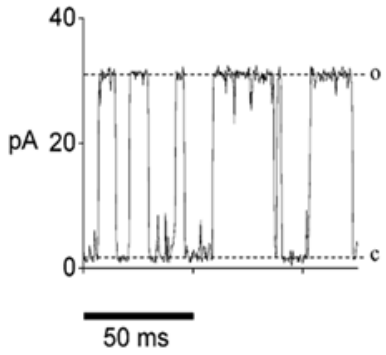

Figure 3.24 Fluctuation of OmpG at pH 5.6 between the opening/closing conformation. The figure was taken from Conlan *et al.,* 2003.

Figure 3.24 describes the OmpG situation in lipid bilayer at pH 5.6: there are two chambers separated from a phospholipid bilayer in which OmpG is embedded. The pH 5.6 was obtained by adding 1M $NaCH_3COO$. A voltage was applied and the conductance was measured. OmpG fluctuated between the opening/closing conformations. According to this electrophysiological study OmpG at pH 4.7 is primarily in the closing conformation.

3.1.5.2 Going new ways

The labelled sample at pH 5.6 is unstable under the influence of 235.000 g force when prepared directly in acid condition, or under g force from MAS frequency. It misfolds from the lipid environment and aggregates with other misfolded OmpG proteins, but the g force of both the ultracentrifugation and the spinning of the rotor at MAS frequency is so high that the sample precipitates on the pellet. For this reason, the SDS-PAGE analysis of the three different diluted states presents 50 % of unfolded protein. It is unknown what can interfere with the stability of the labelled sample at pH 5.6, where there seems to be a biophysical problem. To overcome it, the more rational consideration was to change the preparation of

the OmpG labelled samples at different pH's. Therefore the concentrations of the mono- and di-hydrogenphosphate in PPi were altered. To prove if this can be the reason for the partial unfolding of the protein at pH 5.6, a new labelled acid sample at pH 4.7 was prepared in a different way. The target is always to prepare OmpG at acid condition but not more than pH 5.6, as was done by the X-ray crystallographer (Yildiz *et al.,* 2006), but at pH 4.7, as was shown by electrophysiological method (Conlan *et al.,* 2003). The preparation of the labelled sample at acid pH was improved following some consideration of the publication of Lü (Lü *et al.,* 2011). The crystal pellet at pH 7.5 is resuspended in different buffer systems at different pH's (Table 3.2) and centrifuged at 14.000 rpm for 5 min at room temperature. This was done twice as shown in figure 3.25 (the composition of the different buffer systems at different pH's is shown in table 3.2). Then they were resuspended again in different buffer systems at different pH's and ultracentrifuged at 235.000 g for 1 h at 8 °C. Finally the crystal pellets were again resuspended in different buffer systems at different pH's to be analysed by SDS-PAGE and EM.

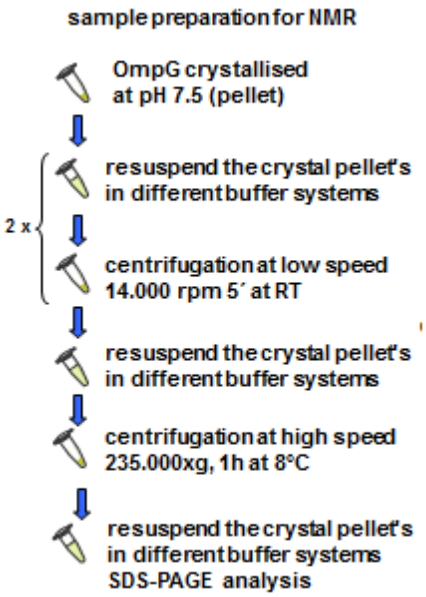

Figure 3.25 Schematic protocol for the preparation of the labelled OmpG sample at acid pH.

Phosphate buffers	Na-Citrate buffers
20 mM Phosphate pH 7.5, 5.6 and 4.9 50 mM NaCl 3 mM NaN_3	20 mM Na-Citrate pH 5.6 and pH 4.7 50 mM NaCl 3 mM NaN_3
pH 7.5, 5.6 and 4.9	pH 5.6 and 4.7

Table 3.2 The different buffer compositions.

The SDS-PAGE analysis (figure 3.26) compares these new labelled samples (lanes I, III, V, X, XII), prepared following the protocol shown in figure 3.25, with the labelled sample prepared directly in acid condition (red circle in the figure 3.36 lane VIII and IX), and highlights less content of unfolded protein (especially in the labelled sample at pH 4.7 prepared in Na-citrate buffer, lane XII). The buffers' composition at different pH's is shown in Table 3.2.

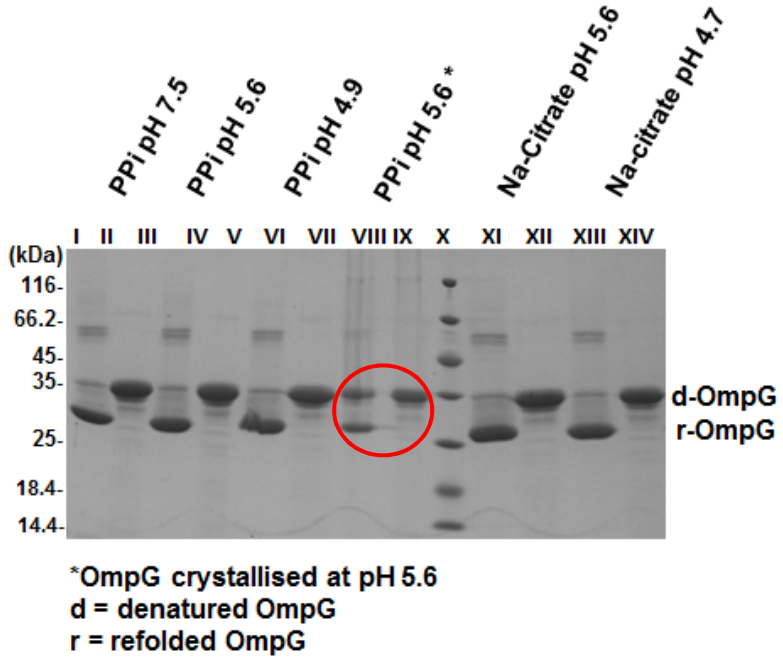

Figure 3.26 SDS-PAGE analysis of 2D OmpG crystals. Lane I = OmpG sample washed in PPi at pH 7.5, refolded form; Lane II = OmpG sample washed in PPi at pH 7.5, denatured form; Lane III = OmpG sample washed in PPi at pH 5.6, refolded form; Lane IV = OmpG sample washed in PPi at pH 5.6, denatured form; Lane V = OmpG sample washed in PPi at pH 4.9, refolded form; Lane VI = OmpG sample washed in PPi at pH 4.9, denatured form; Lanes VII and VIII = 2D OmpG crystals at pH 5.6 prepared directly in acid condition, refolded and denatured form respectively. Lane IX = molecular weight marker (Fermentas); Lane X = OmpG sample washed in Na-citrate at pH 5.6, refolded form; Lane XI = OmpG sample washed in Na-citrate at pH 5.6, denatured form; Lane XII = OmpG sample washed in Na-citrate at pH 4.7, refolded form; Lane XIII = OmpG sample washed in Na-citrate at pH 4.7, denatured form.

In comparison to the refolded sample in which 50 % of the protein is still unfolded (lane VII), the refolded labelled sample at pH 4.7 (lane XII), which was prepared as shown above by different washing steps in Na-Citrate buffer, showed less content of unfolded protein.

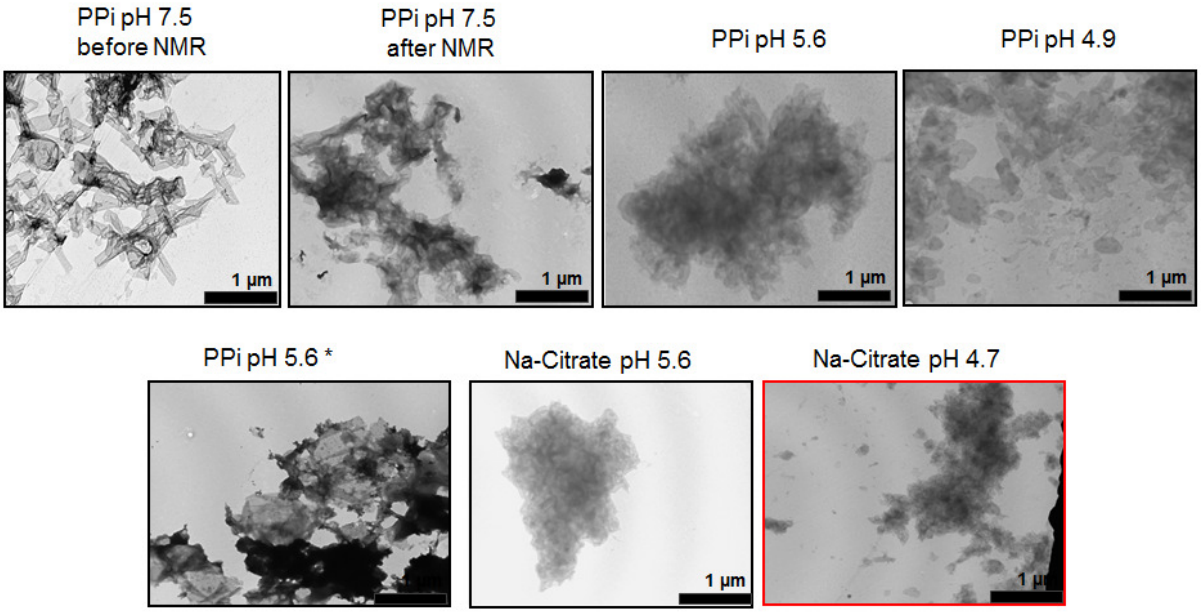

Figure 3.27 EM analysis of 2D crystals of [^{13}C, ^{15}N]-GALVSHF$_{\alpha,\beta}$Y$_{\alpha,\beta}$-OmpG washed in different buffer systems at different pH's.

After the EM analysis (figure 3.27) it is possible to compare the 2D crystals prepared in different buffer systems at different pH's. After NMR measurement the 2D crystals of the labelled sample at pH 5.6 washed in PPi (indicated with an asterisk in figure 3.27) are totally broken, meaning that they are not suitable for NMR measurement. This leads to a reflection about the biophysical problem of this preparation method and a strategy to prepare a new acid labelled sample differently. During the overnight ultracentrifugation the sample started to change colour from a characteristic yellow to white. Maybe this process could be continued during the spinning of the rotor at MAS frequency, considering that after NMR measurements the 2D crystals are totally broken. The other 2D crystals prepared in this way were broken as well, maybe due to the several washing steps in the respective buffers, but there were still enough 2D crystals in a tubular shape suitable for solid-state MAS NMR studies. On the one hand it is very important to obtain 2D crystals especially to investigate the dynamics of this protein in a native environment such as the lipid bilayer. On the other hand the lipids are a better environment in comparison to the detergent, which is why they were used to prepare the labelled sample at pH 4.7 by different washing steps at different rates of Na-citrate. This buffer was chosen over PPi due to the crystals being less tightly packed at pH 4.7. The washing protocol applied was as follows: centrifugation three times at 14.000 rpm for 10 min at room temperature; resuspension in Na-citrate buffer at pH 4.7 and

an overnight centrifugation at 235.000 g at 8 °C. Starting from the 2D crystals of the labelled sample at pH 7, they were washed following the protocol in figure 3.25 and washed in Na-citrate buffer at pH 4.7. An SDS-PAGE analysis (figure 3.28) was done to check if the protein was still refolded in a lipid environment and an EM analysis was done to check if there were 2D crystals in a tubular form. They were broken but still 2D crystals in a tubular form.

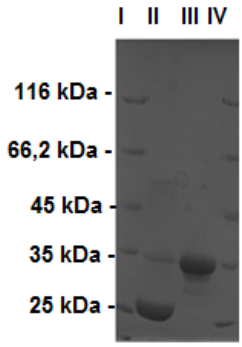

Figure 3.28 SDS-PAGE analysis of 2D crystals at pH 4.7. Lane I = molecular weight marker (Fermentas); Lane II = OmpG at pH 4.7 refolded in a lipid environment; Lane III = OmpG at pH 4.7; Lane IV = molecular weight marker (Fermentas).

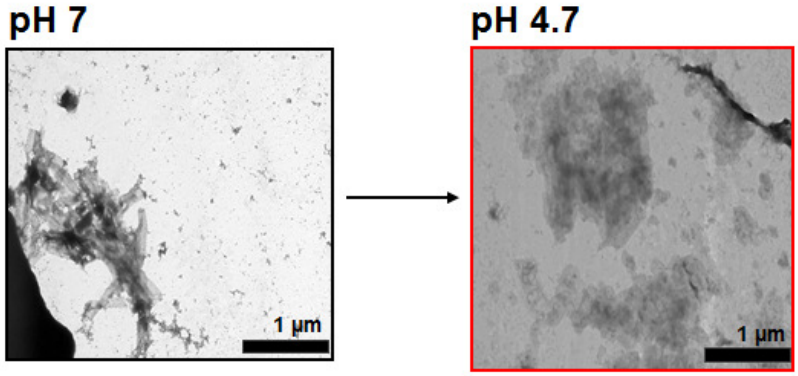

Figure 3.29 EM analysis of 2D crystals of OmpG at pH 7 and at pH 4.7.

3.1.5.3 Final NMR characterisation: [^{13}C, ^{15}N]-GALVSHF$_{\alpha,\beta}$Y$_{\alpha,\beta}$-OmpG

After the preparation of the stable labelled sample at pH 4.7 the characterisation by solid-state MAS NMR was started again with the same procedure shown in the method chapter, but by loading the sample in the 3.2 mm rotor for faster spin to delete the side bands from the region of our interest.

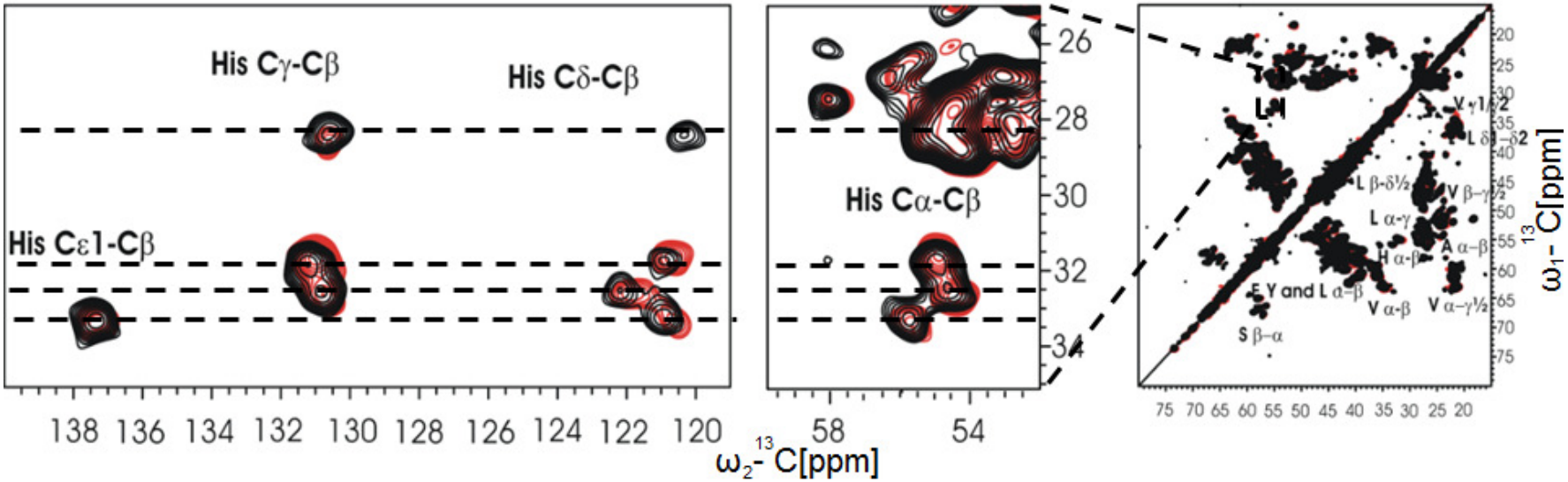

Figure 3.30 Overlay of 2D ^{13}C-^{13}C PDSD NMR spectra of 2D crystals of [GALVSHF$_{\alpha,\beta}$Y$_{\alpha,\beta}$, ^{15}N]-OmpG at pH 7.5 (black) and 4.7 (red). The spectra were recorded at 900 MHz, 280 K, with a mixing time of 50 ms and an MAS frequency of 18 kHz for the samples at pH 7.5 and at pH 4.7.

The overlay of the 2D ^{13}C-^{13}C PDSD spectra at pH 7.5 and at pH 4.7 shows four signals of the His for the labelled sample at pH 7.5 and four signals of the His for the labelled sample at pH 4.7 (figure 3.30). The signals of the His are represented by the black dashed line. It is necessary to detect the other three His signals and to assign the protein. This was the partial conclusion after a first characterisation of OmpG at different pH's by solid-state MAS NMR. A better comparison between the labelled sample at pH 7.5 and the labelled sample at pH 4.7 is shown in figure 3.31. The 2D ^{13}C-^{13}C spectrum of the labelled sample at pH 7.5 (black) and the one at pH 4.7 (red) are compared with the 2D ^{13}C-^{13}C of [^{13}C, ^{15}N]-GANDSH-OmpG at pH 7.5, especially the aromatic region where it is possible to identify the aromatic signal of the carbon of the His imidazole. The [^{13}C, ^{15}N]-GANDSH-OmpG at pH 7.5 is an OmpG sample labelled to characterise the opening conformation of OmpG.

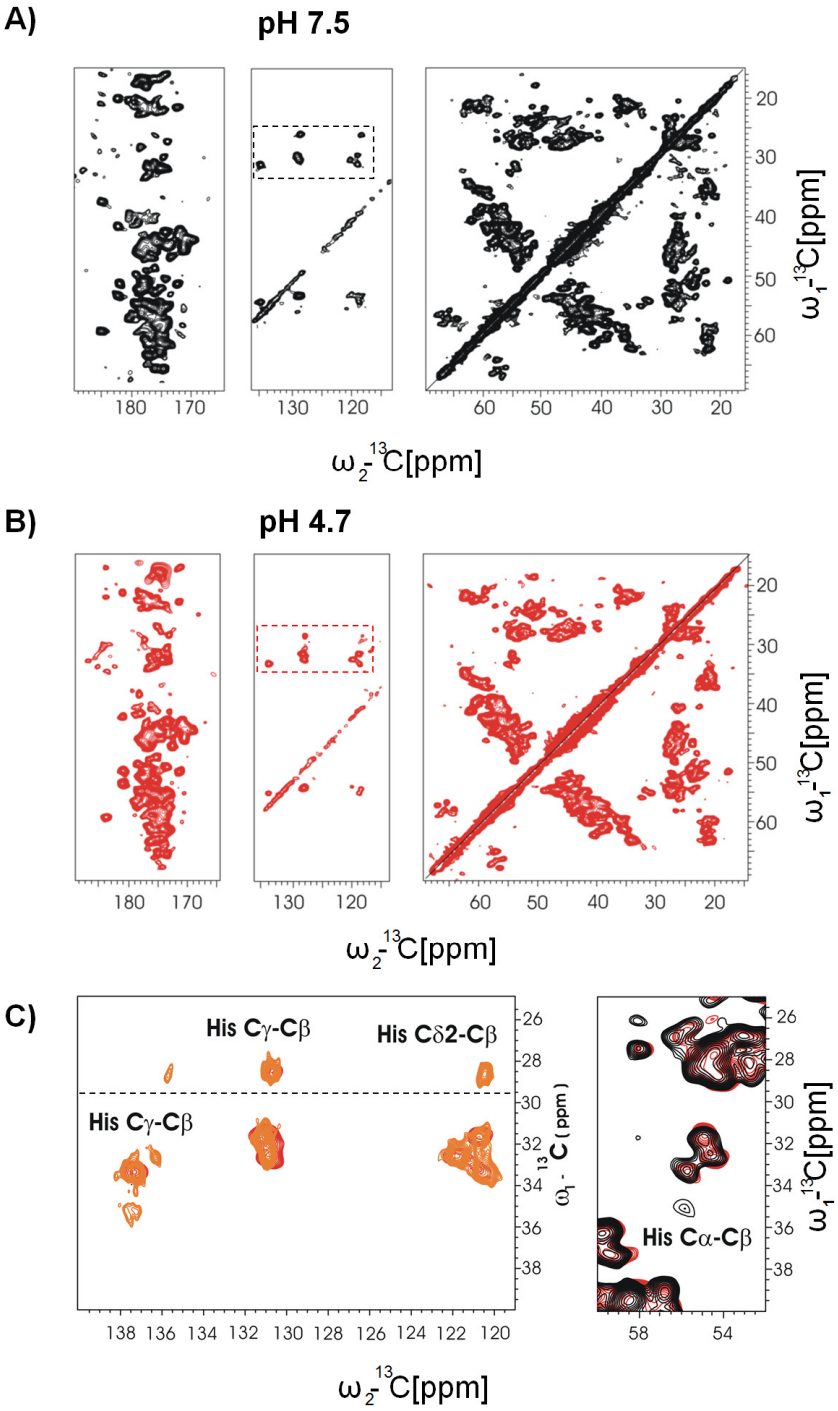

Figure 3.31 2D ^{13}C-^{13}C spectra of [GALVSHF$_{\alpha,\beta}$Y$_{\alpha,\beta}$, ^{15}N]-OmpG and [GANDSH, ^{15}N]-OmpG at different pH's. The spectra of [GALVSHF$_{\alpha,\beta}$Y$_{\alpha,\beta}$, ^{15}N]-OmpG at pH 7.5 (black, A) and at pH 4.7 (red, B) were recorded with a mixing time of 50 ms and an MAS frequency of 18 kHz. The spectrum of the sample of the [GANDSH, ^{15}N]-OmpG at pH 7.5 (yellow, C) was recorded with a mixing time of 20 ms and an MAS frequency of 13 kHz. All spectra were recorded on a 900 MHz machine at 280 K.

The chemical shifts of some Cβ atoms of the histidines are more shielded in comparison to other ones. This might be due to different orientations of the side chains (figure 3.31, C). In addition, one Cγ-Cβ peak has a completely different chemical shift for the Cγ atom (figure 3.31, C). One Cα-Cβ peak of the histidines is overlayed by a Leu Cα-Cγ correlation. In total it is possible to count four of the seven histidines' signals (one signal which was considered as belonging to His was an aliphatic signal of Trp coming from the Ser metabolism, figure 3.30). However, there were not any strong chemical shift changes at different pH values (figure 3.31, C). Perhaps were detected the histidines belonging to the barrel of OmpG and not His 231 and His 261 involved in the opening/closing mechanism of OmpG at different pH's. This lead to reconsidering the overlay between the 1D ^{15}N/CP MAS of the labelled samples at pH 7.5 and at pH 4.7 to find significant differences between the two states at different pH's.

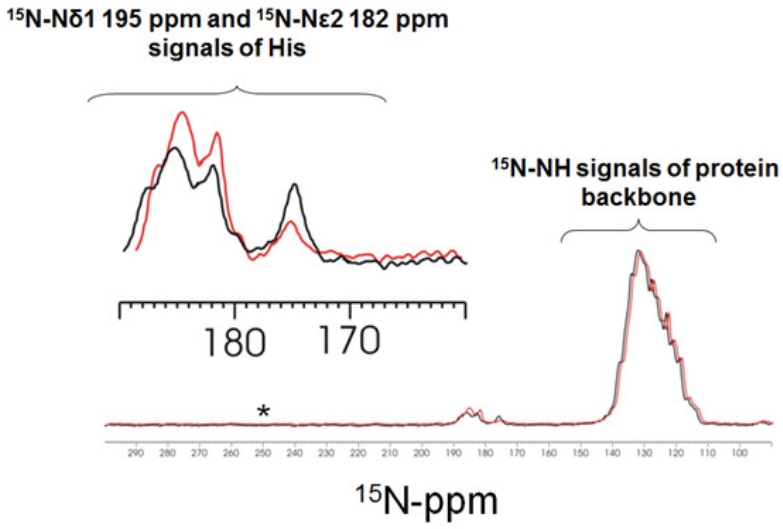

Figure 3.32 Overlay of the 1D ^{15}N-CP/MAS spectra of [GALVSHF$_{\alpha,\beta}$Y$_{\alpha,\beta}$, ^{15}N]-OmpG at pH 7.5 (black) and at pH 4.7 (red). The spectra were recorded on a 900 MHz narrow-bore spectrometer with a spinning frequency of 18 kHz at 280 K. Number of scans = 4096.

The signals of the Nε2 and Nδ1 of the imidazole at pH 7.5 have different intensity than the signals Nε2 and Nδ1 of the imidazole at pH 4.7 (figure 3.32). The chemical shift values of the His imidazole's Nε2 and Nδ1 were taken from www.bmrb.wisc.edu. This led to a change in the state of protonation between the labelled sample at pH 7.5 (in black) and the labelled sample at pH 4.7 (in red). At pH 7.5 the imidazol ring systems of the histidines forms H-bond with other amino acids (figure 3.33). Both nitrogens Nε2 and Nδ1 of these histidines (pH 7.5) were involved in the H-bonds because a signal of the unprotonated form did not appear at 250 ppm (indicated by the asterisk in figure 3.32).

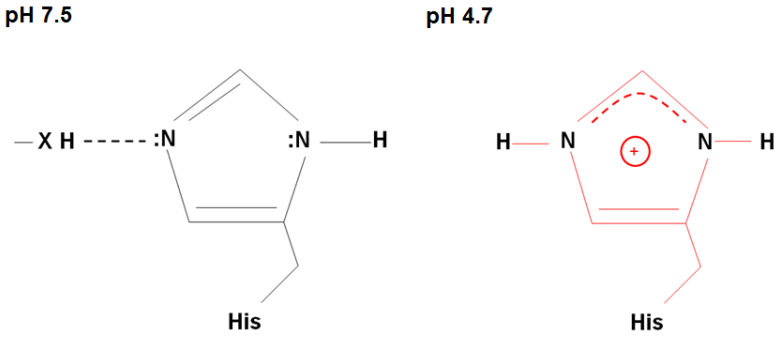

Figure 3.33 Different protonation states of the imidazole ring system of the Histidines at different pH's (Hu *et al.,* 2012; www.bmrb.wisc.edu). X = O or N atom of an amino acid's side-chain involved in H-bond in OmpG

At pH 4.7 the imidazol of these histidines are bi-protonated in cationic form (figure 3.33). These results do not respect the consideration done by the X-ray crystallography, namely that at acid pH the folding of loop 6 inside the channel is caused from the repulsion of the protonated imidazoles of the His 231 and His 261 because these signals are not detected in the spectra.

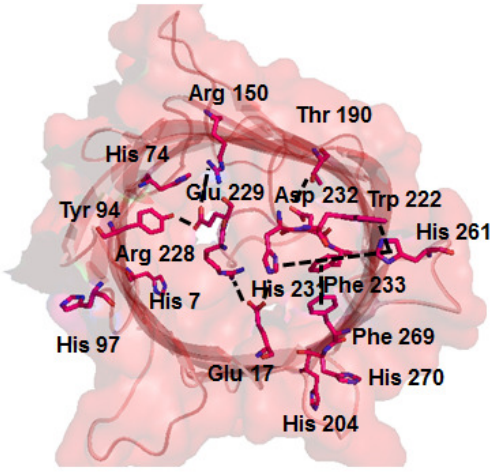

Figure 3.34 AA interactions involved in the closing conformation of OmpG at pH 4.7. Top view of OmpG at pH 4.7 from the extracellular side. The black dotted lines indicate the different interactions (electrostatic, hydrophobic and H-bond interactions) involved in the OmpG closure at pH 4.7. Image of OmpG was taken from PDB (2IWW) and was rendered by PyMOL (http//www.pymol.org).

However, the closing conformation is supported by electrostatic, hydrophobic and H-bond interactions among other AAs. At pH 4.7, the C-terminal part of loop 6 together with β-strand S12 established a strong interaction that was absent at pH 7.0. Again the X-ray structures show that, at acidic pH, the residues of loop 6 form additional interactions between Phe 233 and Phe 269, Asp 232 and Thr 190, His 231/Arg 228 and Glu 17, Glu 229 and Arg 150/Tyr 94, and Trp 222 and His 261 (figure 3.34). In addition to the role of the histidines pair and the loop 6, in situ opening/closing experiments showed that positively and negatively charged AAs residues (Asp, Glu and Arg) also play an active role: interacting with each other inside the pore lumen. Therefore the closing entrance by the folding of the loop 6 is also supported from the changing of the electric potential due to the different state of these charged AAs inside the lumen (Hu *et al.,* 2012, Damaghi *et al.,* 2010, Korkmaz *et al.,* 2012).

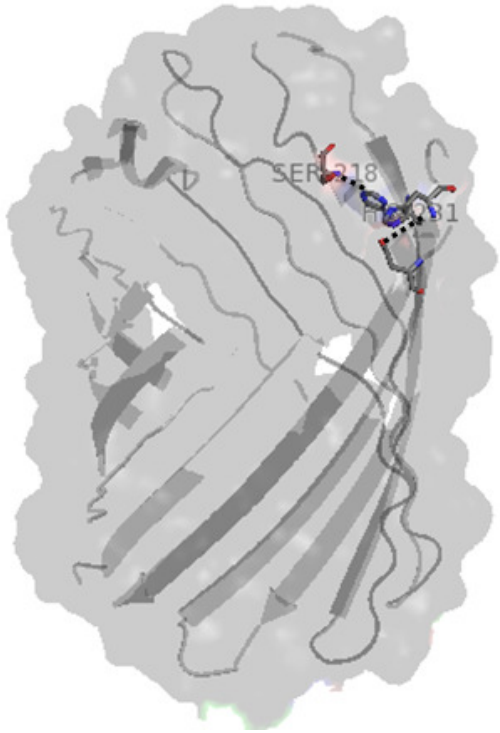

Figure 3.35 AA interactions involved in the opening conformation of OmpG at pH 7.5. Image of OmpG was taken from PDB (2IWV) and was rendered by PyMOL (http//www.pymol.org).

3.2 Protein labelling strategy: [^{13}C, ^{15}N]-GEQNDPASR-OmpG

Yildiz (Yildiz *et al.,* 2006) shows that, at pH 5.6, crystals of OmpG grown in presence of OG (octyl-β-D-glucopyranoside) have two different densities, one of which fitted with an octyl-glucopyranoside (OG) molecule. The other density lacked a clear hydrocarbon tail and it was fitted with a glucose molecule that either represents the head group of a second, partially disordered, detergent molecule or it was picked up from cryoprotectant. The sugar head group of the complete OG molecule is coordinated by hydrogen bonds to residues Arg 168, Tyr 196, Glu 154, Glu 253 and Trp 131, while the adjacent glucose molecule forms hydrogen bonds with Trp 131, Tyr 135 and Glu 152. The glucose molecule and the OG glucoside head group most likely indicate the positions of sugar binding sites in the OmpG pore, and the side chains involved in sugar binding have the same conformation in both structures (figure 3.36).

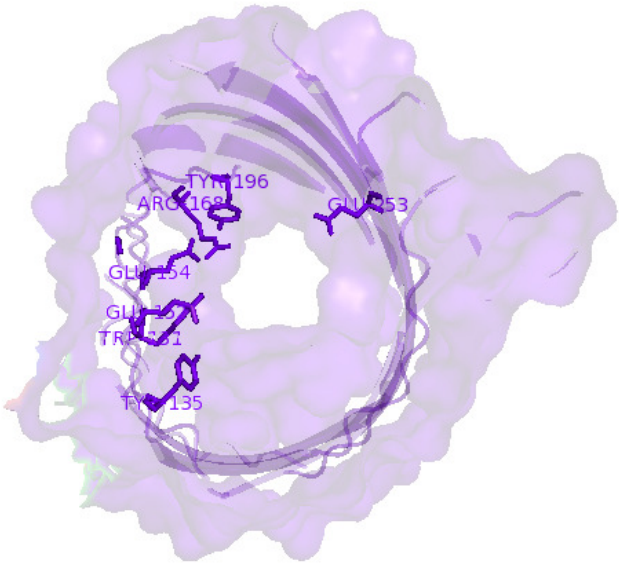

Figure 3.36 Different AAs involved in sugar binding. Image was taken from PDB (2IWV) and rendered by PyMOL (http//www.pymol.org).

The entry of disaccharides into the channel is thought to be facilitated by a line of aromatic residues roughly parallel to the barrel axis, sometimes referred to as the 'greasy slide'. In OmpG was found a strikingly similar arrangement of aromatic residues Tyr 98, Tyr 96, Tyr 94, Phe 66 and Tyr 50, called aromatic slide more for its hydrophobicity than for its line of Tyr-OH. Their presences in OmpG suggest that it is an essential feature for solute uptake. To understand how the sugars can attach to the OmpG channel a labelled [^{13}C, ^{15}N]-GEQNDPASR-OmpG sample was prepared. The preparation of this labelled sample was

achieved by manipulating the end-product feedback inhibition of the *E. coli* amino acid metabolic pathway and using enzyme inhibitors. In this way OmpG was efficiently labelled in vivo. One of the main difficulties is to label the amino acids glutamine, glutamate, aspartate and asparagine in vivo without isotopic scrambling. *E. coli* has got three enzymes that metabolise Q→2E in three consecutive steps (figure 3.37). Tong (Tong *et al.,* 2008) described that these anabolic and catabolic reactions can be inhibited by the addition of different inhibitors to the cultivation medium (figure 3.37). In this way the first two steps are kept in reversible manner and Q and E are labelled (figure 3.37).

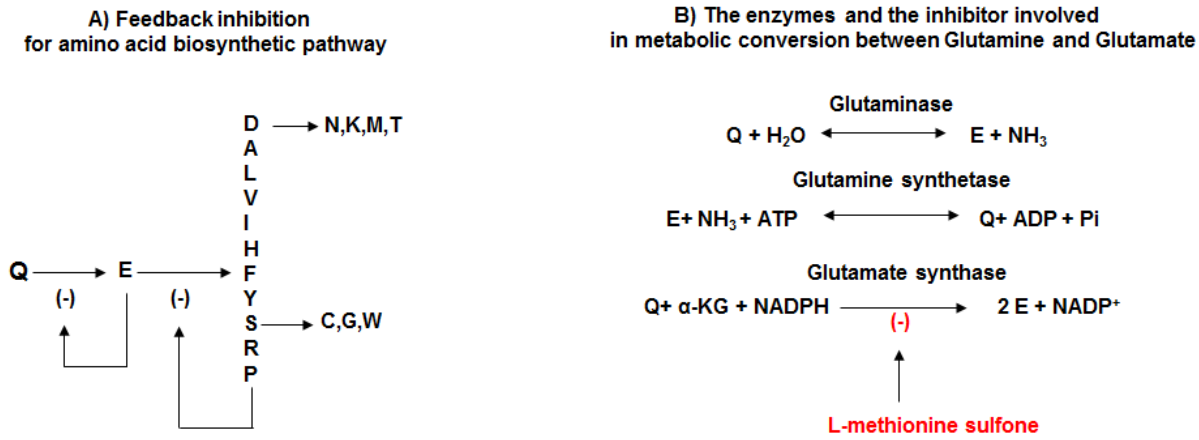

Figure 3.37 Metabolism of glutamine and glutamate. A) A simplified and partial view of the end-product feedback inhibition for amino acid biosynthetic pathway. B) In *E. coli* Q is metabolised in E through three steps. Each of these steps is catalysed by an own enzyme: Glutaminase, glutamine synthetase and glutamate synthase. L-methionine sulfone is the inhibitor of glutamate synthase.

Another problem is the metabolism of aspartate. Asp can be converted to 4-Aspartyl-P by aspartate kinase, to oxalacetate by aspartate transaminase, to fumarate by aspartate ammonia-lyase, to alanine by aspartate 4-decarboxylase and then to pyruvate by ß-alanine pyruvate kinase. All the metabolic pathways can be inhibited by different substances (figure 3.38).

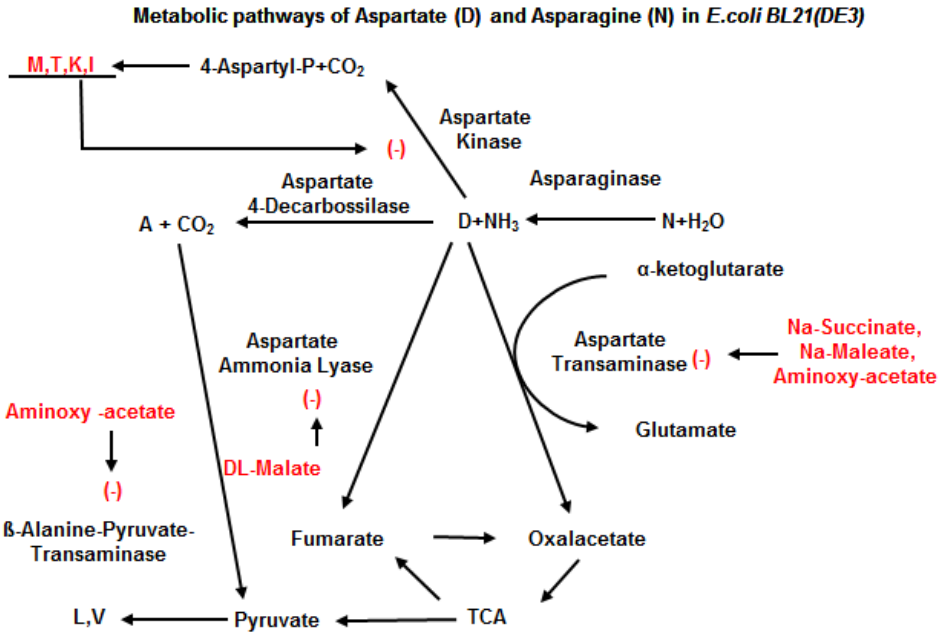

Figure 3.38 Anabolic and catabolic pathways of aspartate and asparagine.

In a first experiment GEQNDPASR-OmpG was prepared in unlabelled form using the inhibitors L-methionine sulfone, Na-succinate, Na-maleate, aminooxyacetate and DL-malate to check the expression of this unlabelled protein in the presence of these inhibitors (Tong *et al.,* 2008; Viola *et al.,* 2001; Michuda and Martinez-Carrion, 1970; Hopper and Segal, 1962; John *et al.,* 1970; Falzone *et al.,* 1998; Miyohara *et al.,* 1994).

3.2.1 Expression and purification of unlabelled GENDQPASR-OmpG in *E. coli* without signal sequence

The expression and purification of unlabelled GEQNDPASR-OmpG was done to test the expression level of the protein in the presence of inhibitors described following the publication of Tong (Tong *et al.,* 2008). The protocols performed in the laboratory are shown in the method part (2.2.7.3.2). The schemes in figure 3.39 sum that up.

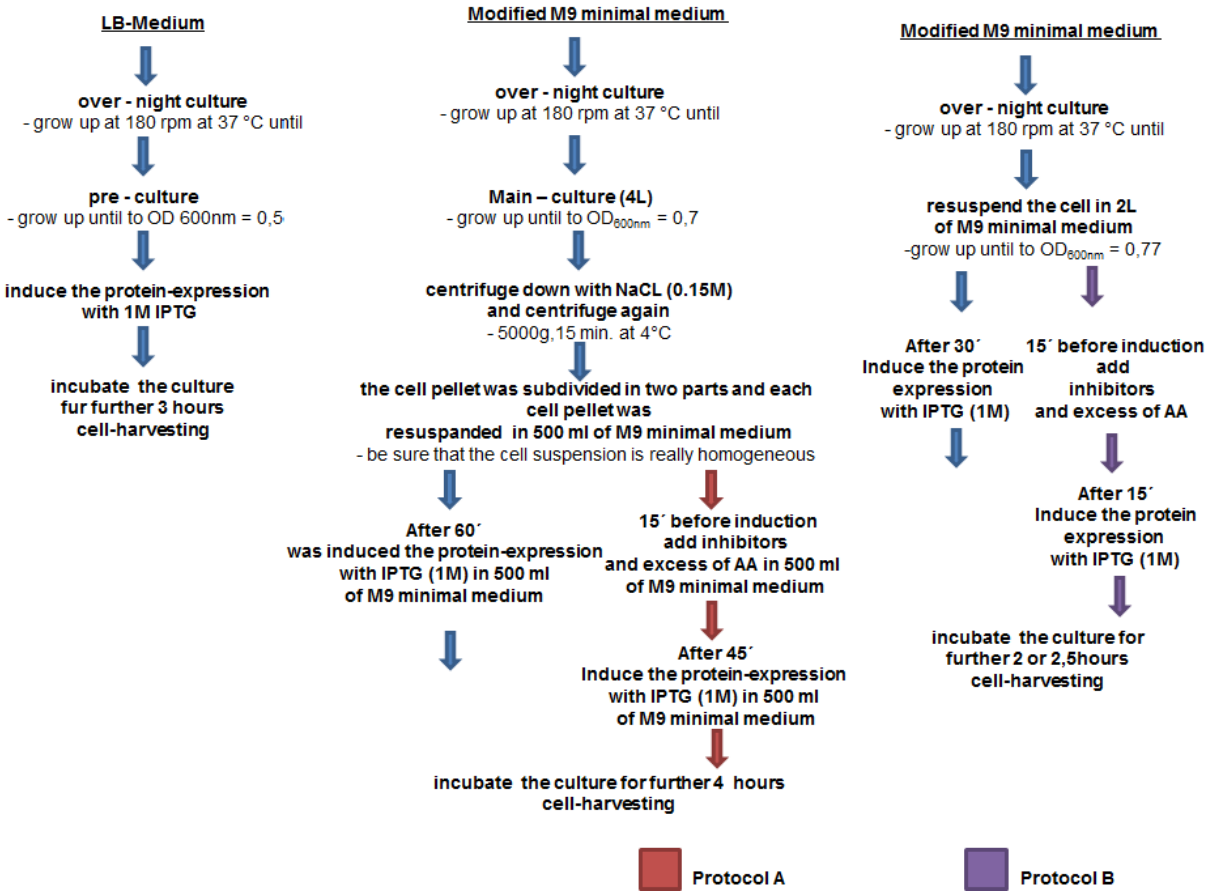

Figure 3.39 Schematic representation of the standard and the modified cultivation protocols (Protocols A and B).

3.2.2 Analysis of the expression and purification in unlabelled form

The different behaviours of the cells in standard and modified M9 minimal medium were monitored by measuring the OD_{600nm} during cultivation (figure 3.40).

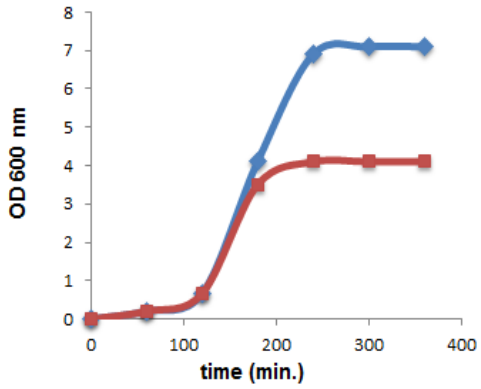

Figure 3.40 Comparison of the growth curve of *E. coli* in standard M9 minimal medium (blue) and in modified M9 medium (red, Protocol A).

In the standard M9 minimal medium the cells grew up to an OD_{600nm} = 7. In the modified M9 minimal medium cells grew up to OD_{600nm} = 4.5. The presence of the inhibitors constrained the growth of the cells (figure 3.40). This result was also confirmed by the obtained bio wet mass (5 g in 500 ml of standard M9 minimal medium and 3.5 g in 500 ml of modified M9 minimal medium). Additionally, the total protein content was analysed during the expression by SDS-PAGE (figure 3.41).

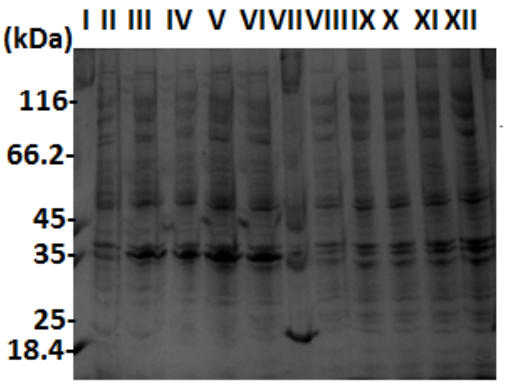

Figure 3.41 SDS-PAGE analysis of the expression of OmpG in standard (left side) and modified M9 Minimal medium (right side, Protocol A). Lane I = molecular weight marker (Fermentas); Lane II = before induction of 1mM IPTG; Lane III = after induction of 1mM IPTG; Lanes IV, V, VI = each lane represents one additional hour after induction of 1 mM IPTG; Lane VIII = before induction of 1mM IPTG in modified M9 minimal medium; Lanes IX, X, XI, XII = each lane represents one additional hour after induction of 1 mM IPTG. Lanes II to VI were all in standard M9 medium. The molecular weight of OmpG is 34 kDa.

In comparison to the standard M9 minimal medium there is the same enhancement of the OmpG expression over the time in modified M9 minimal medium (figure 3.41). However, the total yield of OmpG is drastically decreased. To confirm these data the inclusion body fractions were purified or solubilised under denaturing conditions in 8 M urea (figure 3.42).

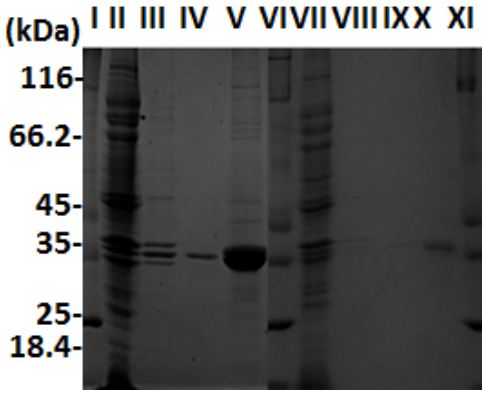

Figure 3.42 Solubilisation of the inclusion body fractions in denaturing condition (8 M urea) in standard (left side) and in modified M9 minimal medium (right side, Protocol A).

Lane I = molecular weight marker (Fermentas); Lane II = supernatant buffer A; Lane III = supernatant washing buffer 1; Lane IV = supernatant washing buffer 2; Lane V = supernatant solubilisation buffer. From lane I to V all samples are in standard M9 medium; Lane VI = molecular weight marker (Fermentas); Lane VII = supernatant buffer A; Lane VIII = supernatant washing buffer 1; Lane IX = supernatant washing buffer 2; Lane X = supernatant solubilisation buffer. Lane XI = molecular weight marker. From lane VII to X all samples are in modified M9 minimal medium (Protocol A).

After the purification of OmpG under denaturing condition 71.54 mg of OmpG were obtained from cells cultivated on standard M9 Minimal medium whereas the yield of OmpG obtained by cultivation on modified M9 minimal medium was only 6 mg. After a discussion with the author of the publication Tong *et al.,* 2008, was the expression protocol was optimised again. Therefore, an excess of amino acids (0.1 g/ ℓ of GNDQEPASR and 1 g/ ℓ of all other amino acids) was added. Protein expression was induced at OD_{600nm} = 0.77. The growth behaviour and the protein expression were monitored by measuring the OD_{600nm} over the time (figure 3.43) and by SDS-PAGE analysis (figure 3.44). Fifteen minutes before the IPTG induction inhibitors and excess of labelled and unlabelled AAs were added. The respective amounts are shown in the method chapter and the schematic protocol B is shown in figure 3.39.

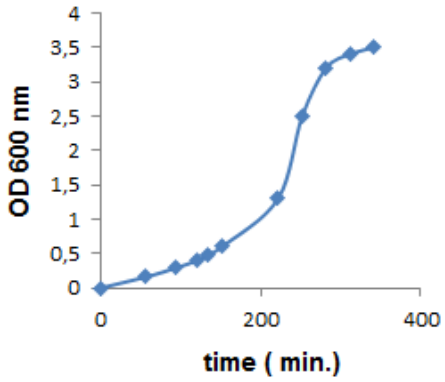

Figure 3.43 Growth curve in modified M9 medium with an excess of AAs and different inhibitor concentrations.

The result in figure 3.43 shows a different growth curve for the *E. coli* strain BL21(DE3) than figure 3.40 due to the use of Protocol A. Using Protocol B the overnight culture was directly used to inoculate the M9 minimal medium. The cells grew up to an OD_{600nm} = 3.5 after IPTG induction, yielding a bio wet mass of 2.4 g. Additionally, the OmpG expression rate was analysed by SDS-PAGE during the cultivation (figure 3.44).

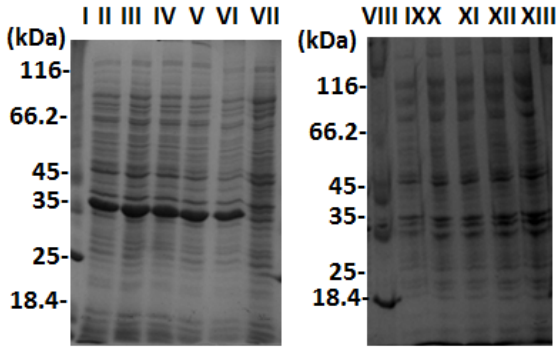

Figure 3.44 Comparison between the expression of unlabelled OmpG in different modified M9 minimal media (using Protocol B on the left and Protocol A on the right side) by SDS-PAGE analysis inducing the cells at OD_{600nm} = 0.77 before and after induction of 1 mM IPTG.

Lane I = molecular weight marker (Fermentas); Lane VII = before induction of 1mM IPTG; Lane II = after induction of 1mM IPTG; Lanes III, IV, V, VI = each lane represents one additional half hour after induction of 1 mM IPTG. Lane VIII = molecular weight marker (Fermentas); Lane IX = before induction of 1mM IPTG. Lane X = after induction of 1mM IPTG; Lanes XI, XII, XIII = each lane represents one additional hour after induction of 1 mM of IPTG.

Comparing the results obtained by using Protocol B to those obtained by using Protocol A it is possible to see an enhancement of the OmpG expression. A little more than half an hour after the induction of 1mM IPTG GENDQPASR-OmpG is already expressed (figure 3.44, Lane VI). After 90 min of IPTG induction, the expression of the protein is constant (figure 3.44). To confirm these results OmpG was purified from the inclusion bodies fraction under denaturing conditions (8 M urea; figure 3.45). From the purification of OmpG were obtained 27.62 mg in 500 ml culture.

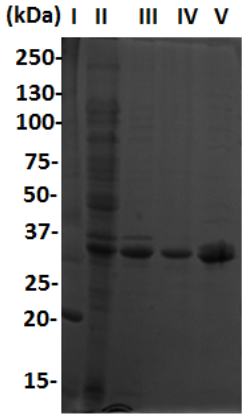

Figure 3.45 Solubilisation of inclusion bodies fraction in denaturing condition (8 M urea). Lane I = molecular weight marker (Biorad); Lane II = supernatant buffer A; Lane III = supernatant washing buffer 1; Lane IV = supernatant washing buffer 2; Lane V = supernatant solubilisation buffer.

3.2.3 Expression and purification of the labelled [^{13}C, ^{15}N]-GENDPQARS-OmpG sample from inclusion bodies

After testing the expression level of the unlabelled sample in a modified M9 minimal medium in presence of inhibitors and an excess of unlabelled AAs using Protocol B, GENDQPASR-OmpG was also expressed in labelled form in a modified M9 minimal medium in presence of inhibitors and an excess of AAs. The concentration of the inhibitors as well as the excess of amino acids was already calculated. The cells were harvested 120 min after IPTG induction because the expression does not increase in time after 90 min (as is shown in figure 3.46). This is also explained in the publication of Tong (Tong *et al.,* 2008). From the expression were obtained 6.2 g of cells from 2 ℓ of culture.

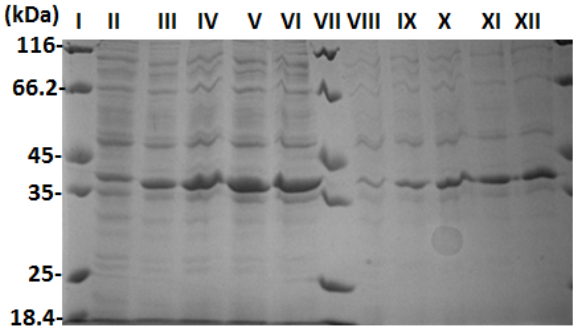

Figure 3.46 Comparison between the expression of labelled OmpG in standard M9 minimal medium and in a modified M9 minimal medium. Lane I = molecular weight marker (Fermentas); Lane II = before induction of 1mM IPTG; Lane III = after induction of 1mM IPTG; Lanes IV, V, VI = each lane represents one additional half hour after induction of 1 mM of IPTG. Lane VII = molecular weight marker (Fermentas); Lane VIII = before induction of 1 mM of IPTG; Lane IX = after induction of 1mM of IPTG; Lanes IX, X, XI, XII = each lane represents one additional half hour after induction of 1 mM of IPTG. Lines II to VI are all in standard M9 medium, lines VIII to XII all are in modified M9 medium. For the expression protocol follow figure 3.39.

The cells were purified according to the protocol shown in the method chapter 2.2.8, getting 210 mg/ 2 ℓ of protein culture. This value is very far from the one was expected. According to the unlabelled procedure for the same protocol, it was expected to get around 60 mg of protein. Maybe during this procedure there was not only the precipitated protein, but also an excess of lipids (figure 3.47).

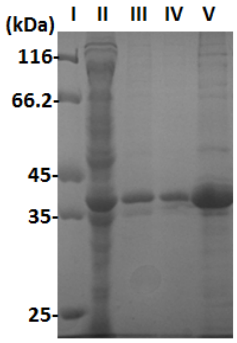

Figure 3.47 Solubilisation inclusion bodies fraction in denaturing condition (8 M urea). Lane I = molecular weight marker (Fermentas); Lane II = supernatant buffer A; Lane III = supernatant washing buffer 1; Lane IV = supernatant washing buffer 2; Lane V = supernatant solubilisation buffer.

After the first anion exchange chromatography (figure 3.48) 57.4 mg of protein/ 2 ℓ culture were obtained. This value confirms the presence of the lipid and accords with what was

expected and what was done in the preparation of the sample in unlabelled form using the same protocol.

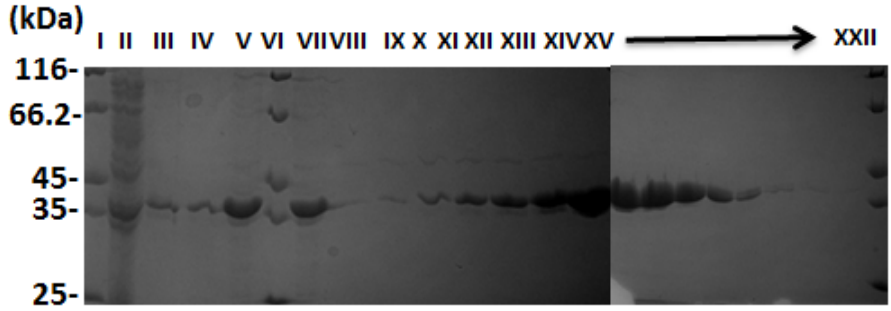

Figure 3.48 Solubilisation of the inclusion body fraction and purification by anion exchange chromatography. Lane I = molecular weight marker (Fermentas); Lane II = soluble protein fraction after homogenisation; Lane III = supernatant after first washing step; Lane IV = supernatant after second washing step; Lane V = inclusion bodies fraction after solubilisation with 8 M urea; Lane VI = molecular weight marker; Lane VII = inclusion body fraction before loading onto the column; Lane VIII to XXII = eluate start at NaCl 300 mM.

3.2.4 Refolding and reconstitution in 2D crystals of the [^{13}C, ^{15}N]-GENDPQARS-OmpG

After the purification procedure the refolding was started in the same way shown for the other labelled sample using refolding buffer containing 1 mM DDM and 0.6 M L-arginine.

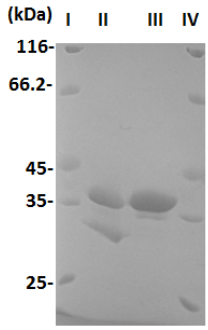

Figure 3.49 Refolding of the [^{13}C, ^{15}N]-GENDPQARS-OmpG sample. Lane I = molecular weight marker (Fermentas); Lane II = OmpG refolded; Lane III = OmpG denatured; Lane IV = molecular weight marker (Fermentas).

Figure 3.49 clearly shows the lesser efficiency of the refolding. Nevertheless a second anion exchange chromatography was applied getting 8 mg of completely refolded OmpG from 2 ℓ of culture. The rest in denatured form was harvested and was loaded into the Vivapure IEX spin columns (Sartorius).

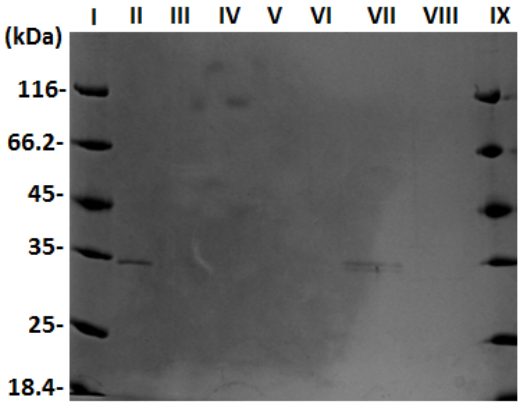

Figure 3.50 SDS-PAGE analysis of the [^{13}C, ^{15}N]-GENDPQARS-OmpG after Vivapure IEX spin columns. Lane I = molecular weight marker (Fermentas); Lane II = loading buffer; Lanes III to VI = washing buffer; Lanes VII and VIII = elution buffer; Lane IX = molecular weight marker (Fermentas).

The aim of the use of Vivapure IEX spin columns is to harvest and concentrate the rest of the denatured protein gained after the second anion exchange chromatography and to retry the refolding procedure. The solution containing the denatured protein is applied on a chromatographic column with a weak matrix (diethyl ammonium). The process consists in:

- loading sample (20 ml) and centrifugation at 500 g for 5 min at room temperature;
- four washing steps with 10 ml of buffer A at 500 g for 5 min at room temperature;
- two washing steps with 19 ml of buffer B at 500 g for 5 min at room temperature.

The protein was concentrated on a membrane cut-off of 10 kDa. 17 mg of completely denatured labelled protein were obtained, which were subsequently refolded under same conditions.

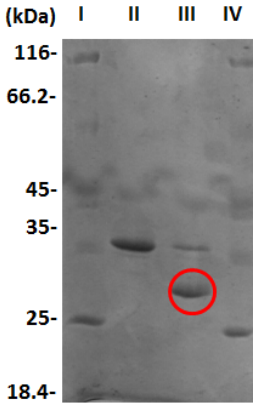

Figure 3.51 Refolding of the [^{13}C, ^{15}N]-GENDPQARS-OmpG sample. Lane I = molecular weight marker (Fermentas); Lane II = OmpG refolded; Lane III = OmpG denatured; Lane IV = molecular weight marker (Fermentas).

From the refolding procedure (figure 3.51) were obtained 17 mg of protein. To avoid losing more protein, a second anion exchange chromatography (to separate the 10 % of unfolded protein and to reduce the detergent concentration from 1 mM to 0.4 mM) was not applied. The refolded form was concentrated using a centrifugal tube with a cut-off of 50 kDa (Amicon Ultra-15 Centrifugal Filters-Millipore). The procedure consists in:

- loading 1 ml of sample in the centrifugal tube and centrifuge at 3.800 g for 21 min;
- four washing steps with 1 ml of buffer B' (pH 8, 10 mM Tris HCL pH 8, DDM 0.4 mM and 300 mM NaCl).

From this procedure 14 mg of completely refolded protein were obtained. Along with the 8 mg of the refolded protein obtained after the second anion exchange chromatography described before (data not shown), 22 mg of completely refolded protein were obtained, which were then reconstituted in a lipid environment at a lipid to protein ratio of 0.5. To crystallise OmpG at pH 7.5 were used the following crystallisation conditions: Crystallisation buffer pH 7.5 (Tris-HCl 20 mM pH 7.5; NaCl 150 mM; $MgCl_2$ 25 mM; NaN_3 3 mM) and Bio-Beads™ for the slow removal of the detergent and the formation of the 2D crystals. Three weeks after the dialysis, SDS-PAGE analysis was done to check if the sample was still folded in a lipid environment and an EM analysis was done to check if the 2D crystals were in a tubular form (figure 3.52).

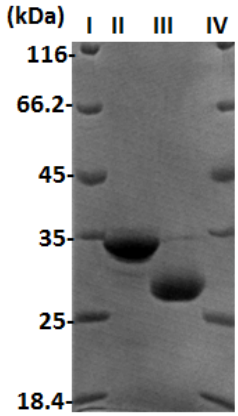

Figure 3.52 SDS-PAGE analysis of 2D crystals of OmpG at pH 7.5. Lane I = molecular weight marker (Fermentas); Lane II = denatured OmpG; Lane III = refolded OmpG; Lane IV = molecular weight marker (Fermentas).

The SDS-PAGE analysis confirmed the stability of our sample in lipid bilayer.

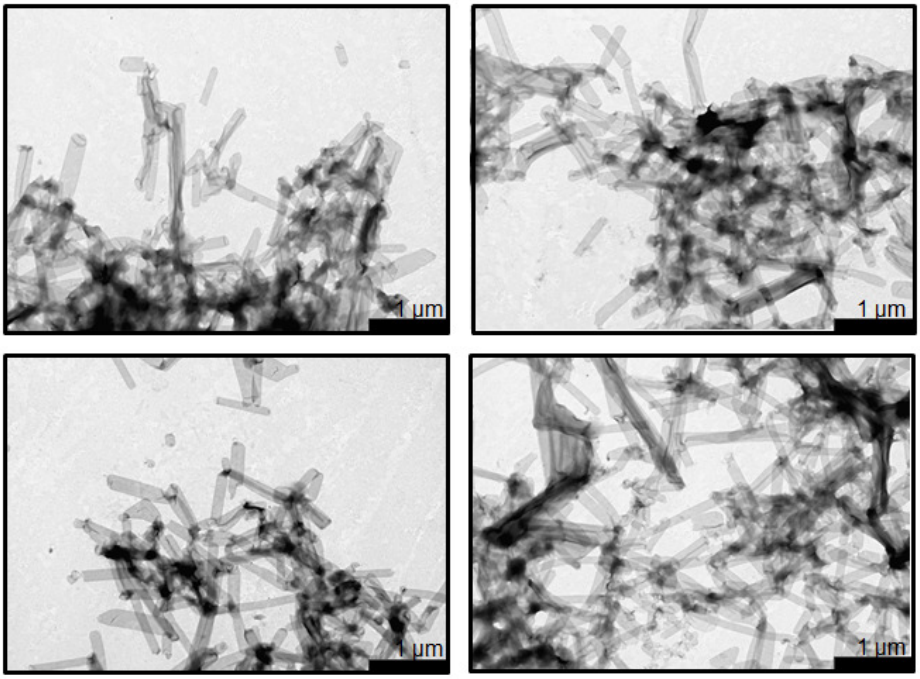

Figure 3.53 EM analysis of the crystallised [^{13}C, ^{15}N]-GENDQPASR-OmpG at pH 7.5.

The EM analysis confirmed that were obtained 2D crystals in a tubular form after four weeks, so these samples were loaded in a 3.2 mm rotor with the same procedure shown in the method chapter 2.2.13, applied the labelled sample [^{13}C, ^{15}N]-GALVSHF$_{\alpha,\beta}$Y$_{\alpha,\beta}$-OmpG, and started the characterisation with solid-state MAS NMR.

3.2.5 Solid-state MAS NMR characterisation of the [^{13}C, ^{15}N]-GENDPQARS-OmpG

As was shown earlier the solid-state MAS NMR characterisation starts with the recordings of the 1D experiment. In figure 3.56 the 1D ^{13}C-CP/MAS of the [^{13}C, ^{15}N]-GENDPQARS-OmpG sample is shown.

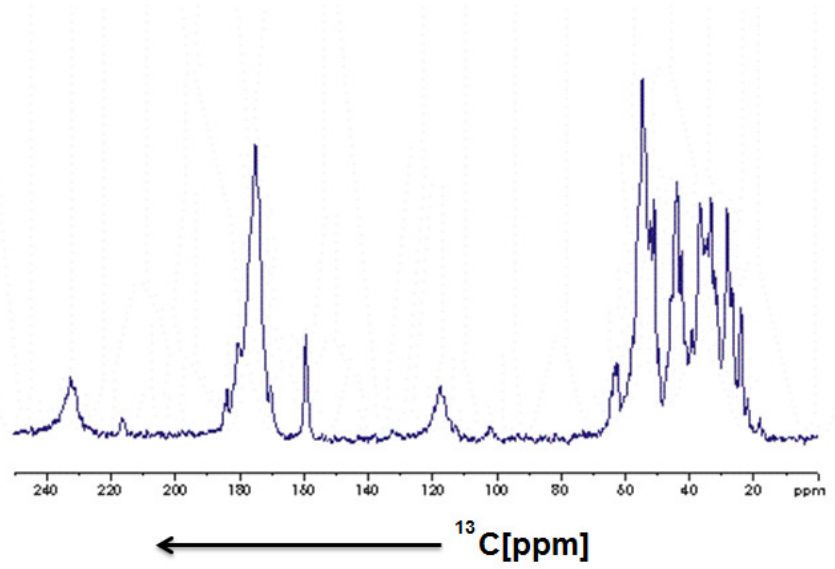

Figure 3.54 1D ^{13}C/CP MAS [^{13}C, ^{15}N]-GENDPQARS-OmpG. The spectrum was recorded on the 900 MHz spectrometer with an MAS frequency of 18 kHz at 280 K.

Figure 3.54 makes it possible to highlight the aliphatic signals of the methyl- and methylen-carbon in the region of 70–20 ppm. Around 120 ppm the characteristic signals of the side bands at a spinning rate of 18 kHz can be seen. It was recognised due to the signal appearing at 240 ppm, which is specular to it. In the carbonyl region there are all signals of the carbonyl and carboxyl groups of the labelled AAs and, more difficult to see, the characteristic signal of the arginine's carbonyl at around 160 ppm.

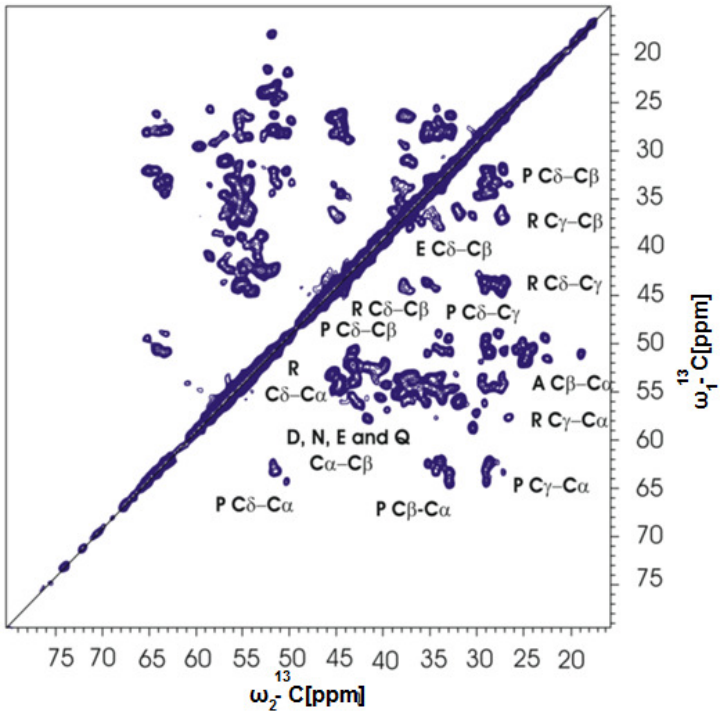

Figure 3.55 2D ^{13}C-^{13}C PDSD spectrum of [GENDQPASR, ^{15}N]-OmpG at pH 7.5. The spectrum was recorded at 900 MHz, 280 K, with a PDSD mixing time of 20 ms and an MAS frequency of 18 kHz.

With this labelling pattern it is possible to visualise the intraresidual correlation of all labelled AAs. The intraresidual correlation of Pro and Arg are highlighted.

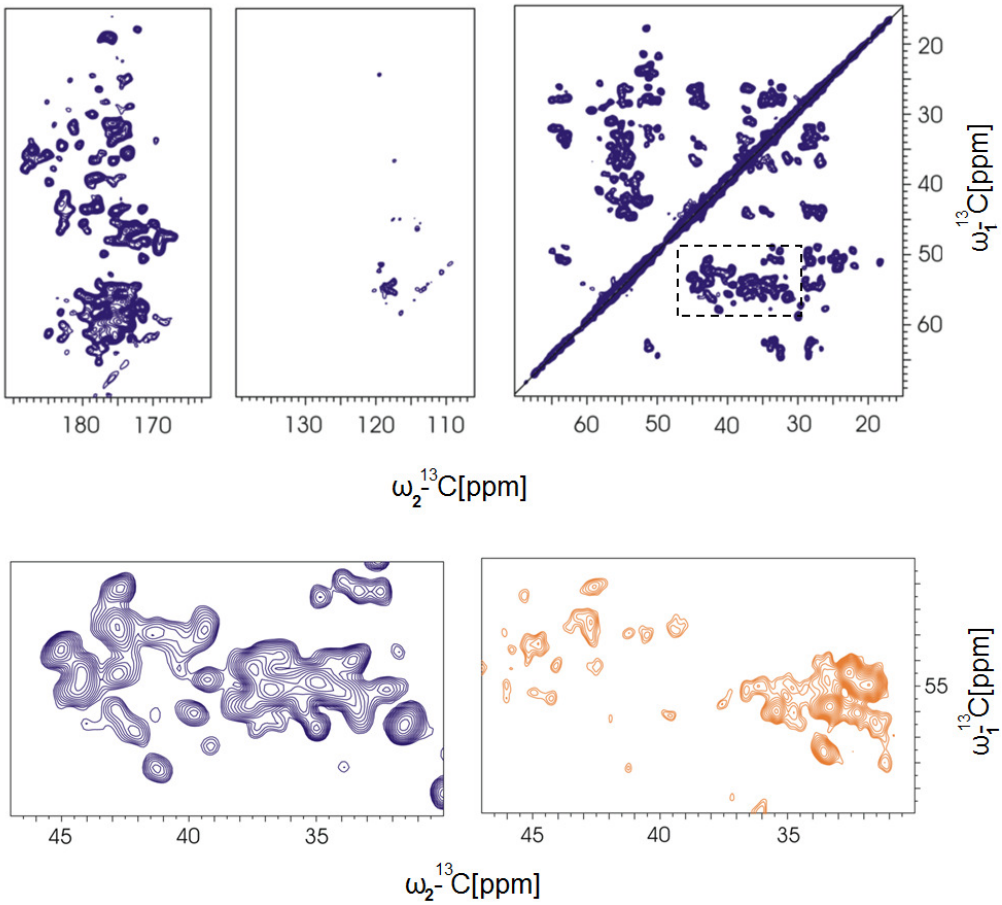

Figure 3.56 2D ^{13}C-^{13}C spectra of [GENDPQARS, ^{15}N]-OmpG and [GANDSH, ^{15}N]-OmpG. The spectrum was recorded at 900 MHz, 280 K, with a PDSD mixing time of 20 ms and an MAS frequency of 18 kHz (blue).

The intraresidual correlations Cα-Cβ of the Glu, Gln, Asp and Asn are shown. Furthermore, any ^{13}C scrambling in other AAs was not observed (like in the yellow spectrum).

3.3 Extending the mixing time: [^{13}C, ^{15}N]-GALVSHF$_{\alpha,\beta}$Y$_{\alpha,\beta}$-OmpG

These experiments contain a mixing time in the pulse sequence during which magnetisation is transferred between different carbons (figure 3.57). Over which distance magnetisation can diffuse depends on the length of said mixing time. Several spectra of the same samples are recorded with different mixing times. This section shows different overlays of the 2D crystals of the labelled samples at pH 7.5 and at pH 4.7 at different mixing times. In these spectra it is possible to observe that at 50 ms primarily intraresidual peaks show up (paragraph 3.1).

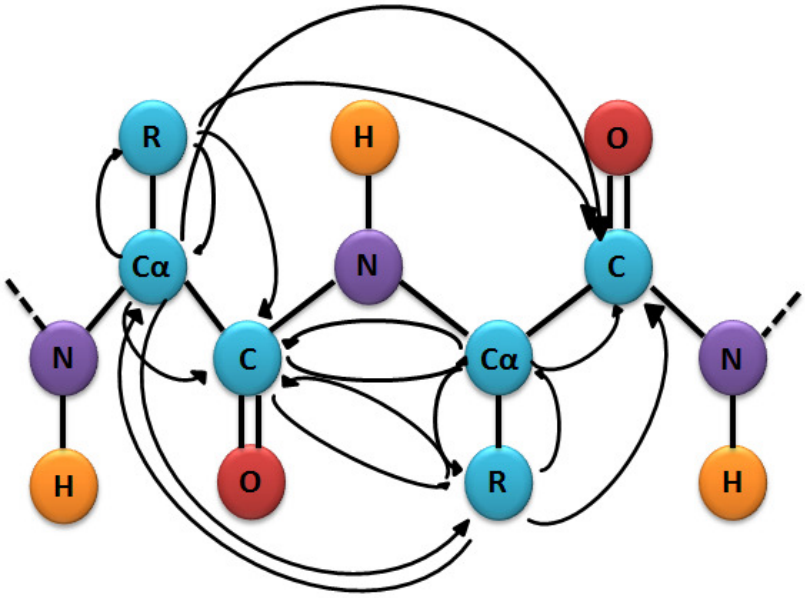

Figure 3.57 2D ^{13}C-^{13}C correlation spectra at different mixing times.

In the 200 ms spectra a sequential peak could be seen and when the mixing time was increased to 400 ms, even a correlation over the β-sheet could be found. However, since the PDSD experiment utilises through-space ^{13}C-^{13}C spin diffusion, these assignments are not unambiguous. Extending ^{13}C-^{13}C mixing time, the magnetisation transfer between Cα carbon atoms of neighbouring β-strands occurs via through-space spin diffusion. Figure 3.58 shows how the extension of the mixing time sequence contained in the pulse sequence is able to detect the interresidual correlations of the aliphatic side chain of the amino acid for the sequential assignment. The interresidual correlations are not assigned but are represented by the overcrowded spectra, especially, in this case, in the aliphatic region, where lots of peaks are present.

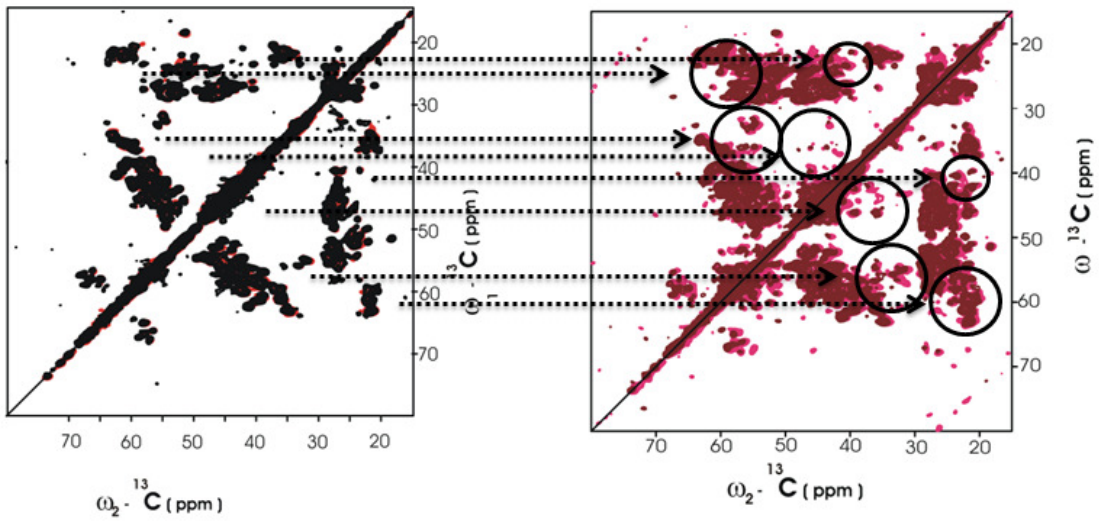

Figure 3.58 Comparison between the overlay of the 2D ^{13}C-^{13}C spectra of the 2D crystals of the labelled sample [^{13}C, ^{15}N]-GALVSHF$_{\alpha,\beta}$Y$_{\alpha,\beta}$-OmpG at pH 7.5 (black) and at pH 4.7 (red) at 50 ms mixing time and the overlay of the 2D ^{13}C-^{13}C spectra of the 2D crystals of the labelled sample [^{13}C, ^{15}N]-GALVSHF$_{\alpha,\beta}$Y$_{\alpha,\beta}$-OmpG at pH 7.5 (brown) and at pH 4.7 (pink) at 400 ms mixing time. All spectra were recorded on the 900 MHz spectrometer.

The extension of the mixing time should result in interresidual correlations between Cβ-Cβ, Cα-Cβ and Cα-Cα carbon atoms becoming visible. With this procedure, and with the use of all specifically labelled OmpG samples, it was possible to assign nearly 50 % of the OmpG amino acid sequence. This strategy was developed because 2D ^{13}C-^{13}C and 3D-NCACX and 3D-NCOCX correlation spectra of uniformly [^{13}C, ^{15}N]-labelled OmpG identified well-separated resonances for some AAs only, for the resonances of all other AA types are mostly overlapped and therefore cannot be identified unambiguously. Therefore, selectively labelled OmpG samples were prepared allowing the identification of assignment starting points.

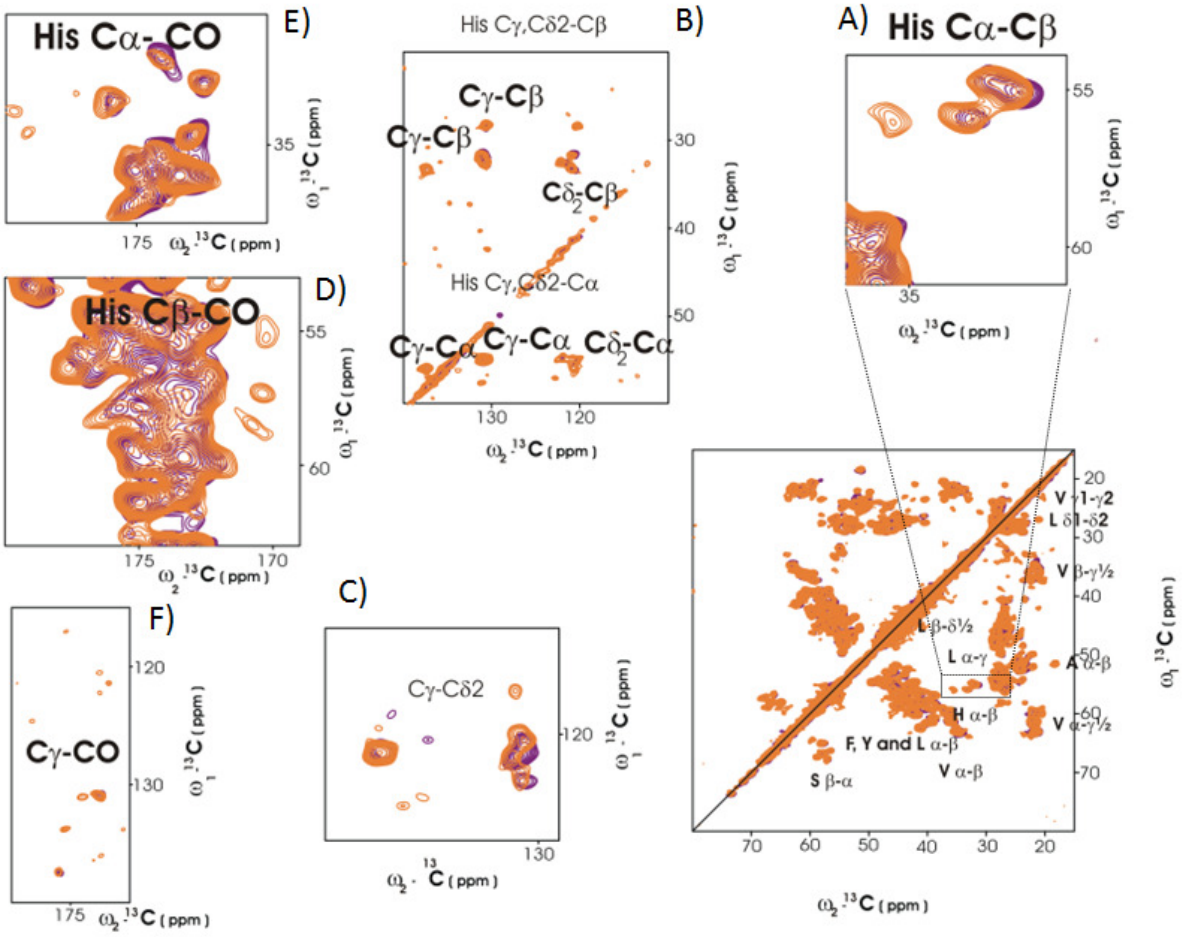

Figure 3.59 Overlay of the 2D ^{13}C-^{13}C spectra of the 2D crystals of the labelled sample [^{13}C, ^{15}N]-GALVSHF$_{\alpha,\beta}$Y$_{\alpha,\beta}$-OmpG at pH 7.5 (yellow) and at pH 4.7 (purple). Both samples were recorded at 50 ms mixing time on the 900 MHz spectrometer with 18 kHz MAS frequency at 280 K.

In figure 3.59 various regions of the 2D spectra at different pH's are overlapped. Different intraresidual correlations are shown: the intraresidual correlations of the aliphatic side chain of the histidines (they were already shown in chapter 3.1 with different colours, A), the intraresidual correlations between the carbons of the imidazole and the aliphatic carbons of the His' side chain (B), the intraresidual correlations among the imidazole carbons (C), the intraresidual correlations between the side chain's aliphatic His carbons and the backbone's carbonyls (D,E) and the intraresidual correlations between the imidazole carbons and the backbone's carbonyls (F).

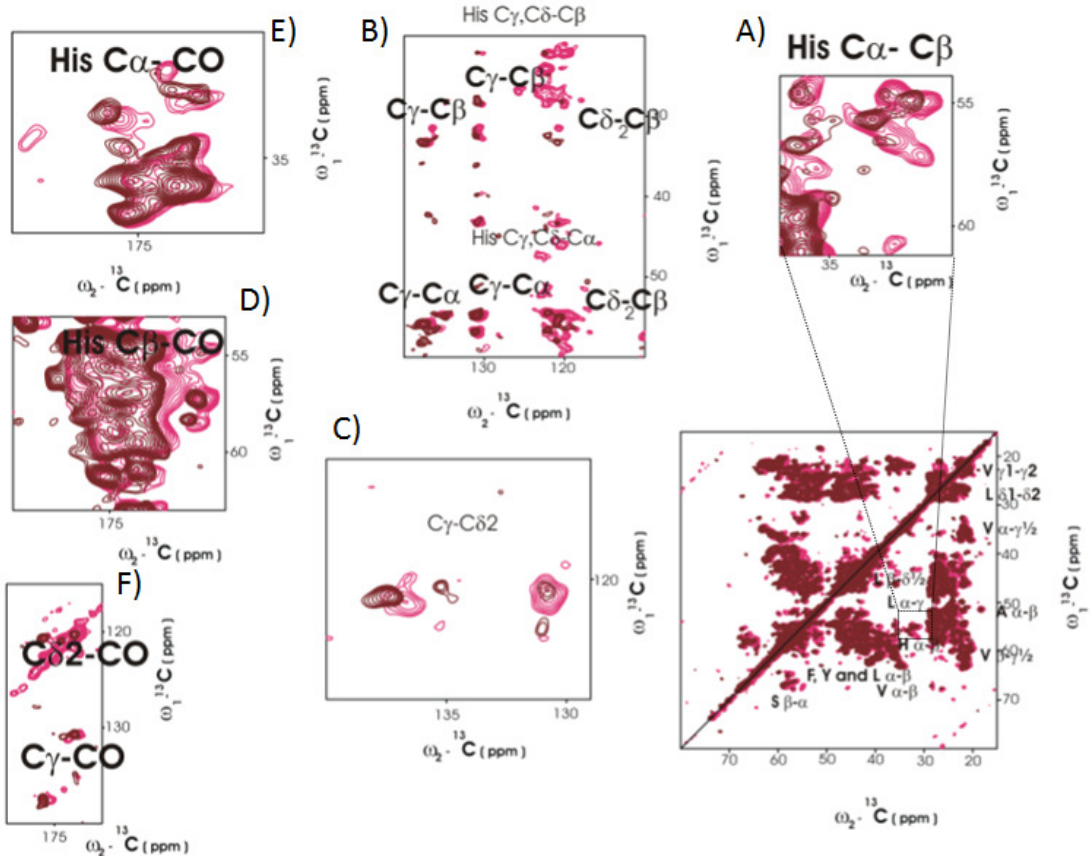

Figure 3.60 Overlay of the 2D ^{13}C-^{13}C spectra of the 2D crystals of the labelled sample [^{13}C, ^{15}N]-GALVSHF$_{\alpha,\beta}$Y$_{\alpha,\beta}$-OmpG at pH 7.5 (brown) and at pH 4.7 (pink). Both spectra were recorded at 900 MHz, at 280 K and with a mixing time sequence of 400 ms. The labelled sample at pH 7.5 was spinned at MAS frequency 18 kHz and the labelled sample at pH 4.7 at MAS frequency 13 kHz.

For both samples the further extension of the mixing time to 400 ms resulted in an enhancement of the peaks in the spectra. The peaks not assigned should represent the interresidual correlations necessary for the sequential assignment. The different MAS frequencies were applied here as well to remove the side bands from the regions of our interest. The difference between the two pH's started to become clearer.

3.4 Low buffer concentration: [^{13}C, ^{15}N]-GALVSHF$_{\alpha,\beta}$Y$_{\alpha,\beta}$-OmpG

This experiment was done to reduce the ion concentration to better irradiate the protein, especially the proton, during the recoupling. The buffer type for NMR experiments in cryogenic probes can have a dramatic effect on the achieved sensitivity (Kelly *et al.,* 2002). Buffers used in protein structure determination add a resistance to the coil, resulting in a reduced signal-to-noise ratio. It is very important for the use of buffer solutions to keep the pH constant and the molecule in a defined protonation state. In other cases some salts have to be added to increase the solubility and to prevent protein aggregation. It is necessary to optimise the buffer conditions by reducing the total salt concentration and the ion mobility to achieve a high sensitivity. Using NMR buffers made of ions with low ion mobility should provide a way to improve the sensitivity in NMR experiments, even though a high salt concentration is necessary. To decrease the ion concentration 20 mM HEPES or 20 mM MOPS buffers were used, both at pH 7.5, to improve the efficiency of the 3D-NCACX. These two buffers are easily prepared in the laboratory. The GANDSH-OmpG sample at pH 5.6 was removed from the 4 mm rotor and washed with buffer PPi 200 mM (containing NaCl 50 mM and NaN_3 2 mM as well) at pH 7.5. The washing step was done three times and consists of centrifugation at 14.000 rpm for 10 min and ultracentrifugation at 235.000 g for 1 hour at 8 ℃.

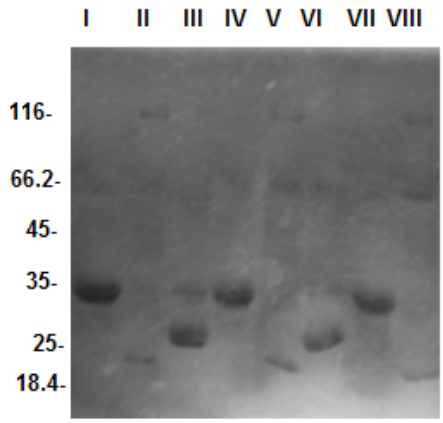

Figure 3.61 SDS-PAGE analysis of the 2D crystals of the [^{13}C, ^{15}N]-GANDSH-OmpG at pH 7.5 washed in 20 mM HEPES and 20 mM MOPS buffer at pH 7.5. Lane I = reference; Lane II = molecular weight marker (Fermentas); Lane III = refolded OmpG in 20 mM HEPES at pH 7.5; Lane IV = denatured OmpG in 20 mM HEPES at pH 7.5; Lane V = molecular weight marker (Fermentas); Lane VI = refolded OmpG in 20 mM MOPS at pH 7.5; Lane VII = denatured OmpG in 20 mM MOPS at pH 7.5; Lane VIII = molecular weight marker (Fermentas).

The sample was divided into two parts before ultracentrifugation. After the ultracentrifugation the two parts were washed separately with 20 mM HEPES (containing 25 mM NaCl and 12.5 mm $MgCl_2$) and 20 mM MOPS (containing 25 mM NaCl and 12.5 mM $MgCl_2$), both at pH 7.5. These two buffers were used to reduce the ion concentration because their conductivity was tested before these experiments: 6.64 mS/ cm for 20 mM HEPES buffer at pH 7.5 and 7.38 mS/ cm for 20 mM MOPS buffer at pH 7.5 using 20 mM of BIS TRIS buffer at pH 7.5 as a reference. After SDS-PAGE analysis, which was done to check whether the protein was still refolded in the lipid bilayer, 1D ^{13}C experiments were recorded (data not shown) to understand which buffer fits best for our purpose. Due to the 1D ^{13}C experiments' results 20mM HEPES at pH 7.5 was chosen, considering the better resolution of the 1D ^{13}C-CP/MAS experiment (although the buffers were not filtered). Subsequently, the experiment was repeated with the 2D crystals of the GALVSHF$_{\alpha,\beta}$Y$_{\alpha,\beta}$-OmpG at pH 7.5 using 20 mM HEPES at pH 7.5. The crystals were washed in PPi buffer (three washing steps at 14.000 rpm for 10 min) and then in 20 mM HEPES at pH 7.5 (three washing steps) and were then ultracentrifuged overnight at 235.000 g at 8 °C. After the overnight ultracentrifugation samples were taken for SDS-PAGE analysis.

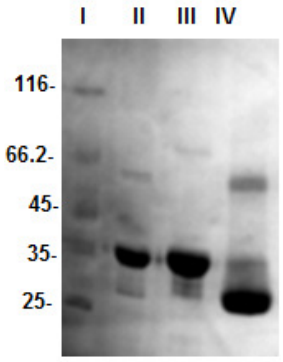

Figure 3.62 SDS-PAGE analysis of the 2D crystals of the [^{13}C, ^{15}N]-GALVSHF$_{\alpha,\beta}$Y$_{\alpha,\beta}$-OmpG at pH 7.5. Lane I = molecular weight marker (Fermentas); Lane II = denatured OmpG control; Lane III = denatured labelled OmpG sample in 20 mM HEPES at pH 7.5; Lane IV = refolded OmpG in 20 mM HEPES at pH 7.5.

After SDS-PAGE analysis a 2D-NCO experiment was recorded to check if it is possible to increase the resolution or signal-to-noise ratio using 20 mM HEPES at pH 7.5. This experiment was planned following the publication of Kelly (Kelly *et al.,* 2003).

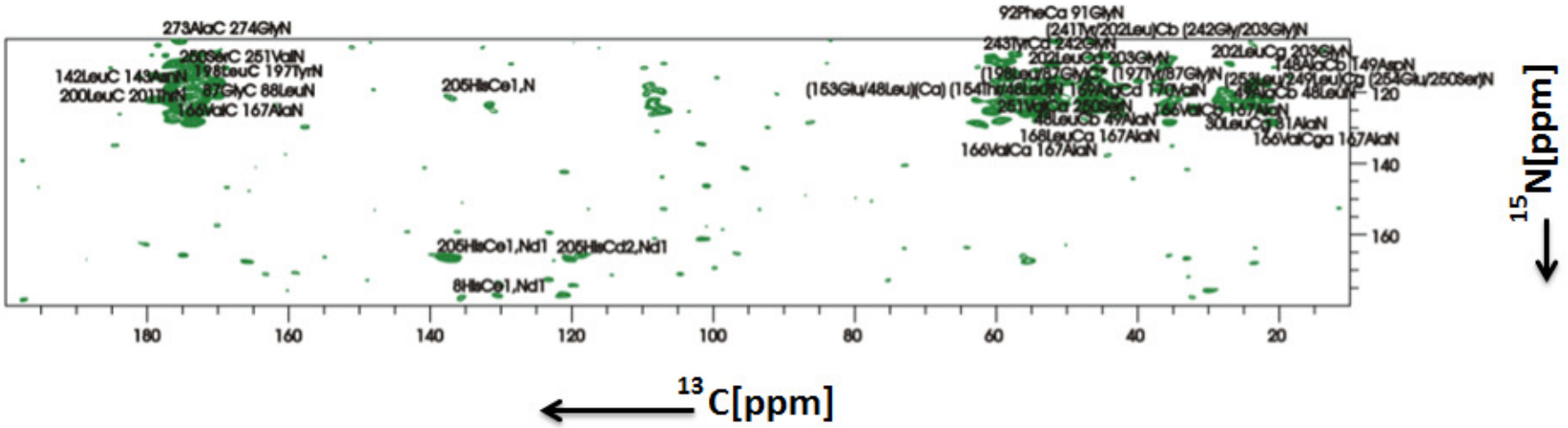

Figure 3.63 2D NCO spectrum of 2D crystals of [^{13}C, ^{15}N]-GALVSHF$_{\alpha,\beta}$Y$_{\alpha,\beta}$-OmpG. The spectrum was recorded on the 700 MHz spectrometer at an MAS frequency of 13 kHz at 280 K.

In this 2D-NCO experiment done on the 700 MHz at MAS 13 kHz it was possible to observe an enhancement of both the resolution, using 20 mM HEPES buffer, and the structural information that can be obtained for different graphic interpretations. Obviously this experiment should be recorded simultaneously with a 2D-NCA for the sequential assignment, but 2D solid-state MAS NMR techniques for the sequential assignment have been overcome by 3D experiments in which 3D-NCACX and 3D NCOCX are used for the sequential assignment, because they provide better structural biological information. What was described above had the purpose of increasing the signal-to-noise ratio. These 2D experiments show the correlation between the N of the AA and the CO^{-i} or $C\alpha^{-i}$ of the previous AA.

4 Conclusions and outlook

This thesis describes the labelling strategies for investigations in membrane protein dynamics and sugar coordination by solid-state MAS NMR. The adapted labelling strategies allow the ambiguous identification of assignment´s starting point of the 281-residue OmpG protein used as a model system.

In general, an essential prerequisite for structural investigation of MPs by NMR is the availability of high amounts of an isotopically labelled MP sample, which should be homogeneous in terms of purity and conformation. In paragraph 3.1, the work focused on the labelling strategy adapted for the preparation of labelled samples designated to be used in investigations in the dynamics of the loops and sugar binding sites of OmpG. In paragraph 3.2, the work focused on the preparation of large amounts of isotopically labelled OmpG, using suitable expression protocols to prepare MP samples of OmpG for solid-state MAS NMR investigation. In paragraph 3.1, the labelling strategy used to study the dynamics of OmpG at different pH's is described. Yildiz (Yildiz *et al.,* 2006) claims that the loop dynamics exist due to two histidines (His 231 on loop 6 and His 261 on loop 7). For this reason, each histidine as well as its anterior and posterior AA was specifically labelled in OmpG for the sequential assignment. The selective labelling scheme was chosen to reduce spectral congestion caused by various AAs as was shown in previous works about uniformly [^{13}C, ^{15}N]-labelled OmpG. The histidines were labelled to check whether they are involved in the opening/closing mechanism of OmpG. F and Y were labelled only in α and β position to have clear peaks of the histidines in the imidazole region between 140–120 ppm. The other AAs' labelling did not give any trace of scrambling in other AAs. It was done considering the metabolism of the AAs in *E. coli*. The sample was expressed as a non-functional inclusion bodies precipitate. It was shown that the purification and the subsequent in vitro refolding yielded high amounts of native OmpG/ ℓ of culture. This section describes the biophysical problem in the preparation of labelled OmpG samples in 2D crystals at acid pH. After the refolding procedure the labelled OmpG sample was reconstituted in a lipid environment to reproduce the native condition, the biological environment. In a first step the membrane protein reconstituted in a lipid environment (at pH 5.6) during the centrifugation or the spinning of the rotor at MAS frequency shows a strange behaviour, namely misfolding from the lipid environment. After the optimisation of the sample preparation at acid condition (the procedure is shown in 3.1.5.2), the labelled OmpG sample was suitable for solid-state MAS NMR studies. The 1D ^{13}C-CP/MAS NMR spectrum, ^{15}N-CP/MAS NMR spectrum and 2D ^{13}C-^{13}C spectrum at pH 4.7 showed a sufficient resolution for structural study. The labelled OmpG sample at pH 7.5 did not present a biophysical problem during its preparation. It was

the first sample analysis by solid-state MAS NMR. It was recorded 1D ^{13}C-CP/MAS NMR spectrum, ^{15}N-CP/MAS spectrum and 2D ^{13}C-^{13}C spectrum showing high resolution for structural study. Both samples were reconstituted in a lipid environment at a lipid-to-protein ratio of 0.5 (for 10 mg of labelled protein 20 mg of lipids were used). The preparation of 2D crystals of the labelled OmpG samples at different pH's produced highly resolved NMR spectra in comparison to the proteoliposome, which, due to the high lipid protein ratio used (50–100:1), decreased the sensitivity of the solid-state MAS NMR experiment drastically. Cause of this effect is that MPs lead to a line broadened spectrum when in inhomogeneous conformational state. This demonstrates how the 2D crystals are the most frequently used preparation type for NMR studies for various reasons. They can be prepared using well-known crystallisation screens. The protein homogeneity and density in this preparation type is high, which guarantees high sensitivity in solid-state MAS NMR experiments.

The solid-state MAS NMR studies of the labelled OmpG samples at different pH's, reconstituted in a lipid environment, showed no significant differences at various pH's when the 2D ^{13}C-^{13}C spectra were recorded. There were some weak differences in the chemical shift of the His region (imidazole and aliphatic side chain regions). It represented the region of our interest considering that, according to the X-ray crystallography (Yildiz *et al.,* 2006), the His 231 and His 261 are responsible to the opening/closing state of OmpG at different pH's. This consideration is additionally supported by site-specific mutagenesis studies (Chen *et al.,* 2008), AFM and SMFS studies (Damaghi *et al.,* 2010, Mari *et al.,* 2010). An FTIR study (Korkmaz *et al.,* 2012) demonstrated that, at different pH's in the closure of the channel, the involved His 231 and His 261 are supported from other AAs.

The overlay of the 2D ^{13}C-^{13}C spectra of the 2D crystals at different pH's shows that some intraresidual correlations of the His in the imidazole region have different chemical shifts in comparison to each other. It could represent the different orientation of the His inside and outside the channel, in the lipid environment. At different pH's, this experiment did not show strong differences. These weak differences between the spectra at different pH's are not only true for the His region (aromatic and aliphatic) but also for the other labelled AAs' intraresidual correlations. In the overlay of the 1D ^{15}N-CP/MAS spectra of the labelled sample at pH 7.5 and at pH 4.7, the Nε2 and Nδ1 signals of the imidazol of the His show different intensity. This difference represents the different state of protonation of the histidine's imidazole at different pH's. At pH 7.5 the imidazol of these Histidines is in neutral form, whereas it is protonated at pH 4.7. The results shown in this thesis cannot support the opening/closing mechanism suggested by the X ray crystallographer because the His signals involved in the dynamics of the loop 6 and 7 are not detected. At different pH's the imidazol of the His show a different protonation state but it is referred to the histidines of the barrel of OmpG. Other authors explain how, using different spectroscopic methods, the closing

conformation is induced not only by the repulsion between the His 231 and His 261 but other interactions (among some AAs of loop 6 and AAs inside the lumen of the pore) can have a rule in opening/closing mechanism (Damaghi *et al.,* 2010). Another group explain that in situ opening/closing experiments shows that the negatively charged AAs (Asp and Glu), and the positively charged Arg residues also play an active role; possibly by interacting with each other inside the pore lumen. Therefore it was suggested that the closure of the channel at acidic pH values is not only via closing the channel entrance by loop 6, but also via changing the electric potential due to the different state of charged amino acid inside the lumen in order to effectively block the gateway (Korkmaz *et al.,* 2012). To confirm these other spectroscopic methods should be prepared other labelled samples of OmpG where are labelled these AAs involved in the opening/closing mechanism. These partial conclusions do not demonstrate the pH gating but require a set of solid-state MAS NMR experiments to detect the other histidine signals. The dynamics of loop 6, where His 231 and His 261 are involved respectively, could be studied with ^{1}H-^{13}C INEPT and ^{1}H-^{13}C CP experiments (to investigate respectively the flexible and rigid part of OmpG as was shown in the publication of Iordanov to study the mobile part of *Klebsiella pneumoniae*'s OmpA transmembrane domain) using the deuterated [^{13}C, ^{15}N]-OmpG sample at different pH's (Iordanov *et al.,* 2012; Linser *et al.,* 2011). A 2D ^{13}C-^{13}C spectra at different pH's could be executed with a TOBSY mixing time sequence (using INEPT to transfer magnetisation from the ^{1}H to ^{13}C), at an MAS spinning frequency of 10 kHz, to characterise the structure and dynamics of OmpG (as was done with the recombinant integral membrane protein PagL in the whole cell, in cell envelope and in proteoliposome; Renault *et al.,* 2012). Other NMR schemes for the detection of mobile protein segments under MAS condition (using TOBSY or NOESY mixing time sequence) are: a) HCC b) HHC or HHN, c) HNCACB or HNCOCACB, and d) HNHHC. These are double and triple channel pulse sequences for two- or three-dimensional NMR experiments. Andronesi (Andronesi *et al.,* 2005) applied these solid-state MAS NMR techniques to a uniform [^{13}C, ^{15}N] variant of the 52-residue polypeptide phospholamban.

Another approach would be to spin faster, at 60 kHz and at 20 kHz using TOBSY mixing time sequence. TOBSY mixing time sequence are also used to investigate the dynamics of the 18.5 kDa myelin basic protein by Zhong (Zhong *et al.,* 2007) and to study another protein by Hardy (Hardy *et al.,* 2000). It is also possible to use Gd^{3+}, a paramagnetic substance. Gd^{3+} is an inhibitor of the channel (Conlan *et al.,* 2003). It binds the OmpG channel on the loop 6, weakening the inward-facing His' signals in the process. The idea was to wash the labelled sample at pH 7.5 and at pH 4.7 with 1 mM of Gd^{3+} to detect and to weaken the signals of the histidines and then to record a 2D ^{13}C-^{13}C spectrum to check the status of the His (imidazole) region. The calculation of the pKa was another method to find out whether lowering the pH to 4.7 was sufficient or not to get the closing conformation. To calculate it, it

is necessary to titrate the signal of the Nε2 or Nδ1 between pH 7.5 and 4.7 (Smith *et al.,* 1989).

After all these experiments it should be possible to build different OmpG models, representing the two different conformation states at various pH's.

The paragraph 3.2 describes the labelling strategy, preparation type and characterisation by solid-state MAS NMR of the labelled OmpG sample to study the sugar binding of OmpG. OmpG is a channel that is, at different pH's, either opening, allowing the entrance of mono-, di- and trisaccharides, or closing. Inside the pore there is an aromatic line (mostly composed of aromatic AAs, especially Tyr) that probably transports the sugar. Inside the pore some sugars can bind the protein. To study this mechanism, the AAs involved in this coordination were labelled. The aromatic AAs were not labelled as this was supposed to be the second part of this project. Some AAs involved in this labelling pattern underwent scrambling in other AAs. To prepare this labelled sample, it was necessary to label those AAs that can scramble in other AAs. Therefore some inhibitors and an excess of AAs were added. This was done especially to label D, N, E and Q.

The preparation of this labelled sample was done following the publication of Tong (Tong *et al.,* 2008). The labelled sample was expressed as a non-functional inclusion bodies precipitate. First, the expression level of the protein in *E.coli* was checked because some inhibitors used to repress the expression of the protein. The protein was expressed in unlabelled form and, after optimisation of the protocol, a sufficient amount of the protein was obtained for solid-state MAS NMR study. In modified M9 minimal medium (Protocol A – figure 3.39) the cells grew less than in standard M9 minimal medium and the expression of GENDQPASR-OmpG was drastically decreased, so a new protocol (called Protocol B) with a different concentration of inhibitors and a different excess of AAs was performed, which allowed the expression of larger amounts of the labelled sample in less time.

After the purification procedure in denaturing condition, the labelled OmpG protein was refolded and reconstituted in a lipid environment at LPR 0.5 to characterise the protein in its biological environment. The crystallisation condition was the same used before but in this case the protein was crystallised at pH 7.5 because it was necessary to have the opening OmpG conformation to study the entering and binding of the sugar.

For solid-state MAS NMR study a 1D ^{13}C-CP/MAS NMR and a 2D ^{13}C-^{13}C were recorded. In 1D ^{13}C-CP/MAS the aliphatic signals of the methyl and methylen of the aliphatic labelled AAs and the carbonylic and carboxylic signals of all labelled AAs are shown. Characteristic is the carboxylic signal of the Arg at 160 ppm. In the 2D ^{13}C-^{13}C it is possible to observe all intraresidual peaks of all labelled AAs. Especially the signals of the proline and arginine are very visible in all intraresidual correlations.

To characterise the sugar binding, further studies with the labelled sample could be done. It is possible to wash the sample with 1 mM of maltose to study the variation of the chemical shift of the labelled AAs, to record a 2D ^{13}C-^{13}C REDOR mixed to the carbons at different pH's (7.5 and 4.7), to study the chemical shift variation of the carboxyl of Asp, Glu and the guanidine group of Arg when they are selectively irradiated and to execute three dimensional experiments for the sequential assignment (3D-NCACX and 3D-NCOCX). In the paragraph 3.3 it is shown how, by extending the mixing time sequence in the pulse sequence, it is possible to visualise interresidual correlations in the aliphatic and aromatic region of the labelled samples at different pH's. Usually this is possible for all labelled samples of every MP. The overlay between labelled samples with different mixing times and pH's should reinforce the differences at different pH's between the spectra as well. This is just one way how the sequential assignment could be done. Other methods might involve other labelling schemes used to prepare OmpG samples that are not discussed in this thesis but in other works. The paragraph 3.4 discusses the importance of the buffer system for NMR study. The concentration of the salts in the buffer is important to keep the pH value fixed, but sometimes the concentration and the mobility of the ions can have an effect on the sensitivity of the measurement, thus making it necessary to decrease the concentration of the salts in the buffers or to use another one. A labelled OmpG sample was washed in PPi buffers and cut into two parts. Each part was washed with two different buffers: 20 mM HEPES and 20 mM MOPS, both at pH 7.5. They were chosen for their low conductivity (Kelly *et al.,* 2002) and for their easy preparation in the laboratory. For our purpose HEPES buffer showed better characteristics. The 1D ^{13}C-CP/MAS obtained demonstrated a good resolution. Another labelled sample of OmpG was taken and washed with HEPES buffer at pH 7.5, resulting in the detection of a 2D NCO showing high resolution.

The work described in this thesis shows the development of new labelling strategies and sample preparation protocols for the structural characterisation of large MPs by solid-state MAS NMR.

Summary

Membrane proteins represent one third of all proteins in most genomes and carry out a wide range of essential cellular functions. They transport ions and metabolites across the lipid membranes that surround cells and intracellular organelles, convert light energy to chemical energy, fuse the membranes of two cells, and transmit chemical signals across the membrane to regulate cell growth and division. It is known that the mutation, the misfolding and malfunctioning of membrane proteins can cause devastating diseases. Thus, membrane proteins are of significant biological and medical importance since they represent over 50 % of the current drug targets. Although a number of biophysical techniques including X-ray crystallography, electron microscopy and solution NMR spectroscopy have been used to determine membrane protein structures, these methods are unable to replicate and accommodate the complexity and diversity of natural membrane proteins. Additionally, X-ray crystallography and electron microscopy require highly diffracting 3D and 2D crystals, respectively. Solid-state MAS NMR is a versatile method for structural biology and can be used to provide new insights into the structures of membrane components and their mutual interactions. The extensive variety of sample forms amenable for study by solid-state MAS NMR allows data to be collected from proteins in conditions that are more similar to those of the native environment, and therefore are much closer to a functional state.

In this thesis, different labelling strategies for structural characterisation of MP studies were tested by solid-state MAS NMR. The determination of large proteins by NMR is frequently hampered by several major problems, including the complexity of crowded spectra, fast nuclear relaxation, low sensitivity and the lack of precise conformational constrains. The development of sample labelling, in particular with NMR visible isotopes, become a commonly employed strategy. In NMR of large proteins sample labelling allows to improve methods for protein production and devise more sophisticated and elegant labelling strategies. The aim of isotope labelling is to increase the sensitivity and resolution, to simplify the complexities of spectra and to narrow the line widths. The labelling strategy used in this thesis is the selective labelling. For the preparation of these labelled samples were considered the cross labelling and isotopic dilution that sometimes can be reduced by increasing and decreasing the concentration of the appropriate unlabelled amino acids in the media as a compensatory effect. Here were produced different selectively labelled OmpG samples and the spectral overlap was decreased in comparison to the uniformly labelled sample of OmpG with the aim to extend the number of assignment possibilities. The assignment used in this thesis is the intraresidual assignment which represents the identification of all the labelled AAs in a spin system. It was done on 2D ^{13}C-^{13}C spectra of

labelled OmpG. The labelling preparation types are described for different labelled OmpG samples for solid-state MAS NMR studies. A prerequisite for NMR study is the amount of recombinant protein (more than 10 mg). This requisite is satisfied in both labelled samples prepared. The results from this work, combined with data found in literature, show that this highly diffracting crystalline material is not a prerequirement for structural analysis of MPs for solid-state MAS NMR. It is possible to use poorly diffracting 2D crystals and it allows the structural investigation in a quasi-native environment. To prepare MP samples suitable for solid-state MAS NMR studies there are well established screening methods for 2D crystallisation of MPs.

The paragraph 3.1 of the chapter 3 shows the labelling strategy to study the mobile part of OmpG, the expression protocol used to achieve the amount of expressed protein suitable for solid-state MAS NMR study, the refolding procedure applied and the reconstitution of the refolded labelled protein into 2D crystals at neutral and at acid pH (to characterise the mobile part of the protein responsible for the pH gating). This paragraph also describes the biophysical problem to prepare 2D crystals of labelled OmpG in acid condition and how they are finally prepared. On these 2D crystals of labelled OmpG at different pH's solid-state MAS NMR experiments were applied to characterise the protein at different conformational states.

The paragraph 3.2 describes the preparation of the second labelled OmpG NMR sample to study the region of the protein involved in the sugar binding. Here the labelling strategy, the expression protocol, the refolding procedure, the reconstitution in 2D crystals and the solid-state MAS NMR characterisation are shown. In this paragraph the expression protocol was necessarily modified to obtain enough labelled OmpG sample for structural studies because some inhibitors were used to minimise isotope dilution and an excess of AAs.

The paragraph 3.3 shows how, by extending the mixing time in the pulse sequence, it is possible to obtain interresidual correlation important for the sequential assignment. Several spectra at different mixing times and different pH's are overlapped to find out whether the chemical shift of these new peaks (the intraresidual correlations) could change at different pH's. At the end the paragraph 3.4 describes the importance of the buffer condition to obtain a high spectrum resolution. A 2D spectrum was recorded and the signal-to-noise ratio was improved.

This thesis wants to establish an approach to the preparation of different samples for NMR, particularly for studies of different regions of large MPs in their biological environment, using different selective labelling schemes for structural analysis by solid-state MAS NMR.

Zusammenfassung

Membranproteine stellen ein Drittel aller Proteine in den meisten Genomen dar und führen eine breite Palette von essentiellen zellulären Funktionen durch. Sie transportieren Ionen und Metaboliten für die Lipidmembranen, die die Zellen und die intrazellulären Organellen umgeben, wandeln Licht in chemische Energie um, verschmelzen die Membranen der beiden Zellen und übertragen chemische Signale über die Membran, um Zellwachstum und -teilung zu regulieren. Es ist bekannt, dass Mutationen, Fehlfaltungen und Fehlfunktionen der Membranproteine verheerende Krankheiten verursachen können. Somit sind Membranproteine von signifikanter biologischer und medizinischer Bedeutung, da sie aktuell mehr als 50 % aller Angriffspunkte von Medikamenten darstellen. Obwohl eine Reihe biophysikalischer Techniken wie Röntgenkristallographie, Elektronenmikroskopie und NMR-Spektroskopie verwendet wurden, um Membran-Protein-Strukturen zu bestimmen, sind diese Methoden nicht in der Lage, die Komplexität und Vielfalt der natürlichen Membranproteine zu replizieren. Außerdem erfordern Röntgenkristallographie und Elektronenmikroskopie stark beugende 3D- und 2D-Kristalle.

Festkörper-MAS-NMR-Spektroskopie ist eine vielseitig anwendbare Methode in der Strukturbiologie und kann verwendet werden, um neue Einblicke in die Strukturen der Membrankomponenten und deren Wechselwirkungen zu liefern. Der Reichtum an für die Festkörper-MAS-NMR-Studie geeigneten Probenarten sorgt dafür, dass Daten über Proteine in einer Umgebung gesammelt werden können, die naturgetreuer und daher viel näher an einem funktionsfähigen Zustand ist.

In dieser Arbeit wurden unterschiedliche Kennzeichnungsstrategien zur strukturellen Charakterisierung von Membranproteinen mittels Festkörper-MAS-NMR getestet. Die Bestimmung der makromolekularen Struktur durch NMR wird häufig von mehreren großen Problemen, wie der Komplexität der überfüllten Spektren, schnellen Kernrelaxationszeiten, geringer Empfindlichkeit und ungenauen Konformativen, stark behindert. Die Entwicklung der Probenbeschriftung, insbesondere mit NMR sichtbarer Isotope, ist eine der üblicherweise eingesetzten Strategien. In NMR mit großen Proteinen, die die Methoden zur Proteinproduktion erlauben, sind anspruchsvollere und elegantere Kennzeichnungsstrategien möglich. Das Ziel der Isotopenmarkierung ist es, die Empfindlichkeit und die Auflösung zu erhöhen, um die Komplexität der Spektren zu vereinfachen und die Linienbreiten einzugrenzen. Die Kennzeichnungsstrategie, welche in dieser Arbeit verwendet wird, ist die selektive Kennzeichnung. Um diese markierten Proben vorzubereiten, wurden die Kreuzkennzeichnung und Isotopenverdünnung berücksichtigt, die manchmal durch Erhöhung und Verringerung der Konzentration der entsprechenden unmarkierten Aminosäuren in den Medien als ausgleichende Wirkung reduziert werden

können. Es wurde auch der Stoffwechsel der Aminosäuren in *E. coli* berücksichtigt. Unter Verwendung der Vorwärtsmarkierung wurden selektiv markierte OMPG-Proben hergestellt und die spektrale Überlappung im Vergleich zur Probe aus gleichmäßigen OMPG reduziert, mit dem Ziel die Anzahl der Zuordnungsmöglichkeiten zu erweitern. Die Zuordnung, die in dieser Arbeit verwendet wird, ist die intraresiduelle Zuordnung, welche die Identifizierung aller markierten Aminosäuren in einem Spin-System darstellt. Es basiert auf zweidimensionalen ^{13}C-^{13}C-Spektren der markierten OMPG. Die verschiedenen Typen von Kennzeichnungsstrategien werden für diverse markierte OMPG-Proben zur Verwendung in Festkörper-MAS-NMR-Studien beschrieben.

Eine Voraussetzung für die NMR-Studie ist die Menge an rekombinantem Protein (mehr als 10 mg). Diese Voraussetzung ist in beiden markierten Proben erfüllt. Es wird auch beschrieben, dass schlecht gebeugte Kristalle von Proteinen der äußeren Membran G (OMPG) als Modellsystem für große Membranproteine dienen. Die Ergebnisse dieser Arbeit kombiniert mit Fachliteratur zeigen, dass die hoch beugenden kristallinen Materialien keine Vorbedingung für die Strukturanalyse von Membranproteinen für Festkörper-MAS-NMR darstellen. Es ist möglich, schlecht beugende 2D-Kristalle zu verwenden und es ermöglicht die strukturelle Untersuchung in einer quasi-natürlichen Umgebung. Um Membranproteinproben für Festkörper-MAS-NMR-Studien vorzubereiten gibt es etablierte Screening-Methoden für die 2D-Kristallisation von Membranproteinen.

In Paragraph 3.1 des Kapitels 3 wird das Verfahren zur Vorbereitung gezeigt, welches der Bezeichnung von OMPG in rekonstituierten 2D-Kristallen bei neutralem und saurem pH-Wert dient (weil die beweglichen Teile des Proteins charakterisiert werden sollen). Besprochen werden außerdem die Probleme, auf die wir bei der Vorbereitung der markierten Probe bei saurem pH-Wert trafen, und wie wir sie überwanden. In Paragraph 3.2 wird auch die Herstellung der zweiten markierten Probe beschrieben. Hierbei geht es um die Region des Proteins in der Zucker-Bindung. Aufgrund der Verwendung von Inhibitoren zur Minimierung der Isotopenverdünnung war es schwierig, eine genügende Menge der markierten Probe für die NMR-Untersuchung zu erhalten. Das Verfahren zur Herstellung der NMR-Probe ist dasselbe wie das im Falle der dynamischen Teile des Proteins bei unterschiedlichen pH-Werten gezeigte, jedoch mit anderem Ziel.

Es wird auch gezeigt (Paragraph 3.3), wie durch Verlängerung der Mischzeit in der Impulsfolge die interresiduelle Korrelation erreicht werden kann, die für die sequentielle Zuordnung wichtig ist. Hierbei werden mehrere Spektren bei unterschiedlichen Mischzeiten und verschiedenen pH-Werten übereinandergelegt, um herauszufinden, wann und ob sich die chemische Verschiebung dieser neuen Höchststände (die Intraresidualkorrelationen) bei verschiedenen pH-Werten verändern könnte.

Zuletzt (Paragraph 3.4) wird die Bedeutung des Pufferzustandes beschrieben, der nötig ist, um eine hohe spektrale Auflösung zu erhalten. Ein 2D-Spektrum wurde aufgenommen und das Signal-Rausch-Verhältnis verbessert.

Diese These will einen Ansatz zur Vorbereitung verschiedener Proben für NMR schaffen, insbesondere zur Erforschung anderer Regionen der großen Membranproteine in ihrer biologischen Umgebung unter Zuhilfenahme verschiedener selektiver Kennzeichnungssysteme zur Strukturanalyse durch Festkörper-MAS-NMR.

References

Andronesi, O. C., Becker, S., Seidel, K., Heise, H., Young, H. S., Baldus, M. Determination of membrane protein structure and dynamics by magic-angle-spinning solid-state NMR spectroscopy (2005). *J. Am. Chem. Soc.* **127** (37), 12965–12974.

Arakawa, T., Ejima, D., Tsumoto, K., Obcjama, L., Tanaka, Y., Kita, Y., Timasheff, S. N. Suppression of protein interactions by Arginine: A proposed mechanism of the arginine effects (2007). *Biophysical chemistry* **127**, 1–8.

Baldermann, C., Engelhardt, H. Expression, two-dimensional crystallization, and three-dimensional reconstruction of the h8 outer membrane protein Omp21 from Comamonas acidovorans (2000). *J. Struct. Biol.* **131,** 96–107.

Baldus, M., Geurts, D. G., Hediger, S., Meier, B. H. Efficient N-15-C-13 polarization transfer by adiabatic-passage Hartmann-Hahn cross polarization (1996). *J. Magn. Reson. A* **118**, 140–144.

Baldus, M., Petkova, A. T., Herzfeld, J., Griffin, R. G. Cross polarization in the tilted frame: assignment and spectral simplification in heteronuclear spin systems (1998). *Mol. Phys.* **95**, 1197–1207.

Basle, A., Rummel, G., Storici, P., Rosenbusch, J. P., Schirmer, T. Crystal structure of osmoporin OmpC from *E. coli* at 2.0 Å (2006). *Journal of Molecular Biology* **362** (5), 933–942.

Bannwarth, M., Schulz, G.E. The expression of outer membrane proteins for crystallization (2003). *Biochimica et Biophysica Acta – Biomembranes* **1610**, 37–45.

Bayburt, T. H., Carlson, J. W., Sligar, S. G. Reconstitution and imaging of a membrane protein in a nanometer-size phospholipid bilayer (1988). *J. Struct. Biol.* **123**, 37–44.

Bayley, H., Cremer, P.S. Stochastic sensors inspired by biology (2001). *Nature* **413**, 226–230.

Becker, J. Ferguson, N., Flinders, J., van Rossum B. J., Fersht A. R., Oschkinat H. A sequential assignment procedure for proteins that have intermediate line widths in MAS NMR spectra: amyloid fibrils of human CA150.WW2 (2008). *Chembiochem.* **9**, 1946–1952.

Beher, M. G., Schnaitman, C. A., Pugsley, A. P. Major Heat-Modifiable Outer-Membrane Protein in Gram-Negative Bacteria – Comparison with the OmpA Protein of *Escherichia-Coli* (1980). *Journal of Bacteriology* **143**, 906–913.

Behlau, M., Mills, D. J., Quader, H., Kühlbrandt, W., Vonck, J. Projection structure of the monomeric porin OmpG at 6 angstrom resolution (2001). *Journal of Molecular Biology* **305**, 71–77.

Bennett, A. E., Ok, J. H., Griffin, R. G., Vega, S. Chemical-Shift Correlation Spectroscopy in Rotating Solids – Radio Frequency-Driven Dipolar Recoupling and Longitudinal Exchange (1992). *J. Chem. Phys.* **96**, 8624–8627.

Bennett, A. E., Rienstra, C. M., Auger, M., Lakshmi, K. V., Griffin, R. G. Heteronuclear decoupling in rotating solids (1995). *J. Chem. Phys.* **103**, 6951–6958.

Berman, H.M. Westbrook, J., Feng, Z., Gilliland, G, Bhat, T.N., Weissig, H., Shindyalov, I.N., Bourne, P.E. The Protein Data Bank (2000). *Nucleic Acids Research* **28**, 235–242.

Binda, C., Newton-Vinson, P., Hubalek, F., Edmondson, D. E., Mattevi, A. Structure of human monoamino oxidase B, a drug target for the treatment of neurological disorders (2002). *Nat. Struct. Biol.* **9**, 22–26

Blaauw, M., Dekker, N., Verheij, H. M., Kalk, K. H., Dijkstra, B. W. Crystallization and preliminary X-ray analysis of outer membrane phospholipase A from *Escherichia coli* (1995). *FEBS Lett.* **373**, 10–12.

Blanchette, C. D., Law, R., Benner, W. H., Pesavento, J. B., Cappuccio, J. A., Walsworth, V., Kuhn, E. A., Corzett, M., Chromy, B. A., Segelke, B. W. Coleman, M.A., Bench, G., Hoeprich, P.D., Sulchek, T.A. Quantifying size distributions of nanolipoprotein particles with single-particle analysis and molecular dynamic simulations (2008). *J. Lipid. Res.* **49**, 1420–1430.

Bloch, F. Theory of Line Narrowing by Double-Frequency Irradiation (1958). *Physical Review* **111**, 841–853.

Bloembergen, N. On the interaction of nuclear spins in a crystalline lattice (1949). *Physica* **15**, 386–426.

Bocharov, E. V., Mineev, K. S., Volynsky, P. E., Ermolyuk, Y. S., Tkach, E. N., Sobol, A. G., Chupin, V. V., Kirpichnikov, M. P., Efremov, R. G., Arseniev, A. S. Spatial structure of the dimeric transmembrane domain of the growth factor receptor ErbB2 presumably corresponding to the receptor active state (2008). *J. Biol. Chem.* **283**, 6950–6956.

Booth, P. J., Templer, R. H., Meijberg, W., Allen, S. J., Curran, A. R., Lorch, M. In vitro studies of membrane protein folding (2001). *Crit. Rev. Biochem. Mol. Biol.* **36,** 501–603.

Breyton, C., Pucci, B., Popot, J. L. Amphipols and fluorinated surfactants: two alternatives to detergents for studying membrane proteins in vitro (2010). *Methods Mol. Biol.* **601**, 219–245.

Buchanan, S. K. Overexpression and refolding of an 80-kDa iron transporter from the outer membrane of *Escherichia coli* (1999). *Biochem. Soc. Trans.* **27**, 903–908.

Cantor, R. S. Lipid composition and the lateral pressure profile in bilayers (1999). *Biophys. J.* **76**, 2625–2639.

Castellani, F. Structure determination of immobilized proteins by solid-state NMR spectroscopy (2003).

Catoire, L. J., Zoonens, M., van Heijenoort, C., Giusti, F., Guittet, E., Popot, J. L. Solution NMR mapping of water-accessible residues in the transmembrane beta-barrel of OmpX (2010). *Eur. Biophys. J.* **39**, 623–630.

Charbonnier, F., Köhler, T., Pechère, J. C., Ducruix, A. Overexpression, refolding, and purification of the histidine-tagged outer membrane efflux protein OprM of *Pseudomonas aeruginosa* (2001). *Protein Expr. Purif.* **23**, 121–127.

Chen, G. Q., Gouaux, E. Overexpression of a glutamate receptor (GluR2) ligand binding domain in *Escherichia coli*: application of a novel protein folding screen (1997). *Proc. Natl. Acad. Sci. U. S. A.* **94**, 13431–13436.

Chen, M., Khalid, S., Sansom, M. S., Bayley, H. Outer membrane protein G: Engineering a quiet pore for biosensing (2008). *Proc. Natl. Acad. Sci. U. S. A.* **105**, 6272–6277.

Cherezov, V., Rosenbaum, D. M., Hanson, M. A.,Rasmussen, S. G., Thian, F. S., Kobilka, T. S., Choi, H. J., Kuhn, P., Weis, W. I., Kobilka, B. K., Stevens, R. C. High-resolution crystal structure of an engineered human beta2-adrenergic G protein-coupled receptor (2007). *Science* **318** (5854), 1258–1265.

Civjan, N. R., Bayburt, T. H., Schuler, M. A., Sligar, S. G. Direct solubilisation of heterologously expressed membrane proteins by incorporation into nanoscale lipid bilayers (2003). *Biotechniques* **35**, 556–560.

Conlan, S., Zhang, Y., Cheley, S., Bayley, H. Biochemical and biophysical characterization of OmpG: A monomeric porin (2000). *Biochemistry* **39**, 11845–11854.

Conlan, S., Bayley, H. Folding of a monomeric porin, OmpG, in detergent solution (2003). *Biochemistry* **42**, 9453–9465.

Cowan, S. W., Schirmer, T., Rummel, G., Steiert, M., Ghosh, R., Pauptit, R. A., Jansonius, J. N., Rosenbusch, J. P. Crystal structures explain functional properties of two *E. coli* porins (1992). *Nature* **358**, 727–733.

Dahmane, T., Damian, M., Mary, S., Popot, J. L., Baneres, J. L. Amphipol assisted in vitro folding of G protein-coupled receptors (2009). *Biochemistry* **48**, 6516–6521.

Damaghi, M., Köster, S., Bippes, C. A., Yildiz, O., Müller, D. J. One β hairpin follows the other: exploring refolding pathways and kinetics of the transmembrane β-barrel protein OmpG (2010). *Angew. Chem. Int. Ed. Engl.* 1 **50** (32), 7422–7424.

De Bernadez-Clark, E., Schwarz, E., Rudolph, R. Inhibition of aggregation side reactions during in vitro protein folding (1999). *Methods Enzymol.* **309**, 217–236.

Denisov, I. G., Grinkova, Y. V., Lazarides, A. A., Sligar, S. G. Directed self-assembly of monodisperse phospholipid bilayer nanodiscs with controlled size (2004). *J. Am. Chem. Soc.* **126**, 3477–3487.

Dekker, N., Merck, K., Tommassen, J., Verheij, H. M. In vitro folding of *Escherichia coli* outer-membrane phospholipase A (1995). *Eur. J. Biochem.* **232**, 214–219.

Diab, C., Tribet, C., Gohon, Y., Popot, J. L., Winnik, F. M. Complexation of integral membrane proteins by phosphorylcholine-based amphipols (2007). *Biochim. Biophys. Acta* **1768**, 2737–2747.

Dolder, M., Zeth, K., Tittmann, P., Gross, H., Welte, W., Wallimann, T. Crystallization of the human, mitochondrial voltage-dependent anion selective channel in the presence of phospholipids (1999). *J. Struct. Biol.* **127**, 64–71.

Dong, C., Beis, K., Nesper, J., Brunkan-Lamontagne, A. L., Clarke, B. R., Whitfield, C., Naismith, J.H. Wza the translocon for *E. coli* capsular polysaccharides defines a new class of membrane protein (2006). *Nature* **444** (7116), 226–229.

Engel, A, Müller, D. J. Observing single biomolecules at work with the atomic force microscope (2000). *Nat. Struct. Biol.* **7**(9), 715–718.

Etzkorn, M., Seidel, K., Li, L., Martell, S., Geyer, M., Engelhard, M., Baldus, M. Complex formation and light activation in membrane-embedded sensory rhodopsin II as seen by solid-state NMR spectroscopy (2010). *Structure* **18**, 293–300.

Fajardo, D. A. Cheung, J., Ito, C., Sugawara, E., Nikaido, H., Misra, R. Biochemistry and regulation of a novel Escherichia coli K-12 porin protein, OmpG, which produces unusually large channels (1998). *Journal of Bacteriology* **180**, 4452–4459.

Falzone J. C., Karsten W. E., Conley J. D., Viola R. E. L-Aspartase from *Escherichia coli*: Substrate specificity and role of divalent metal ions (1988). *Biochemstry* **27**, 9089–9093.

Ferguson, A. D., Breed, J., Diederichs, K., Welte, W., Coulton, J. W. An internal affinity-tag for purification and crystallization of the siderophore receptor FhuA, integral outer membrane protein from *Escherichia coli* K-12 (1998). *Protein Sci.* **7**, 1636–1638.

Ferguson, A. D., Welte, W., Hofmann, E., Lindner, B., Holst, O., Coulton, J. W., Diederichs, K. A conserved structural motif for lipopolysaccharide recognition by procaryotic and eucaryotic proteins (2000). *Structure* **8** 585–592.

Ferguson, A. D., Ködding, J., Walker, G., Bös, C., Coulton, J. W., Diederichs, K., Braun, V., Welte, W. Active transport of an antibiotic rifamycin derivative by the outer-membrane protein FhuA (2001). *Structure* **9**, 707–716.

Ferguson, N. Becker, J., Tidow, H., Tremmel, S., Sharpe, T.D., Krause, G., Flinders, J., Petrovich, M., Berriman, J., Oschkinat, H., Fersht, A.R. General structural motifs of amyloid protofilaments (2006). *Proc. Natl. Acad. Sci. U. S. A.* **103**, 16248–16253.

Fernández, C., Hilty, C., Wider, G., Guntert, P., Wuthrich, K. NMR structure of the integral membrane protein OmpX (2004). *J. Mol. Biol.* **336**, 1211–1221.

Fleishman, S. J., Harrington, S. E., Enosh, A., Halperin, D., Tate, C. G., Ben-Tal, N. Quasi-symmetry in the cryo-EM structure of EmrE provides the key to modelling its transmembrane domain (2006). *Journal of Molecular Biology* **364** (1), 54–67.

Forst, D., Schülein, K. Wacker, T., Diederichs, K., Kreutz, W., Benz, R., Welte, W. Crystallization and preliminary X-ray diffraction analysis of ScrY, a specific bacterial outer membrane porin (1993). *J. Mol. Biol.* **229**, 258–262.

Fung, B.M., Khitrin, A.K. and Ermolaev, K. An improved broadband decoupling sequence for liquid crystals and solids (2000). *J. Magn. Reson.* **142**, 97-101.

Garavito, R. M., Rosenbusch, J. P. Three-dimensional crystals of an integral membrane protein: an initial x-ray analysis (1980). *J Cell Biol.* **86** (1), 327–329.

Garavito, R. M., Picot, D., Loll, P. J. Strategies for crystallizing membrane proteins (1995). *J. Bioenerg. Biomembr.* **28**, 1–8.

Gill, S. C., Vonhippel, P. H. Calculation of protein extinction coefficients from amino-acid Sequence Data (1989). *Analytical Biochemistry* **182**, 319–326.

Gohon, Y., Dahmane, T., Ruigrok, R. W., Schuck, P., Charvolin, D., Rappaport, F., Timmins, P., Engelman, D. M., Tribet, C., Popot, J. L. Ebel, C. Bacteriorhodopsin/ amphipol complexes: structural and functional properties (2008). *Biophys. J.* **94**, 3523–3537.

Gonen, T., Sliz, P., Kistler, J., Cheng, Y., Walz, T. Aquaporin-0 membrane junctions reveal the structure of a closing water pore (2004). *Nature* **429**, 193–97.

Gonen, T., Cheng, Y., Sliz, P., Hiroaki, Y., Fujiyoshi, Y. Harrison, S.C., Walz, T. Lipid-protein interactions in double-layered two-dimensional AQP0 crystals (2005). *Nature* **438**, 633–638.

Gorzelle, B. M., Hoffman, A. K., Keyes, M. H., Gray, D. N., Ray, D. G., Sanders, C. R. Amphipols can support the activity of a membrane enzyme (2002). *J. Am. Chem. Soc.* **124**, 11594–11595.

Gouaux, E. Alpha-Hemolysin from *Staphylococcus aureus*: an archetype of beta-barrel, channel-forming toxins (1998). *Journal of Structural Biology* **121** (2), 110–122.

Grosse, W., Reiss, P., Reitz, S., Cebi, M., Lübben, W., Koert, U., Essen, L. O. Structural and functional characterization of a synthetically modified OmpG (2010). *Bioorg Med Chem* **18** (22), 7716–7723.

Gu, L. Q., Braha, O., Conlan, S., Cheley, S., Bayley, H. Stochastic sensing of organic analytes by a pore-forming protein containing a molecular adapter (1999). *Nature* **398**, 686–690.

Gullion, T., Schaefer, J. Rotational-Echo Double-Resonance Nmr (1989). *J. Magn.* Reson. 81, 196–200.

Hardy. H. H., Verel, R., Meier B. H. Fast MAS Total Through-Bond Correlation Spectroscopy (2000). *Journal of Magnetic Resonance* **148**, 459–464.

Hasler, L., Heymann, J. B., Engel, A., Kistler, J., Walz, T. 2D crystallization of membrane proteins: Rationales and examples (1998). *Journal of Structural Biology* **121**, 162–171.

Heise, H. Hoyer, W., Becker, S., Andronesi, O.C., Riedel, D., Baldus, M. Molecular-level secondary structure, polymorphism, and dynamics of full-length alpha-synuclein fibrils studied by solid-state NMR (2005). *Proc. Natl. Acad. Sci. U. S. A.* **102**, 15871–15876.

Helenius, K. S. Solubilization of membranes by detergents (1975). *Biochim. Biophys. Acta* **415**, 29–79.

Henderson, R. Realizing the potential of electron cryo-microscopy (2004). *Quarterly Reviews of Biophysics* **37** (1), 3–13.

Henderson, R., Baldwin, J. M., Ceska, T. A., Zemlin, F., Beckmann, E., Downing, K. H. Model for the structure of bacteriorhodopsin based on high-resolution electron cryo-microscopy (1990). *J. Mol. Biol.* **213**, 899–929.

Hiller, M., Krabben, L., Vinothkumar, K. R., Castellani, F., van Rossum, B. J., Kühlbrandt, W., Oschkinat, H. Solid-state magic-angle spinning NMR of outer-membrane protein G from *Escherichia coli* (2005). *Chembiochem.* **6** (9), 1679–1684.

Hiller, S., Garces, R. G., Malia, T. J., Orekhov, V. Y., Colombini, M., Wagner, G. Solution structure of the integral human membrane protein VDAC-1 in detergent micelles (2008). *Science* **321**, 1206–1210.

Hiller, M. Sample preparation of membrane proteins suitable for solid-state MAS NMR and development of assignment strategies (2009).

Hing, A. W., Vega, S. & Schaefer, J. Transferred-Echo Double-Resonance Nmr (1992). *J. Magn. Reson.* **96**, 205-209.

Hiroaki, Y., Tani, K., Kamegawa, A., Gyobu, N., Nishikawa, K. Suzuki, H., Walz, T., Sasaki S, Mitsuoka, K., Kimura, K., Mizoguchi, A., Fujiyoshi, Y. Implications of the aquaporin-4 structure on array formation and cell adhesion (2006). *J. Mol. Biol.* **355**, 628–639.

Holm, P. J., Bhakat, P., Jegerschold, C., Gyobu, N., Mitsuoka, K., Fujiyoshi, Y., Morgenstern, R., Hebert, H. Structural basis for detoxification and oxidative stress protection in membranes (2006). *J. Mol. Biol.* **360**, 934–945.

Hong, M., Zhang, Y., Hu, F., Membrane protein structure and dynamics from NMR spectroscopy (2012). *Annu. Rev. Phys. Chem.* **63**, 1–24.

Hoogenboom, B. W., Hug, H. J., Pellmont, Y., Martin, S., Frederix, P.L.T.M., Fotiadis, D., Engel A. Quantitative dynamic-mode scanning force microscopy in liquid (2006). *Appl. Phys. Lett.* **88**, 193109.

Hopper, S., Segal, H. L. Kinetic studies of rat liver glutamic-alanine transaminase (1962). *The journal of biological chemistry* **237**, 3189–3195.

Hu, F., Schmidt-Rohr, K., Hong, M. NMR detection of pH-dependent histidine-water proton exchange reveals the conduction mechanism of a transmembrane proton channel (2012). *J Am Chem Soc.* **134** (8), 3703–3713.

Hubner, C. A., Jentsch, T. J. Ion channel diseases (2002). *Hum. Mol. Genet.* **11**, 2435–2445.

Hunte, C., Michel, H. Crystallisation of membrane proteins mediated by antibody fragments (2002). *Curr. Opin. Struct. Biol.* **12**, 503–508.

Hunte, C., Richters, S. Lipids and membrane protein structures (2008). *Curr. Op. Struc. Biol.* **18**, 1–6.

Hwang, P. M. & Kay, L. E. Solution structure and dynamics of integral membrane proteins by NMR: A case study involving the enzyme PagP (2005). *Methods Enzimol* **394**, 335-350.

Igumenova, T. I., Wand, A. J., McDermott, A. E. Assignment of the backbone resonances for microcrystalline ubiquitin (2004). *J. Am. Chem. Soc.* **126**, 5323–5331.

Iordanov, I., Renault, M., Réat, V., Bosshart, P. D., Engel, A., Saurel, O., Milon, A. Dynamics of *Klebsiella pneumoniae* OmpA transmembrane domain: The four extracellular loops display restricted motion behavior in micelles and in lipid bilayers (2012). *Biochim. Biophys. Acta.* **1818** (9), 2344–2353.

Iwahara, J., Clore, G. M. Detecting transient intermediates in macromolecular binding by paramagnetic NMR (2006). *Nature* **440**, 1227–1230.

Jaakola, V. P., Griffith, M. T., Hanson, M. A., Cherezov, V., Chien, E. Y., Lane, J. R., Ijzerman, A. P. and Stevens, R. C. The 2.6 Ångstrom crystal structure of a human A2a adenosine receptor bound to an antagonist (2008). *Science* **322**(5905), 1211–1217.

Jegerschold, C., Pawelzik, S. C., Purhonen, P., Bhakat, P., Gheorghe, K. R., Gyobu, N., Mitsuoka, K., Morgenstern, R., Jakobsson, P. J., Hernert, H. Structural basis for induced formation of the inflammatory mediator prostaglandin E2 (2008). *Proceedings of the National Academy of Sciences of the United States of America* **105** (32), 11110–11115.

John, R. A., Charteris A., Fowler, L. J. The reaction of Amino-oxyacetate with Pyridoxal phosphate-dependent enzymes (1978). *Biochem. J.* **171**, 771–779.

Jonas, A. Reconstitution of high-density lipoproteins (1986). *Methods Enzymol.* **128**, 553–582.

Kedrov, A., Janovjak, H., Sapra, K. T., Müller, D. J. Deciphering molecular interactions of native membrane proteins by single-molecule force spectroscopy (2007). *Annu. Rev. Biophys. Biomol. Struct.* **36**, 233–260.

Kelly, A. E., Ou, H. D., Withers R., Dötsch, V. Low-conductivity buffers for high-sensitivity NMR Measurements (2002). *American Chemical Society* **124**, 12013–12019.

Kimura Y., Vassylyev, D. G., Miyazawa, A., Kidera, A., Matsushima, M. Surface of bacteriorhodopsin revealed by high-resolution electron crystallography (1997). *Nature* **389**, 206–11.

Kleinschmidt, J. H., Wiener, M. C., Tamm, L. K. Outer membrane protein A of *E. coli* folds into detergent micelles, but not in the presence of monomeric detergent (1999). *Protein Sci.* **8**, 2065–2071.

Koppel, D. A., Kinnally, K. W., Masters, P., Forte, M., Blachly-Dyson, E., Mannella, C. A. Bacterial expression and characterization of the mitochondrial outer membrane channel (1998). *J. Biol. Chem.* **273**, 13794–13800.

Koronakis, V., Li, J., Koronakis E., Stauffer K. Structure of TolC, the outer membrane component of the bacterial type I efflux system, derived from two-dimensional crystals (1997). *Mol. Microbiol.* **23**, 617–623.

Korkmaz, F., Köster, S., Yildiz, O., Mäntele, W. The role of lipids for the functional integrity of porin: an FTIR study using lipid and protein reporter groups (2008). *Biochemistry* **47** (46), 12126–12134.

Korkmaz, F., Ozkan, F., Köster, S., Kühlbrandt, W., Mäntele, W., Yildiz, O. Correlation between the OmpG secondary structure and its pH-dependent alterations monitored by FTIR (2010). *J. Mol. Biol.* **401**, 56–67.

Korkmaz, F., Köster, S., Yildiz, O., Mäntele, W. In situ opening/ closing of OmpG from E. coli and the splitting of β-sheet signals in ATR-FTIR spectroscopy (2012). *Spectrochim. Acta A Mol. Biomol. Spectrosc.* **91**, 395–401.

Kramer, R. A., Zandwijken, D., Egmond, M. R., Dekker, N. In vitro folding, purification and characterization of *Escherichia coli* outer membrane protease OmpT (2000). *Eur. J. Biochem.* **267**, 885–893.

Kreusch, A., Neubüser, A., Schiltz, E., Weckesser, J., Schulz, G. E. The structure of the membrane channel porin from *Rhodopseudomonas blastica* at 2.0 Å resolution (1994). *Protein Sci.* **3**, 58–63.

Kühlbrandt, W. Three-dimensional crystallization of membrane proteins (1988). *Quarterly Reviews of Biophysics* **21** (4), 429–477.

Kühlbrandt, W. Two-dimensional crystallization of membrane proteins (1992). *Q.Rev. Biophys.* **25**, 1–49.

Kühlbrandt W., Wang D. N., Fujiyoshi Y. Atomic model of plant light-harvesting complex by electron crystallography (1994). *Nature* **367**, 614–621.

Kuruma, Y., Suzuki, T., Ueda, T. Production of multi-subunit complexes on liposome through an *E. coli* cell-free expression system (2010). *Methods Mol. Biol.* **607**,161–171.

Lacapère, J. J., Stokes, D., Olofsson, A. J. L., Rigaud, J. L. Two dimensional crystallization of Ca-ATPase by total detergent removal (1998). *Biophys. J.* **75**, 1319–1329.

Laemmli, U.K. Cleavage of Structural Proteins during the Assembly of the Head of Bacteriophage T4 (1970). *Nature* **227**, 680–685.

Lange, A. Giller, K., Hornig, S., Martin-Eauclaire, M.F., Pongs, O., Becker, S., Baldus, M. Toxin-induced conformational changes in a potassium channel revealed by solid-state NMR (2006). *Nature* **440**, 959–962.

Lau, F. W., Bowie, J. U. A method for assessing the stability of a membrane protein (1997). *Biochemistry* **36**, 5884–5892.

Lau, T. L., Kim, C., Ginsberg, M. H., Ulmer, T. S. The structure of the integrin alphabeta3 transmembrane complex explains integrin transmembrane signalling (2009). *EMBO J.* **28**, 1351–1361.

Laws, D. D., Bitter, H. M., Jerschow, A. Solid-state NMR spectroscopic methods in chemistry (2002). *Angew. Chem. Int. Ed Engl.* **41**, 3096–3129.

Le Maire, M., Champeil, P., Møller, J. V. Interaction of membrane proteins and lipids with solubilizing detergents (2000). *Biochim. Biophys. Acta* **1508**, 86–111.

Lee, D., Walter, K. F., Bruckner, A. K., Hilty, C., Becker S., Griesinger, C. Bilayer in small bicelles revealed by lipid–protein interactions using NMR spectroscopy (2008). *J. Am. Chem. Soc.* **130**, 13822–13823.

Lévy, D., Bluzat A., Seigneuret, M., Rigaud, J. L. A systematic study of liposome and proteoliposome reconstitution involving Bio-Bead-mediated Triton X100 removal (1990). *Biochim. Biophys. Acta* **1025**, 179–190.

Lian, L. Y., Middleton, D. A. Labelling approaches for protein structural studies by solution-state and solid-state NMR (2001). *Prog. Nucl. Magn. Reson. Spectrosc.* **39**, 171–190.

Liang, B. & Tamm, L. K. Structure of outer membrane protein G by solution NMR spectroscopy (2007). *Proceedings of the National Academy of Sciences* **104**, 16140–16145.

Linke, D., Frank, J., Holzwarth, J. F., Soll, J., Boettcher, C., Fromme, P. In vitro reconstitution and biophysical characterization of OEP16, an outer envelope pore protein of pea chloroplasts (2000). Biochemistry **39**, 11050–11056.

Linser, R., Dasari, M., Hiller, M., Higman, V., Fink, U., Lopez del Amo, J. M., Markovic, S., Handel, L., Kessler, B., Schmieder, P., Oesterhelt, D., Oschkinat, H., Reif, B. Proton-detected solid-state NMR spectroscopy of fibrillar and membrane proteins (2011). *Angew. Chem. Int. Ed. Engl.* **50** (19), 4508–4512.

Locher, K. P., Rosenbusch, J. P. Oligomeric states and siderophore binding of the ligand-gated FhuA protein that forms channels across *Escherichia coli* outer membranes (1997). *Eur. J. Biochem.* **247**, 770–775.

Locher, K. P., Rees, B., Koebnik, R., Mitschler, A., Moulinier, L., Rosenbusch, J. P., Moras, D. Transmembrane signalling across the ligand gated FhuA receptor: crystal structures of free and ferrichrome-bound states reveal allosteric changes (1998). *Cell.* **95**, 771–778.

Long, S. B., Campbell, E. B., Mackinnon, R. Voltage sensor of Kv1.2: structural basis of electromechanical coupling (2005). *Science* **309** (5736), 903–908.

Long, S. B., Tao, X., Campbell, E. B., MacKinnon, R. Atomic structure of a voltage-dependent K^+ channel in a lipid membrane-like environment (2007). *Nature* **450** (7168), 376–382.

Luirink, J., von Heijne, G., Houben, E., de Gier, J. W. Biogenesis of inner membrane proteins in *Escherichia coli* (2005). *Annu. Rev. Microbiol.* **59**, 329–355.

Lü, W., Du, J., Wacker, T., Gerbig-Smentek, E., Andrade, S. L., Einsle, O. pH-dependent gating in a FocA formate channel (2011). *Science* **332** (6027), 352–354.

Mannella, C. A. On the structure and gating mechanism of the mitochondrial channel, VDAC (1997). *J. Bioenerg. Biomembranes.* **29**, 525–531.

Mannella, C. A. Conformational changes in the mitochondrial channel protein, VDAC, and their functional implications (1998). *J. Struct. Biol.* **121**, 207–218.

Mari, S. A., Koster, S., Bippes, C. A., Yildiz, O., Kühlbrandt, W., Müller, D. J. pH-induced conformational change of the beta-barrel-forming protein OmpG reconstituted into native *E. coli* lipids (2010). *J. Mol. Biol.* **396**, 610–616.

Marley, J., Lu, M., Bracken, C. A method for efficient isotopic labeling of recombinant proteins (2001). *J. Biomol. NMR.* **20**, 71–75.

Martin, R. W., Zilm, K.W. Preparation of protein nanocrystals and their characterization by solid state NMR (2003). *J. Magn. Reson.* **165**, 162–174.

McDermott, A. E. Structural and dynamic studies of proteins by solid-state NMR spectroscopy: rapid movement forward (2004). *Curr. Opin. Struct. Biol.* **14**, 554–561.

McDermott, A. E. Structure and dynamics of membrane proteins by magic angle spinning solid-state NMR (2009). *Annu. Rev. Biophys.* **38**, 385–403.

Metz, G., Wu, X.L. and Smith, S.O. Ramped-Amplitude Cross-Polarization in Magic Angle-Spinning Nmr (1994). *J. Magn. Reson.* A **110**, 219-227.

Meyer, J. E. W., Hofnung, M., Schulz, G. E., Structure of maltoporin from *Salmonella typhimurium* ligated with a nitrophenyl-maltotrioside (1997). *J. Mol. Biol.* **266**, 761–775.

Michel, H. Crystallization of Membrane Proteins (1983). *Trends in Biochemical Science* **8** (2), 56–59.

Michuda, C. M. and Martinez-Carrion M. The isozymes of Glutamate-Aspartate transaminase (1970). *The journal of biological chemistry* **245**, 262–269.

Miller, J. H. A short course in bacterial genetics. A Laboratory Manual and Handbook for *Escherichia coli* and related bacteria (1992). *Cold Spring Harbor, New York*.

Minoia, A. NMR Stato Solido: principi applicazioni e strumentazioni. Brucker.

Miroux, B. and Walker, J. E. Over-production of proteins in *Escherichia coli*: Mutant hosts that allow synthesis of some membrane proteins and globular proteins at high levels (1996). *Journal of Molecular Biology* **260**, 289–298.

Misra, R., Benson, S. A. A Novel Mutation, Cog, Which Results in Production of A New Porin Protein (OmpG) of *Escherichia-Coli* K-12 (1989). *Journal of Bacteriology* **171**, 4105–4111.

Miyazawa A, Fujiyoshi Y, Unwin N. Structure and gating mechanism of the acetylcholine receptor pore (2003). *Nature* **423**, 949–955.

Miyahara I., Hitotsu K., Hayashi H., Kagamyama H. X-ray Crystallographic study of pyridoxamine 5'-phosphate type aspartate aminotransferases from *Escherichia coli* in three forms (1994). *J. Biochem.* **116**, 1001–1012.

Müller, D. J., Büldt, G., Engel A. Force-induced conformational change of bacteriorhodopsin (1995). *J. Mol. Biol.* **249**, 239–243.

Murata, K., Mitsuoka, K., Hirai, T., Walz, T., Agre, P. Structural determinants of water permeation through aquaporin-1 (2000). *Nature* **407**, 599–605.

Nelson, D. L., Cax, M. M. Lehninger principles of Biochemistry (2005). W. H. Freeman and Company, Cambridge.

Nevzorov, A. A., Mesleh, M. F., Opella, S. J. Structure determination of aligned samples of membrane proteins by NMR spectroscopy (2004). *Magn Reson. Chem.* **42**, 162–171.

Nikaido, H. Molecular basis of bacterial outer membrane permeability revisited (2003). *Microbiology and Molecular Biology Reviews* **67** (4), 593–656.

Nogales, E., Wolf, S. G., Downing, K. H. Visualizing the secondary structure of tubulin: three dimensional map at 4 Å (1997). *Journal of Structural Biology* **118** (2), 119–127.

Nollert, P., Royant, A., Pebay-Peyroula, E., Landau, E. M. Detergent-free membrane protein crystallization (1999). *FEBS Letters* **457** (2), 205–208.

Oesterhelt, F., Oesterhelt, D., Pfeiffer, M., Engel, A., Gaub, H. E., Müller, D. J. Unfolding pathways of individual bacteriorhodopsins (2000). *Science* 288, 143–146.

Opella, S. J., Marassi, F. M. Structure determination of membrane proteins by NMR spectroscopy (2004). *Chemical Reviews* **104**, 3587–3606.

Ostermeier, C., Michel, H. Crystallization of membrane proteins (1997). *Current Opinion in Structural Biology* **7** (5), 697–701.

Ostermeier, C., Iwata, S., Michel, H. Cytochrome c oxidase (1996). *Curr. Opin. Struct. Biol.* **6**, 460–466.

Otting, G. Prospects for lanthanides in structural biology by NMR (2008). *J. Biomol. NMR* **42**, 1–9.

Oxenoid, K., Chou, J. J. The structure of phospholamban pentamer reveals a channel-like architecture in membranes (2005). *Proc. Natl. Acad. Sci. U. S. A.* **102**, 10870–10875.

Palczewsky, K., Kumasaka, T., Hory, T., Behnke, C. A., Motoshima, H., Fox, B. A., Le Trong, I., Teller, D. C., Okada, T., Stenkamp, R. E., Yamamoto, M. and Miyano, M. Crystal structure of rhodopsin: A G protein-coupled receptor (2000). *Science* **289**(5480), 739–745

Pautsch, A., Vogt, J., Model, K., Siebold, C., Schulz, G. E. Strategy for membrane protein crystallization exemplified with OmpA and OmpX Proteins (1999). *Struct. Funct. Genet.* **34**, 167–172.

Pauli, J., van Rossum, B., Forster, H., de Groot, H. J. M., Oschkinat, H. Sample optimization and identification of signal patterns of amino acid side chains in 2D RFDR spectra of the alpha-spectrin SH3 domain (2000). *J. Magn. Reson.* **143**, 411–416.

Pauli, J., Baldus, M., van Rossum, B., de Groot, H., Oschkinat, H. Backbone and side-chain C-13 and N-15 signal assignments of the alpha-spectrin SH_3 domain by magic angle spinning solid-state NMR at 17.6 tesla (2001). *Chembiochem* **2**, 272–281.

Pebay-Peyroula, E., Dahout-Gonzalez, C., Kahn, R., Trezeguet, V., Lauquin, G. J., Brandolin, G. Structure of mitochondrial ADP/ATP carrier in complex with carboxyatractyloside (2003). *Nature* **426** (6962), 39–44.

Petkova, A. T., Ishii, Y., Balbach, J. J., Antzutkin, O. N., Leapman, R.D., Delaglio, F., Tycko, R.A. structural model for Alzheimer's beta-amyloid fibrils based on experimental constraints from solid state NMR (2002). *Proc. Natl. Acad. Sci. U. S. A.* **99**, 16742–16747.

Petkova, A. T., Yau, W. M., Tycko, R. Experimental constraints on quaternary structure in Alzheimer's beta-amyloid fibrils (2006). *Biochemistry* **45**, 498–512.

Phale, P. S., Schirmer, T., Prilipov, A., Lou, K. L. Hardmeyer, A., Rosenbusch, J. P. Voltage gating of *Escherichia coli* porin channels: role of the constriction loop (1997). *Proc. Natl. Acad. Sci. U. S. A.* **94**, 6741–6745.

Pines, A., Waugh, J. S., Gibby, M. G. Proton-Enhanced Nuclear Induction Spectroscopy-Method for High-Resolution Nmr of Dilute Spins in Solids (1972). *J. Chem. Phys.* **56**(4), 1776–1777.

Prince, S. M., Feron, C., Janssens, D., Lobet, Y., Achtman, M., Kusecek, B., Bullough, P. A., Derrick, J. P. Expression, refolding and crystallization of the OpcA invasin from *Neisseria meningitidis* (2001). *Acta Crystallogr.* D **57**, 1164–1166.

Prive, G. G. Detergents for the stabilization and crystallization of membrane proteins (2007). *Methods* **41** (4), 388–397.

Pocanschi, C. L., Dahmane, T., Gohon, Y., Rappaport, F., Apell, H. J., Kleinschmidt, J. H., Popot, J. L. Amphipathic polymers: tools to fold integral membrane proteins to their active form (2006). *Biochemistry* **45**, 13954–13961.

Poget, S. F., Girvin, M. E. Solution NMR of membrane proteins in bilayer mimics: small is beautiful, but sometimes bigger is better (2007). *Biochim. Biophys. Acta* **1768**, 3098–3106

Pohlmayer, K., Soll, J., Steinkamp, T., Hinnah, S., Wagner, R. Isolation and characterization of an amino acid-selective channel protein present in the chloroplastic outer envelope membrane (1997). *Proc. Natl. Acad. Sci. U. S. A.* **94**, 9504–9509.

ProtParam. www.expasy.ch.

Remaut, H., Tang, C., Henderson, N. S., Pinker, J. S., Wang, T., Hultgren, S. J., Thanassi, D. G., Waksam, G., Li, H. Fiber formation across the bacterial outer membrane by the chaperone/ usher pathway (2008). *Cell.* **133** (4), 640–652.

Renault, M., Tommassen-van Boxtel, R., Bos, M. P., Post, J. A., Tommassen, J., Baldus, M. Cellular solid-state nuclear magnetic resonance spectroscopy (2012). *Proc. Natl. Acad. Sci. U. S. A.* **109** (13), 4863–4868.

Ren, G., Reddy, V. S., Cheng, A., Melnyk, P., Mitra, A. K. Visualization of a water-selective pore by electron crystallography in vitreous ice (2001). *Proc. Natl. Acad. Sci. U. S. A.* **98**, 1398–1403.

Rhee, M., Burns, M. A. Nanopore sequencing technology: nanopore preparations (2007). *Trends Biotechnol.* **25**, 174–181.

Rigaud, J. L., Pitard, B., Lévy, D. Reconstitution of membrane proteins into liposomes: application to energy-transducing membrane proteins (1995). *Biochim. Biophys. Acta* **1231**, 223–246.

Rigaud, J. L., Mosser, G., Lacapère, J. J., Olofsson, A., Lévy, D., Ranck, J. L. Bio-Beads: an efficient strategy for two dimensional crystallization of membrane proteins (1997). *J. Struct. Biol.* **118**, 226–235.

Rigaud, J. L., Lévy, D., Mosser, G., Lambert, O., Detergent removal by Bio-Beads. Applications to membrane protein reconstitution and 2D crystallization (1998). *Eur. Biophys. J.* **27** 305-319.

Rigaud, J. L., Chami, M., Lambert, O., Lévy, D., Ranck, J. L. Use of detergents in two-dimensional crystallization of membrane proteins (2000). *Biochimica et Biophysica Acta* **1508**, 112–128.

Rinas, U., Bailey, J. E. Protein compositional analysis of inclusion bodies produced in recombinant *Escherichia coli* (1992). *Appl. Microbiol. Biotechnol.* **37**, 609–614.

Rogl, H., Kosemund, F., Kühlbrandt, W., Collinson, I. Refolding of *Escherichia coli* produced membrane protein inclusion bodies immobilized by nickel chelating chromatography (1998). *FEBS Lett.* **432**, 21–26.

Roosild T.P., Greenwald J., Vega M., Castronovo S., Riek R., Choe S. NMR structure of Mistic, a membrane-integrating protein for membrane protein expression (2005). *Science* **307**, 1317-1321.
Rosenbusch, J. P. Stability of membrane proteins: relevance for the selection of appropriate methods for high-resolution structure determinations (2001). *J. Struct. Biol.* **136**, 144–157.

Sambrook, J., Fritsch, E. F., Maniatis, T. Molecular cloning. A Laboratory Manual. 2nd Ed. (1989). *Cold. Spring. Harbor. Press. Cold Spring Harbor, New York.*

Sanders, C. R., Landis, G. C. Reconstitution of membrane proteins into lipid-rich bilayered mixed micelles for NMR studies (1995). *Biochemistry* **34**, 4030–4040.

Schaefer, J., Stejskal, E. O. C-13 Nuclear Magnetic-Resonance of Polymers Spinning at Magic Angle (1976). *J. Am. Chem. Soc.* **98**, 1031–1032.

Schägger, H., von Jagow, G. Tricine-Sodium Dodecyl Sulfate-Polyacrylamide Gel Electrophoresis for the Separation of Proteins in the Range from 1 to 100 kDa (1987). *Analytical Biochemistry* **166**, 368–379.

Schein, C. H. Solubility as a function of protein structure and solvent components (1990). *Biotechnology (NY)* **8**(4), 308–316.

Scheuring, S, Müller, D. J., Stahlberg, H., Engel, H. A., Engel, A. Sampling the conformational space of membrane protein surfaces with the AFM (2002). *Eur. Biophys. J.* **31**, 172–178.

Schiltz, E., Kreusch, A., Nestel, U., Schulz, G. E. Primary structure of porin from *Rhodobacter capsulatus* (1991). *Eur. J. Biochem.* **199**, 587–594.

Schirmer, T., Keller, T. A., Wang, Y. F., Rosenbusch, J. P. Structural basis for sugar translocation through maltoporin channels at 3.1 Å resolution (1995). *Science* **267**, 512–514.

Schmid, B., Krömer, M., Schulz, G. E. Expression of porin from *Rhodopseudomonas blastica* in *Escherichia coli* inclusion bodies and folding into exact native structure (1996). *FEBS Lett.* **381**, 111–114.

Schmid, B., Maveyraud, L., Krömer, M., Schulz, G. E. Porin mutants with new channel properties (1998). *Protein. Sci.* **7**, 1603–1611.

Schmid, K., Ebner, R., Jahreis, K., Lengeler, J. W., Titgemeyer, F. A sugar specific porin, ScrY, is involved in sucrose uptake in enteric bacteria (1991). *Mol. Microbiol.* **5**, 941–950.

Schöneberg, T., Schulz, A., Biebermann, H., Hermsdorf, T., Römpler, H., Sangkuhl, K. Mutant G-protein-coupled receptors as a cause of human diseases (2004). *Pharmacol. Ther.* **104**, 173–206.

Schulz, G. E. Bacterial porins: structure and function (1993). *Curr. Opin. Cell Biol.* **5**, 701–707.

Schulz, G. E. Beta-barrel membrane proteins (2000). *Curr. Opin. Struct. Biol.* **10**, 443–447.

Schulz, G. E. The structure of bacterial outer membrane proteins (2002). *Biochim. Biophys. Acta* **1565**, 308–317.

Siemer, A. B. Ritter, C., Steinmetz, M.O., Ernst, M., Riek, R., Meier, B.H. ^{13}C, ^{15}N resonance assignment of parts of the HET-s prion protein in its amyloid form (2006). *J. Biomol. NMR* **34**, 75–87.

Smith, S. O., Farr-Jones, S., Griffin, R. G., Bachovchin, W. W. Crystal versus solution structures of enzymes: NMR spectroscopy of a crystalline serine protease (1989) *Science* **244**, (4907), 961–964.

Smith, B.S., Kobe, B., Kurumbail, R., Buchanan, S.K., Venkatramoni, L., van der Helm, D., Deisenhofer, J. Crystallization and preliminary X-ray analysis of ferric enterobactin receptor

FepA, an integral membrane protein from *Escherichia coli* (1998). *Acta Crystallogr.,* D **54** 697–699.

Smith S.O. Structure and activation of the visual pigment rhodopsin (2010). *Ann. Rev. Biophys.* **39**, 309-328.

Snijder, H. J., Ubaretxena-Belandia, I., Blaauw, M., Kalk, K. H., Verheij, H. M., Egmond, M. R., Dekker, N., Dijkstra, B. W. Structural evidence for dimerization-regulated activation of an integral membrane phospholipase (1999). *Nature* **401** (6754), 717–721.

Sobhanifar, S., Reckel, S., Junge, F., Schwarz, D., Kai, L., Karbyshev, M., Löhr, F., Bernhard, F., Dötsch, V. Cell-free expression and stable isotope labelling strategies for membrane proteins (2010). *J Biomol NMR.* **46**(1):33-43.

Stauffer, K. A., Page, M. G. P., Hardmeyer, A., Keller,T. A., Pauptit, R. A. Crystallization and preliminary X-ray characterization of maltoporin from *Escherichia coli* (1989). *J. Mol. Biol.* **211**, 297–299.

Stroud, R. M., Agard, D. A. Structure determination of asymmetric membrane profiles using an iterative Fourier method (1979). *Biophys. J.* **25**, 495–512.

Subbarao, G. V. & van den Berg, B. Crystal structure of the monomeric porin OmpG (2006). *Journal of Molecular Biology* **360**, 750–759.

Subramaniam, S., Henderson, R. Molecular mechanism of vectorial proton translocation by bacteriorhodopsin (2000). *Nature* **406** (6796), 653–657.

Sui, H., Han, B. G., Lee, J. K., Walian, P. and Jap, B. K. Structural basis of water-specific transport through the AQP1 water channel (2001). *Nature* **414**(6866), 872–878.

Suter, D. & Ernst, R. R. Spin diffusion in resolved solid-state NMR spectra (1985). *Physica Rev. B Condens. Matter,* **32**, 5608–5627.

Szeverenyi, N. M., Sullivan, M. J., Maciel, G. E. Observation of Spin Exchange by Two Dimensional Fourier-Transform C-13 Cross Polarization-Magic-Angle Spinning (1982). *J. Magn. Reson.* **47**, 462–475.

Szmelcman, S., Schwartz, M., Silhavy, T. T. J., Boos, W. Maltose transport in *Escherichia coli* K12. A comparison of transport kinetics in wild-type and lambda-resistant mutants as measured by fluorescence quenching (1976). *Eur. J. Biochem.* **65**, 13–19.

Tang, C., Iwahara, J., Clore, G. M. Visualization of transient encounter complexes in protein-protein association (2006). *Nature* **444**, 383–386.

Tang, C., Schwieters, C. D., Clore, G. M. Opening-to-closing transition in apo maltose-binding protein observed by paramagnetic NMR (2007). *Nature* **449**, 1078–1082.

Tate, C. G. Comparison of three structures of the multidrug transporter EmrE (2006). *Curr. Opin. Struct. Biol.* **16** (4), 457–64.

Tate, C. G. Practical considerations of membrane protein instability during purification and crystallisation (2010). *Methods Mol. Biol.* **601**, 187–203.

Tamm, L. K., Liang, B. Y. NMR of membrane proteins in solution (2006). *Prog. Nucl. Magn. Reson. Spectrosc.* **48**, 201–210.

Takegoshi, K., Nakamura, S., Terao, T. C-13-H-1 dipolar-assisted rotational resonance in magic-angle spinning NMR (2001). *Chem. Phys. Lett.* **344**, 631–637.

Tong, K. I., Yamamoto, M., Tanaka, T. A simple method for amino acid selective isotope labeling of recombinant proteins in *E. coli* (2008). *J. Biomol. NMR* **42** (1), 59–67.

Tonellato M. INTRODUZIONE ALLA SPETTROSCOPIA NMR.

Toyoshima, C. Structural aspects of ion pumping by Ca2+-ATPase of sarcoplasmic reticulum (2008). *Archives of Biochemistry and Biophysics* **476**(1), 3–11.

Tycko, R. Molecular structure of amyloid fibrils: insights from solid-state NMR (2006). *Q. Rev. Biophys.* **39**, 1-55.

Tycko R. Solid-state NMR studies of amyloid fibril structure (2011). *Annu. Rev. Phys. Chem.* **62**, 279–299.

Ultrafiltration application guides (Millipore, Schwalbach, Germany).

Unwin, N. Structure and action of the nicotinic acetylcholine receptor explored by electron microscopy (2003). *FEBS Lett.* **555**, 91–95.

Unwin, N. Refined structure of the nicotinic acetylcholine receptor at 4 Á resolution (2005). *J. Mol. Biol.* **346**, 967–989

van den Brink-van der Laan, E., Chupin, V., Killian, J. A., de Kruijff, B. Stability of KcsA tetramer depends on membrane lateral pressure (2004). *Biochemistry* **43**, 4240–4250.

Vandeputte-Rutten, L., Kramer, R. A., Kroon, J., Dekker, N., Egmond, M. R., Gros, P. Crystal structure of the outer membrane protease OmpT from *Escherichia coli* suggests a novel catalytic site (2001). *EMBO J.* **20**, 5033–5039.

Vinothkumar, K. R., Henderson, R. Structures of membrane proteins (2010). *Q. Rev. Biophys.* **43** (1), 65–158.

Viola, R. E. The central enzymes of the aspartate family of amino acid biosynthesis (2001). *Acc. Chem. Res.* **34**, 339–349.

Vivapure IEX Maxi Sartorium Stedim Biotech. Sartorius, Göttingen, Germany.

Vogt, J., Schultz, G. E. The structure of the outer membrane protein OmpX from Escherichia coli reveals possible mechanisms of virulence (1999). *Structure* **7** (10), 1301–1309.

Vold, R. R., Prosser, R. S. Magnetically oriented phospholipid bilayered micelles for structural studies of polypeptides. Does the ideal bicelle exist? (1998). *J. Magn. Reson. Series B* **113**, 267–271.

Volkov, A. N., Worrall, J. A. R., Holtzmann, E., Ubbink, M. Solution structure and dynamics of the complex between cytochrome c and cytochrome c peroxidase determined by paramagnetic NMR (2006). *Proc. Natl. Acad. Sci.* **103**, 18945–18950.

Vranken, W. F. Boucher, W., Stevens, T. J., Fogh, R. H, Pajon, A, Llinas, M., Ulrich E. L., Markley, J.L., Ionides, J., Laue, E.D. The CCPN data model for NMR spectroscopy: Development of a software pipeline (2005). *Proteins-Structure Function and Bioinformatics* **59**, 687–696.

Weiss, M. S., Schulz, G. E. Structure of porin refined at 1.8 Å resolution (1992). *J. Mol. Biol.* **227**, 493–509.

White, S. Membrane Protein Resources (1998). http://blanco.biomol.uci.edu/mpstruc/

Wickner, W., Schekman, R. Protein translocation across biological membranes (2005). *Science* **310**, 1452–1456.

Wind, R. A., Ded, S. F., Lock, H., Maciel, G. E. ^{13}C CP MAS and high-speed magic-angle spinning (1988). *Journal of Magnetic Resonance* **79** (1), 136–139.

Wu, X. L., Zilm, K. W. Cross polarization with high-speed magic-angle spinning (1993). *Journal of Magnetic Resonance* Series A **104** (2), 154–165.

Wu, C. H., Ramamoorthy, A., Opella, S. J. High resolution heteronuclear dipolar solid-state NMR spectroscopy (1994). *J. Magn. Reson. A* **109**, 270–272.

www.bmrb.wisc.edu

Yamashita, E., Zhalnina, M. V., Zakharov, S. D., Sharma, O., Cramer, W. A. Crystal structures of the OmpF porin: function in a colicin translocon (2008). *Embo Journal* **27** (15), 2171–2180.

Yang, C. R., Shapiro, B. E., Hung, S. P., Mjolsness, E. D., Hatfield, G. W. A mathematical model for the branched chain amino acid biosynthetic pathways of *Escherichia coli* K12 (2005). *J.Biol. Chem.* **280** (12), 11224–11232.

Yildiz, O., Vinothkumar, K. R., Goswami, P., Kühlbrandt, W. Structure of the monomeric outer-membrane porin OmpG in the opening/closing conformation (2006). *Embo Journal* **25**, 3702–3713.

Zeth, K., Diederichs, K., Welte, W., Engelhardt, H. Crystal structures of Omp32, the anion-selective porin from Comamonas acidovorans, in complex with a periplasmic peptide at 2.1 Å resolution (2000). *Structure* **8**, 981–992.

Zhang, H. H., Blanco, D. R., Exner, M. M., Shang, E. S., Champion, C. I., Phillips, M. L., Miller, J. N., Lovett, M. A. Renaturation of recombinant *Treponema pallidum* rare outer membrane protein 1 into a trimeric hydrophobic, and porin-active conformation (1999). *J. Bacteriol.* **181**, 7168–7175.

Zhang, H., Kurisu, G., Smith, J. L., Cramer, W. A. A defined protein-detergent-lipid complex for crystallization of integral membrane proteins: The cytochrome b6f complex of oxygenic photosynthesis (2003). *Proc. Natl. Acad. Sci. U. S. A.* **100**, 5160–5163.

Zhong, L., Bamm, V. V., Ahmed, M. A. M., Harauz, G., Ladizhansky, V. Solid-state NMR spectroscopy of 18.5 kDa myelin basic protein reconstituted with lipid vesicles: Spectroscopic characterisation and spectral assignments of solvent-exposed protein fragments (2007). *Biochimica et Biophysica Acta* **1768**, 3193–3205.

Zhou, Y., Bowie, J. U. Building a thermostable membrane protein (2000). *J. Biol. Chem.* **275**, 6975–6979.

Zoonens, M., Catoire, L. J., Giusti, F., Popot, J. L. NMR study of a membrane protein in detergent-free aqueous solution (2005). *Proc. Natl. Acad. Sci. U. S. A.* **102**, 8893–8898.

Appendix

Index of figures:

Index of Table:

For reasons of data protection,
the curriculum vitae is not included in the online version